THE UNIVERSITY OF CALGARY

LARGE DEFORMATION BEHAVIOUR OF AN INFLATABLE ARCH STRUCTURE

by

LESZEK BALAS

A THESIS

SUBMITTED TO THE FACULTY OF GRADUATE STUDIES

IN PARTIAL FULFILLMENT OF THE REQUIREMENTS FOR THE

DEGREE OF

MASTER OF SCIENCE

DEPARTMENT OF MECHANICAL ENGINEERING

CALGARY, ALBERTA

JULY, 1988

ISBN 0-315-46561-1

THE UNIVERSITY OF CALGARY

FACULTY OF GRADUATE STUDIES

The undersigned certify that they have read, and recommend to the Faculty of Graduate Studies for acceptance, a thesis entitled, "Large Deformation Behaviour of an Inflatable Arch Structure" submitted by Leszek Balas in partial fulfillment of the requirements for the degree of Master of Science in Engineering.

Dr. S.A. Lukasiewicz (Supervisor)
Department of Mechanical Engineering

Dr. M.C. Singh
Department of Mechanical Engineering

Dr. O. Vinogradov
Department of Mechanical Engineering

Dr. W.H. Dilger
Department of Civil Engineering

July 1988

ABSTRACT

This thesis deals with the large deflection and stability behaviour of extensible double-surface pneumatic arch structures subjected to axisymmetrical line load. It was found that, if the applied load exceeds the first wrinkling load, the structure breaks into stiff inflatable segments connected by extensible pneumatic hinges. The problem is reduced to a set of nonlinear equations which are minimized numerically to determine the parameters defining the deflected shape of the inflatable arch structure.

The thesis is also devoted to the theoretical formulation of the three-dimensional geometry of a cylindrical pneumatic hinge. First, the geometry of the hinge is described in parametric form. Next, by applying an external bending moment, the hinge membrane undergoes prescribed cross-sectional deformation. The solution is obtained by minimizing the total potential energy of the system with respect to the parameter describing the shape of the hinge.

Finally, the theoretical predictions given in non-dimensional form are compared to the experimental results obtained from tests on small scale models.

ACKNOWLEDGEMENTS

The author wishes to express his sincere gratitude and appreciation to his supervisor, Dr. S. Lukasiewicz, for his conscientious guidance, support and encouragement throughout the course of this work.

Thanks are due to the staff and fellow students of the Department of Mechanical Engineering for their advice and cooperation. Thanks are extended to Mrs. Karen Undseth and Miss Moira Clarke for the help in typing the manuscript. The financial assistance provided by the Department of Mechanical Engineering of the University of Calgary is gratefully acknowledged.

TABLE OF CONTENTS

LIST OF TABLES

LIST OF FIGURES

LIST OF PLATES

NOMENCLATURE

LETTERS

A	Cross-section area
A_β	Cross-section area at angle β
a	Height of stretched segment
a_β	Geometrical parameter; long axis of an elipse
$a_{i=1,5}$	
$a'_{i=1,2}$	Chord length of an arch segment
b_β	Geometrical parameter; short axis of an elipse
c_β	Geometrical parameter; short axis of an elipse
DY	Vertical displacement
E	Young's modulus; numerical constant
EPS	Length of an interval; numerical constant^2
f	Function
g	Function
h	Height of hinge cross-section
K	Stiffness coefficient
k	Numerical constant
ℓ	Mean length of membrane
$L_{1\beta}$, $L_{2\beta}$	Circumference of an upper and lower elipse
m	Number of integration intervals, unit length (metre)
$M_{i=1,3}$	External bending moment
M_P,$M_{Pi=1,3}$	Pressure moment
M_W	Wrinkling moment
N	Axial force, unit force (newton)

N_a	Resultant axial force
p, p_o	Inflation pressure
Q	Applied load
Q_{min}	Numerical value of calculated Q
R	Radius of cylindrical membrane
R_o	Radius of the arch
R_α^E	Experimental radius of the hinge
$R_{\alpha i=1,3}$	Theoretical radius of the hinge
R_β	Radius of centroid
SP	Flexibility parameter; numerical constant
t	Membrane thickness
V	Total potential function
V*	Total potential function under constraint
W	Potential energy of pneumatic hinge
W_p	Work done by internal pressure
W_Q	Work done by applied load
$X_D, X_{i=0,1,2}$	Horizontal displacement
XL	Left end of search interval
XR	Right end of search interval
XL1	Left-hand interior search point
XR1	Right-hand interior search point
X_{min}	Numerical variable
$y_D, y_{i=0,1,2}$	Vertical displacement
$Y_D, Y_{i=0,1,2}$	
Y_β	Centroid of eliptic cross-section
z	Geometrical parameter

GREEK LETTERS

$\alpha_1, \alpha_{i=1,3}$	Hinge angle
α_E	Angle of elastic deformation
$\alpha^E_{i=1,3}$	Experimental deformation angle
β	Angle of a cross-section
δ	Variational operator
ΔV	Total change in volume
ΔV_D	Change in volume of downward hinge
ΔV_U	Change in volume of upward hinge
ΔX	Horizontal displacement
ΔY	Vertical displacement
ϕ	Meridianal angle of spread of wrinkling
$\phi_{i=1,3}$	Angle of static forces
ψ	Meridianal angle of membrane segment
ρ	Radius of curvature
π	Numerical constant
$\gamma_{i=1,3}$	Meridianal angle of arch segment
$\kappa_{i-1,5}$	Chord angle of arch segment
σ_M	Stress due to bending moment
σ_p	Stress due to inflation pressure
Θ_o	Central half angle
λ	Lagrange multiplier

CHAPTER 1

INTRODUCTION

1.1 INTRODUCTION

The use of air-supported structures has become increasingly common for providing low-cost temporary enclosures for exhibitions and construction sites as well as for the permanent covering of warehouses, greenhouses and athletic facilities [4]*. Although cost-effective these structures have the disadvantage that during sunlit periods their internal temperature is very high due to the greenhouse effect and during the absence of sunlight they require too much heat for comfort temperatures. Another disadvantage is that the internal pressure is higher than the atmospheric pressure and so requires constant ventilation. These types of structures also require anchorage in order to conduct the vertical and horizontal forces carried by the membrane to the ground.

Another type of inflatable structure is an air-inflated structure which is a pneumatically stabilised membrane structure consisting of membrane-like elements. A typical example would be an inflatable beam or inflatable arch structure [1]. These structures are used when requirements such as easy erection and dismantling, low weight, and low transport volume are the decisive factors in the choice a of structural system. However, a complete method for the design of air-inflated structures is not yet available. At present, the design practice is to employ the theory of elastic membranes to determine the

---

*Numbers in square brackets are listed under References.

wrinkling or buckling loads of the structure [21-22]. One of the peculiar aspects of inflatable structures which has been given only limited attention is the possibility of collapse by the accumulation of rain, ice or snow on their surfaces. Investigations of ponding collapse were carried out for spherical air-supported membranes [14-18] and a theory for ponding instability of elastic spherical and cylindrical membranes has been developed.

In the present study, the problem of large-deflection and stability behaviour of double-surface air-inflated toroidal arch structures subjected to concentrated line loads applied at the apex is analysed. Deflections are allowed to become large compared to the initial radius of the arch membrane. Local and global deformation patterns of the arch structure are established. The governing equations of the force equilibrium are solved and the problem of finding the critical load is reduced to the minimization of a trigonometric expression subjected to a displacement equation constraint.

The extremization problem is solved numerically and the non-dimensional load-displacement relationship for a range of various stiffnesses of the membrane is obtained and presented in graphical form. The numerical results are compared to the experimental data obtained from the tests on the small scale model.

The study also investigates post wrinkling local deformation of a cylindrical membrane, which is described as a 'pneumatic hinge', with the help of a deformation model describing the extend and the shape of the deformed section of the membrane. The theoretical predictions of the geometry of the pneumatic hinge are compared to the experimentally obtained local deformation pattern of the test model.

1.2 LITERATURE REVIEW

1.2.1 Review of Air-Supported Structures

The development of pneumatic structures started out shortly after the Second World War. One of the first air structures was a radome, conceived and developed to meet the needs of the Royal Air Force for a thin, non-metallic protective covering for the large ground radar installations. As a result a study program was carried out which included analytical design studies, model construction and testing.

Since then many research projects have been undertaken over the years. Based on membrane theory of small deformations, solutions for the most common engineering problems in air-supported structures have been found. The best overview of these is presented by Frei Otto in [21] and [22].

Although air-supported structures are designed not to deform to the point where membrane wrinkling is caused under normal working conditions, they are sometimes subjected to excessive loading due to snow or water accumulation. The aspect of collapse by ponding of air-supported structures has gained considerable interest from researchers. D.J. Malcolm investigated the possibility of collapse through an accumulation of rain. His studies were limited to symmetric problems including the collapse of cylindrical [7] and spherical [8] membranes subjected to an axisymmetric load in the presence of a ponding medium.

S. Lukasiewicz and P.G. Glockner [12] extended the analysis to the non-symmetrically loaded cylindrical membrane and admit the extensibility of the inflatable structure. The dead weight of the structure was also included in the analysis. They concluded that applying the concentrated line load non-symmetrically increases the

value of the critical load. They also found that the effect of the elasticity of the membrane material is to decrease the value of the critical load.

W. Szyszkowski and P.G. Glockner [14,15,16] analysed spherical membranes undergoing very large axi-symmetric deformations and wrinkling under the action of concentrated loads applied at the apex using equations of equilibrium and the Gauss-Codazzi relations. The deflections of the membrane were allowed to grow larger than the initial height of the structure, and even larger than the initial radius of curvature R_o. The analysis establishes certain height to span ratios above which there exist critical loads beyond which the structure will 'snap-through' and collapse. If, in addition to a concentrated load, an accumulating medium is also present filling the depression completely the instability may occur even for central angles β_o less than than 90°, Fig. 1.

A complete analysis of the nonlinear load-deflection and stability behaviour of cylindrical membranes without end 'shear walls' subjected to longitudinal symmetric line loads is presented in [18] by W. Szyszkowski and P.G. Glockner. The analysis includes low and high profile structures as well as lateral stability behaviour. The analyses were carried out for two different support characteristics, Fig. 2:

- a support which is raised above the exterior ground surface adjacent to the structure and above the interior floor surface so as to allow arbitrary deflections and rotations of the membrane at the support as well as to permit vertical deflections under the line load which are equal to or larger than the initial rise of the structure, Fig. 2a,
- a support where a horizontal ground surface exists next to and

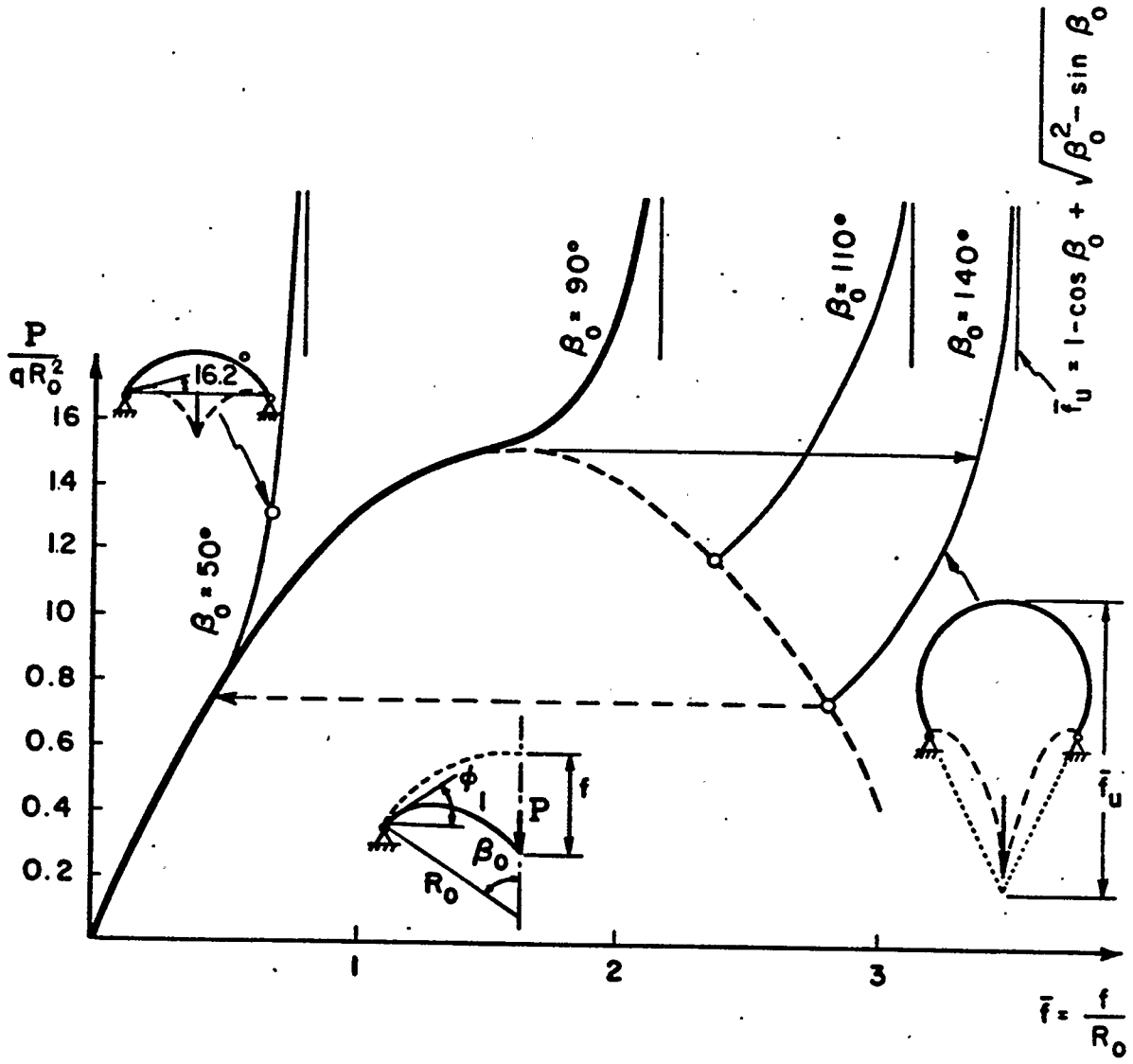

Fig. 1. Load-Deflection Plots for Various Values of the Central Half Angle, β_o.

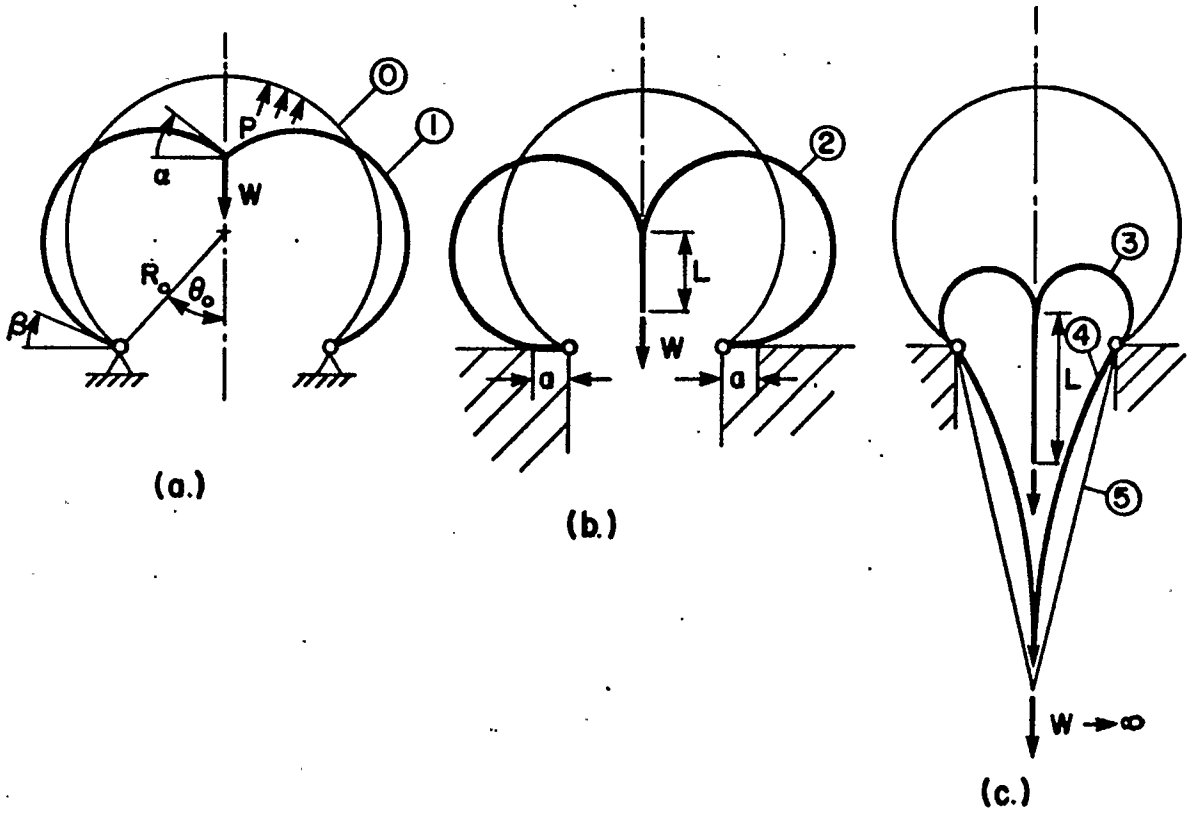

FIG. 2 MODES OF SYMMETRICAL DEFORMATION OF CYLINDRICAL INFLATABLE

at the elevation of the support thereby restricting the rotation and deflection of the membrane at the support to $\beta \geq 0°$, Fig. 2b,c.

The analysis indicates that the behaviour of such structures falls into one of three modes of deformation, Fig. 3:

- the 'first mode', during which there may exist large deflections and rotations in the structure but the membrane is not in contact with the ground nor are portions of the membrane in contact with one another,
- the 'second mode', during which portions of the membrane to either side of the line load are in contact, forming the so-called vertical contact zone of length $\bar{L}$,
- the 'third mode', during which the membrane is in contact with the horizontal ground surface adjacent to the support, forming the so-called horizontal contact zone of length a.

Similar analyses were presented by S. Lukasiewicz, L. Balas and P.G. Glockner [24] for the non-symmetrically loaded cylindrical membrane. This analysis clearly indicates vertical as well as lateral instability at certain load levels and shows that the governing mode of failure is very much influenced by the initial geometry. The results also indicate that the onset of lateral instability is not identical to the configuration when contact between the membrane and the horizontal surface is first established, nor does the onset of vertical instability signify the existence or beginning of vertical contact. Extensive experimental data obtained from tests on a small-scale cylindrical inflatable model are presented and compared with analytical predictions, Fig. 4. Excellent agreement between the numerical and

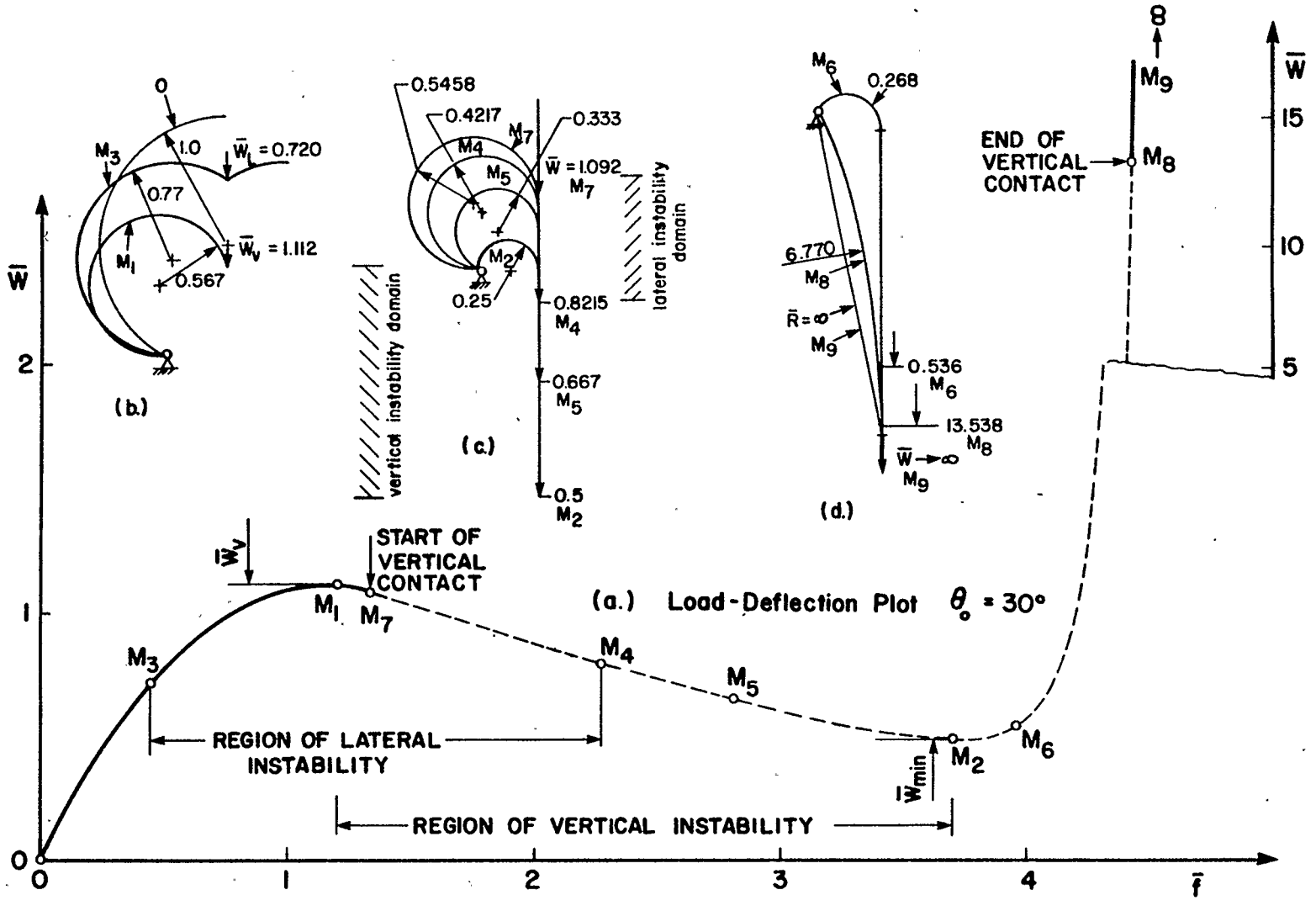

FIG. 3 COMPLETE LOAD-DEFLECTION PLOT FOR CYLINDRICAL MEMBRANE WITH CENTRAL ANGLE, θ_o = 30°

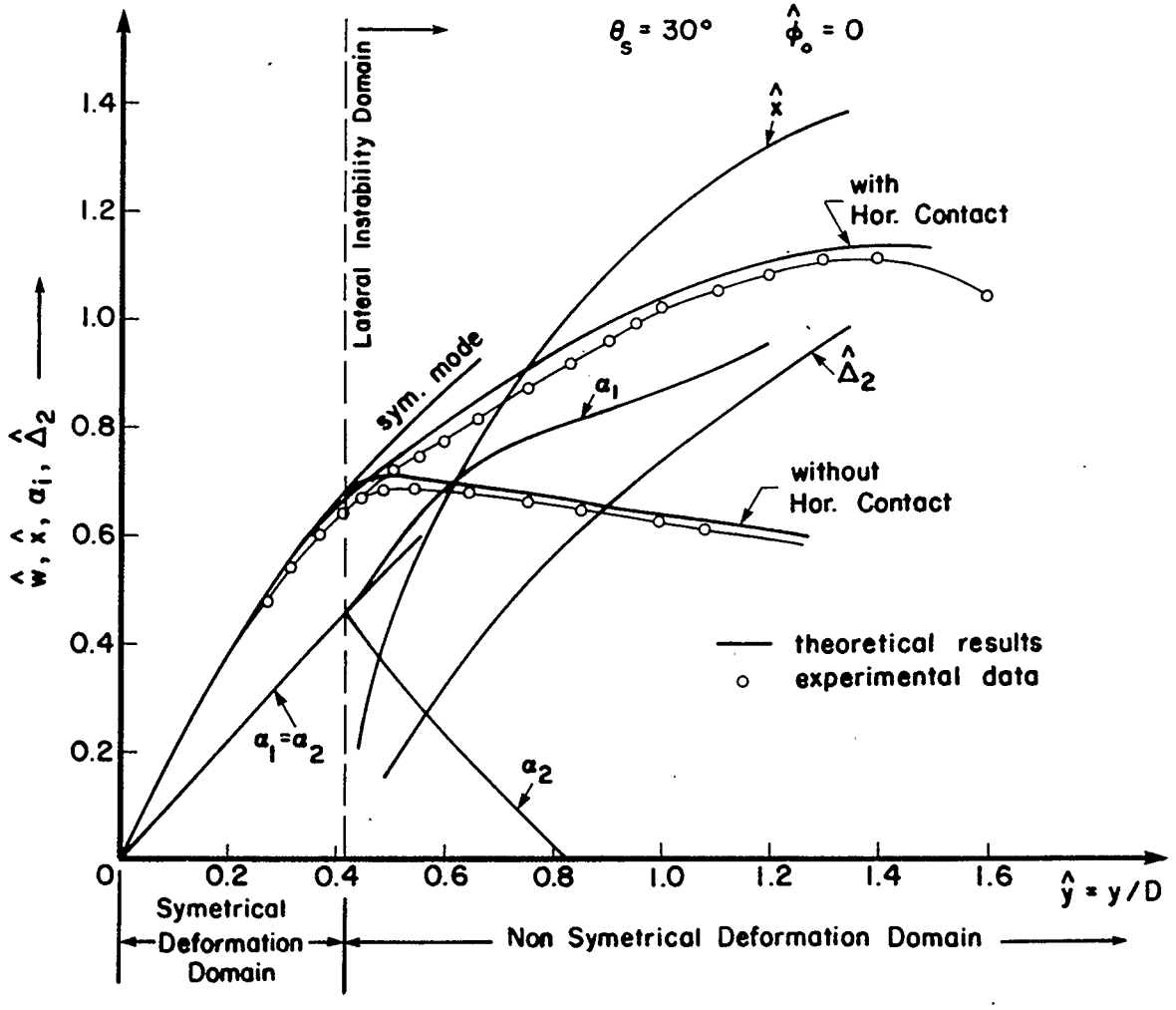

Fig. 4: Variation of Key Parameters with Vertical Deflection

experimental results confirm the validity of the theory and the assumptions used in its derivations.

1.2.2 Review of Inflatable Structures

The theoretical solution of problems of the stability and large deformations of air inflated structures is difficult. Despite substantial theoretical achievements in the area of air supported structures the progress in developing a theory which will describe the behaviour of inflated beams or arches is slow and still limited to calculating the deformations and wrinkling loads on the basis of classical methods of analysis.

A numerical analysis of the nonlinear behaviour of pneumatic structures was first presented by J.T. Oden and W.K. Kubitza [10]. They used finite element representation of flexible pneumatic structures to describe the general kinematic properties of thin membranes. Using the first law of thermodynamics, a general relationship between the kinematic and kinetic variable associated with the behaviour of finite elements of arbitrary pneumatic structures was obtained. This led to the general equation of the motion of the finite elements of thin membranes, and included such properties as anisotropy, nonlinear viscoelasticity, thermoviscoelasticity, unhomogeneity, and plasticity, with no restrictions on the magnitudes of the deformations. Finally, the general formulation was modified and applied to a number of special cases, i.e. the stretching of square and circular rubber membranes.

P.S. Bulson [11] analysed inflated beam structures. One of these was a pure inflated fabric envelope with three longitudinal unproofed diaphragms to maintain a reasonably rectangular cross-section, Fig. 5. The other incorporated top and bottom flanges made from sheets

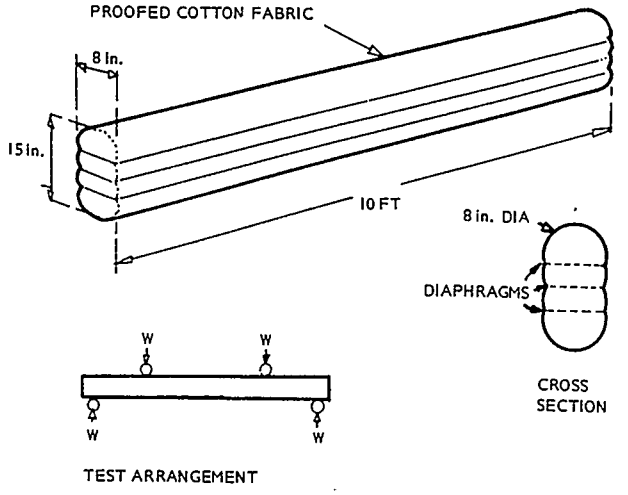

Fig. 5. Inflated beam 1; unreinforced

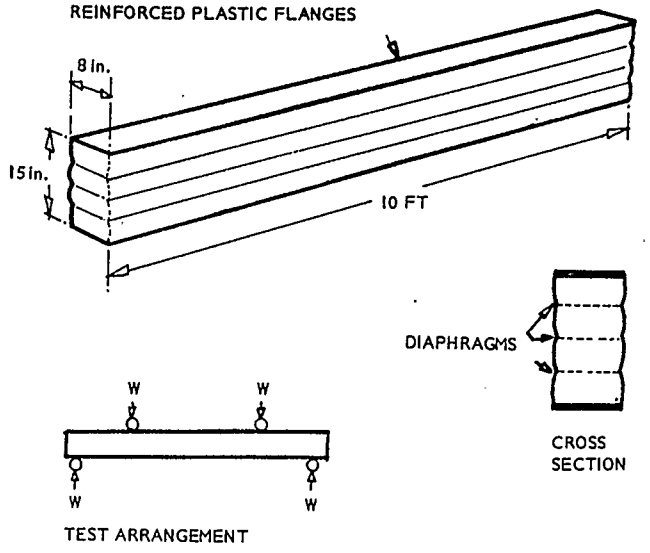

Fig. 6. Inflated beam 2; reinforced

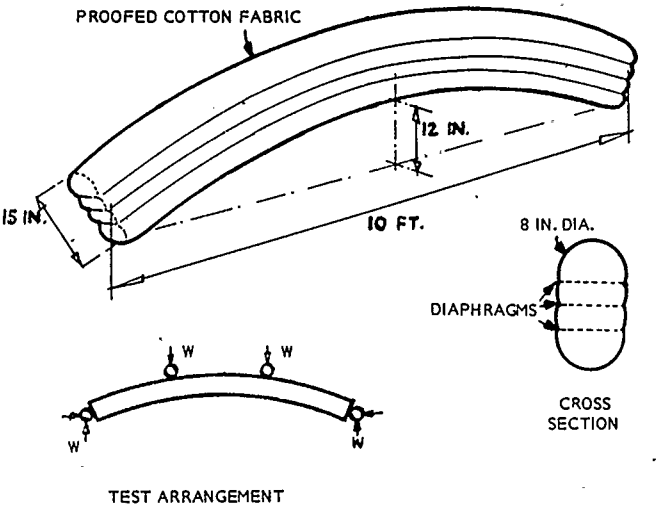

Fig. 7. Inflated arch rib

of glass-reinforced plastic, Fig. 6. Tests were also made on a simple inflated arch rib similar in construction and size to the first beam, Fig. 7. This research established that for an unreinforced beam the load/deflection relationship was non-linear because of the local deformation over the point supports and creep in the fabric. The stiffness was found to diminish rapidly but smoothly until collapse took place. The fabric on the sides of the beam wrinkled under the high shear loads in the neighbourhood of the load joints and this was followed by collapse. It was found that the critical shear stress is proportional to inflation pressure and is given by

$$\tau_{cr} = \frac{p_o R}{2} \qquad (1.2.2.1)$$

where p_o - is inflation pressure,

R - is radius of curvature of the cylindrical cross section.

Comparing the ultimate loads for the beam and the arch under 2-point loading, it has been found that the ultimate loads for the arch are 50% greater than those for the beam.

1.3 OBJECTIVE AND OUTLINE

The aim of this thesis is to examine the large deformation and stability behaviour of toroidal air-inflated arch structures under a concentrated load applied at the apex. Specifically, the objectives for the present investigation are:

1) to formulate a theoretical model based on the total potential energy approach of the deformed structure and to obtain a system equation leading to the solution of the problem by direct application of the Method of Lagrange Multipliers,

2) to formulate a theoretical model based on the static

equilibrium of the forces acting on the structure and by minimization of the load function with the constraint set on horizontal movement of the load to obtain the load-deflection relationship,

3) to verify the performance of the model against the experimental data obtained from tests on a small scale model,

4) to present comments on the accuracy of the results obtained and recommendations for future work.

Based on the objectives presented above, the approach in this thesis, devoted to the theory of the large deformations of inflatable structures, is as follows. The concept of the toroidal arch membrane and the basic geometrical relations of the shape of the structure are reviewed in Chapter 2. Chapter 3 is devoted to the concept of the minimization of the total potential function using the method of Lagrange multipliers as a tool to obtain a system equation for the structure and it introduces a new geometrical model for an inflatable hinge. Chapter 4 attacks the same problem from the static point of view. Numerical procedures are described in Chapter 5. Tests on a small scale model are described in Chapter 6. Comments on the results obtained are summarised in Chapter 7. Finally, some recommendations for further work and the overall conclusions are presented in Chapter 8.

CHAPTER 2

GEOMETRY OF THE THEORETICAL MODEL

The model under consideration was a circular hose or torus which can be imagined as the tangential surface formed by an infinite number of spheres strung in a circle. The surface of a torus is doubly curved in the same sense (dome-like) on the outside and in the opposite sense (saddle-like) on the inside. The arch structure under consideration, made out of a torus is shown in Fig. 8.

The undeformed geometry of the toroidal arch is described by the central half angle θ_o, the radius of central line R_o and the radius of the cylindrical shell R. The support ends of the arch are assumed to be fixed. The external load Q is applied in the plane of symmetry of the structure. The membrane is under internal pressure p.

Consider the shape of the deformed arch as shown in Fig. 9. It is assumed that the membrane is, in general, inextensible. If the load increases above the first wrinkling load the continuous arch begins to break into segments described by angles γ_1, γ_2 connected by pneumatic hinges made of partially wrinkled and partially tensioned membranes described by angles α_1, α_2, α_3. It is further assumed that the membrane segments described by angles γ_1 and γ_2 are rigid and the elastic deformations are local and take place only over that part of the surface of the hinge which is under severe tension.

Let us first discuss the model of the pneumatic hinge shown in Fig. 10. If we assume that the membrane wrinkles only in the plane DO, the isometry of the membrane requires the discontinuity of its surface at this plane (see point D). Such discontinuity is impossible because

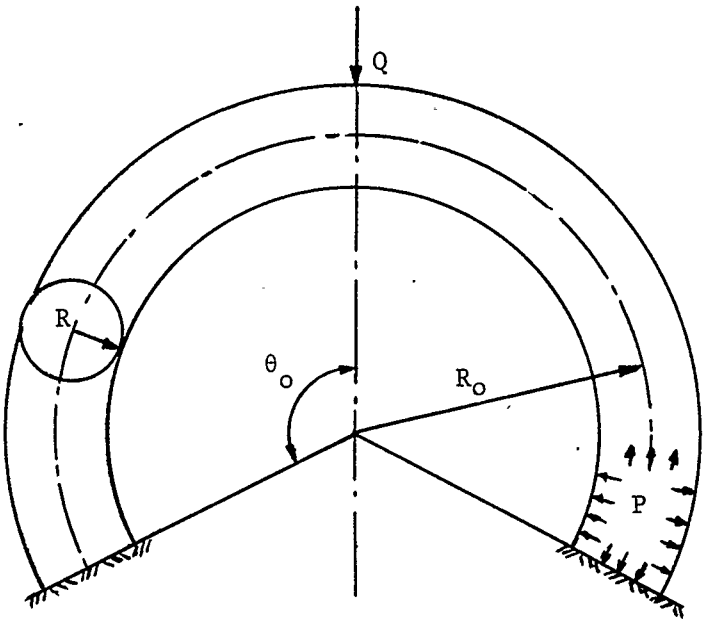

Fig. 8 Toroidal Arch Structure

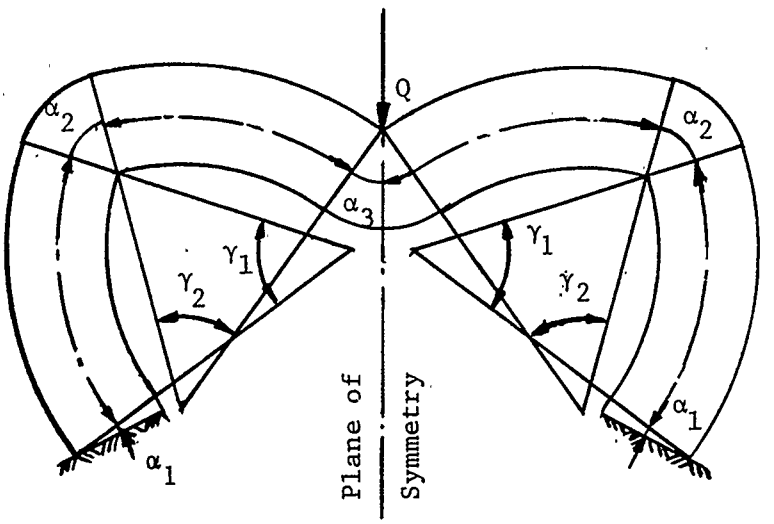

Fig. 9 Deformed Arch Structure

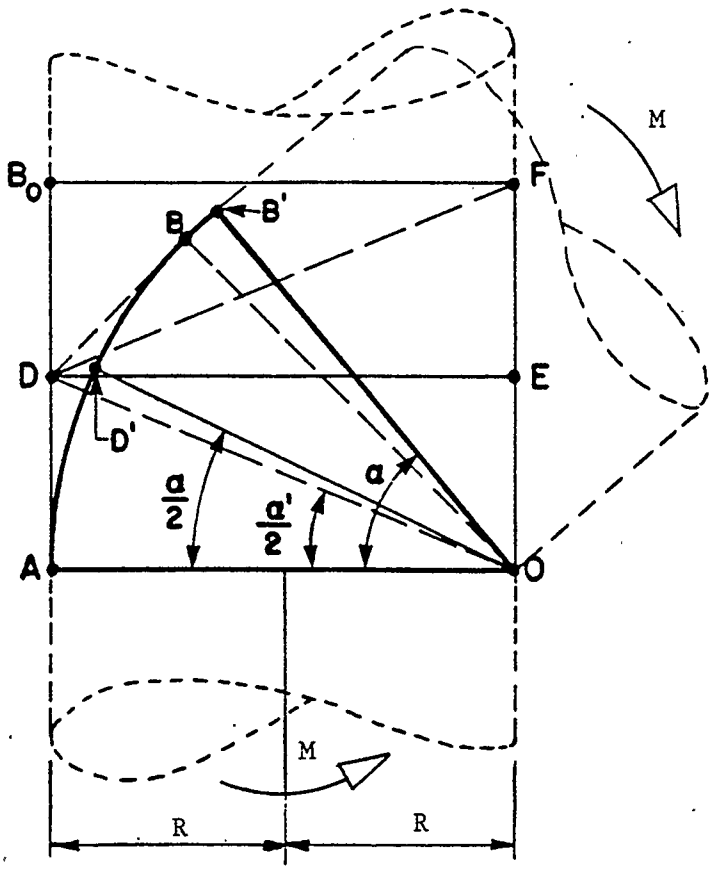

Fig. 10 The Area of Severe Wrinkling

the equations of equilibrium require the continuity of the membrane forces. This in turn means that the membrane must also be wrinkled slightly in the area OADBO. Such wrinkling occurs on the compressive side only and manifests itself along the lines which are perpendicular to the arc AD'B'. The wrinkling changes the configurations of the membrane and therefore the area OADBO may be considered to be a segment of a toroidal surface [25]. Note that the angle α defining the inclination of the upper part of the membrane is not equal to α' with the latter being slightly smaller and its value obtained from the condition of isometry AD = AD'.

The work done by the external moment, M, is obtained as

$$W_M = M\alpha \tag{2.1}$$

The work done during deformation by the internal pressure, p, is obtained from

$$W_p = p\Delta V \tag{2.2}$$

where

$$\Delta V = \pi R^3 \alpha \tag{2.3}$$

is the change in volume due to the collapse of the wall of the membrane. Therefore,

$$W_M = W_p, \tag{2.4}$$

$$M\alpha = p\pi R^3 \alpha , \tag{2.5}$$

or

$$M = p\pi R^3 \tag{2.6}$$

is the maximum bending moment the inflatable hinge can support.

The first wrinkling occurs when the stress in the axial direction of the membrane caused by the internal pressure σ_p is equal to

the stress from the bending moment σ_M.

$$\sigma_M = \frac{M_W . R}{\pi R^3 t} \tag{2.7}$$

$$\sigma_p = \frac{pR}{2t} \tag{2.8}$$

The condition for the first wrinkling is given by

$$\sigma_M = \sigma_p \tag{2.9}$$

$$\frac{M_W . R}{\pi R^3 t} = \frac{pR}{2t}$$

$$M_W = \tfrac{1}{2}\, p\pi R^3 \ . \tag{2.10}$$

This result shows that the pneumatic hinge can support twice the first wrinkling moment M_W

$$M = 2M_W \ . \tag{2.11}$$

Let us return now to the overall geometry of the structure. Because of the symmetry only half of the arch membrane is considered. Fig. 11 shows all the geometrical parameters used later in derivation. Not all parameters are assumed to be positive. The exact derivation of angles κ_i, $i = 1,4$ and other parameters is given in Appendix A.

The total vertical displacement ΔY of the point of application of the load when the reference level is a horizontal line passing through point B on Fig. 11 is obtained as

$$\overline{\Delta Y} = \overline{Y_0} - \overline{Y_D} \tag{2.12}$$

where

$$\overline{Y_0} = (\overline{R_o} - 1)(1 + \cos(\pi - \theta_o)) \tag{2.13}$$

is an initial vertical position of the load when the membrane at points A', B', C' is just beginning to wrinkle.

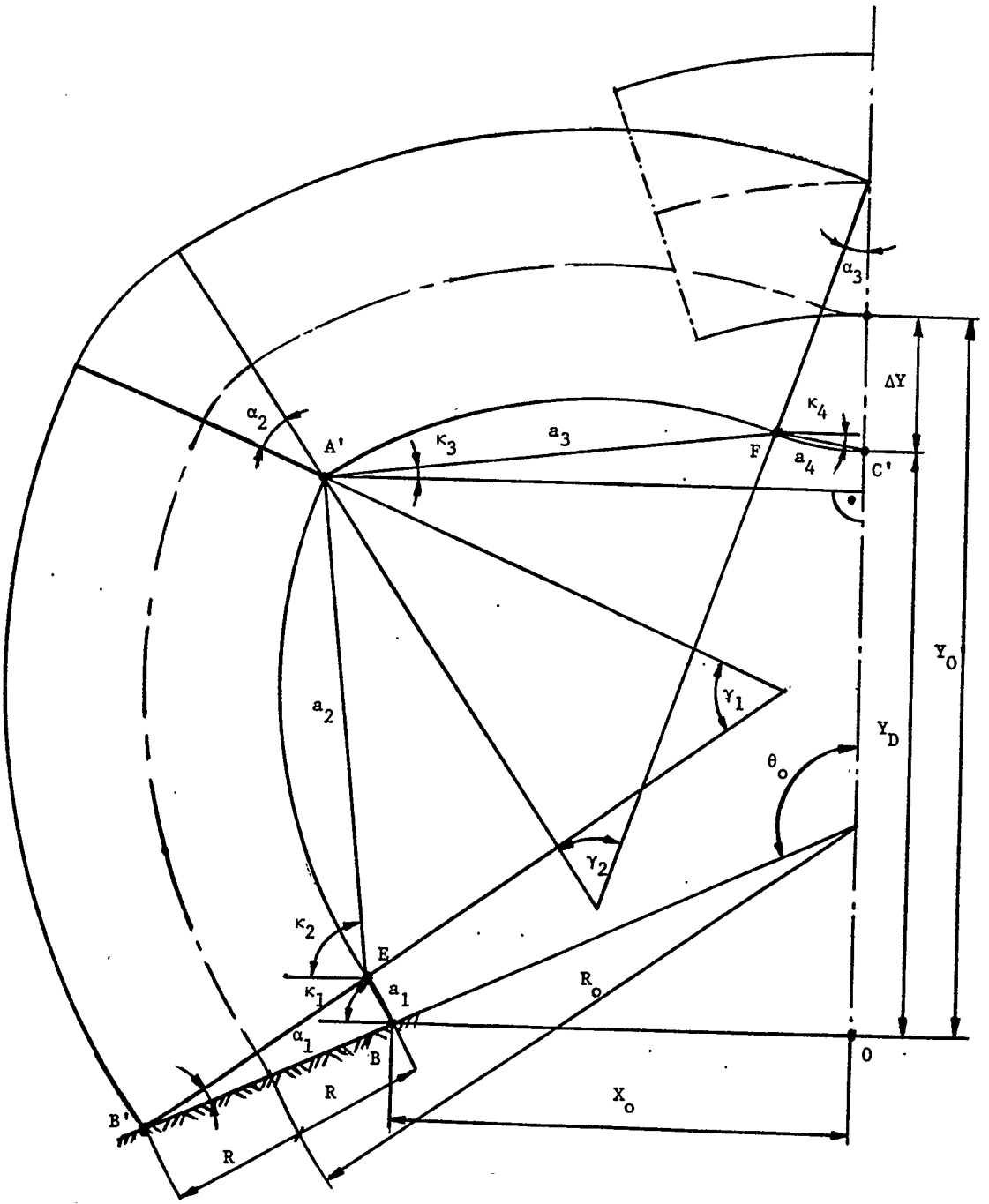

Fig. 11 Geometry of Deformed Toroidal Arch

$$\overline{Y_D} = \overline{a_1} \sin \kappa_1 + \overline{a_2} \sin \kappa_2 + \overline{a_3} \sin \kappa_3 - \overline{a_4} \sin \kappa_4 \qquad (2.14)$$

is the vertical displacement of the load when the pneumatic hinges are fully developed.

$$\overline{a_1} = 4 \sin \left(\frac{\alpha_1}{2}\right) \qquad (2.15)$$

$$\overline{a_2} = 2 \left(\overline{R_o}-1\right) \sin \left(\frac{\gamma_1}{2}\right) \qquad (2.16)$$

$$\overline{a_3} = 2 \left(\overline{R_o}-1\right) \sin \left(\frac{\gamma_2}{2}\right) \qquad (2.17)$$

and

$$\overline{a_4} = 4 \sin \left(\frac{\alpha_3}{2}\right) \qquad (2.18)$$

are distances between points BE, EA', A'F, FC' respectively, as shown on Fig. 11.

$$\alpha_1 = \frac{\left(\overline{R_o}-1\right)^2}{4\overline{R_o}} \left(\theta_o-\gamma_1-\gamma_2\right) - \alpha_3 \qquad (2.19)$$

$$\alpha_2 = \frac{\left(\overline{R_o}-1\right)^2}{4\overline{R_o}} \left(\theta_o-\gamma_1-\gamma_2\right) \qquad (2.20)$$

are hinge angles at the support and in the middle of the arch respectively. Angle α_3 is an angle of the apex hinge. Angles κ_i, $i = 1,4$ are obtained as

$$\kappa_1 = \pi - \left[1 + \frac{\left(\overline{R_o}-1\right)^2}{8\overline{R_o}}\right] \theta_o + \frac{\alpha_3}{2} + \frac{\left(\overline{R_o}-1\right)^2}{8\overline{R_o}} \left(\gamma_1+\gamma_2\right) \qquad (2.21)$$

$$\kappa_2 = \pi - \left[1 + \frac{\left(\overline{R_o}-1\right)^2}{4\overline{R_o}}\right] \theta_o + \alpha_3 + \left[\tfrac{1}{2} + \frac{\left(\overline{R_o}-1\right)^2}{4\overline{R_o}}\right] \gamma_1 + \frac{\left(\overline{R_o}-1\right)^2}{4\overline{R_o}} \gamma_2$$

$$\kappa_3 = \frac{\gamma_2}{2} - \alpha_3 \tag{2.23}$$

$$\kappa_4 = \frac{\alpha_3}{2} . \tag{2.24}$$

A dash over the symbol of the parameter means that it is given in a non-dimensional form.

$$\overline{Y_o} = \frac{Y_o}{R} ; \quad \overline{Y_D} = \frac{Y_D}{R} ; \quad \overline{R_o} = \frac{R_o}{R}$$

$$\overline{a_1} = \frac{a_1}{R} ; \quad \overline{a_2} = \frac{a_2}{R} ; \quad \overline{a_3} = \frac{a_3}{R} ; \quad \overline{a_4} = \frac{a_4}{R} .$$

The horizontal displacement of the point of application of the load is obtained as

$$\overline{\Delta X} = \overline{X_o} - \overline{X_D} \tag{2.25}$$

where

$$\overline{X_o} = (\overline{R_o}-1) \sin (\pi-\theta_o) \tag{2.26}$$

is the initial horizontal position of the point of application of the load with respect to point 0.

$$\overline{X_D} = \overline{a_3} \cos \kappa_3 + \overline{a_4} \cos \kappa_4 - \overline{a_1} \cos \kappa_1 - \overline{a_2} \cos \kappa_2 \tag{2.27}$$

is the horizontal position of the point of application of the load with respect to point C'.

The symmetry of the structure requires horizontal displacement ΔX to disappear over the entire range of the vertical displacement ΔY and is given by

$$\overline{\Delta X} = 0 . \tag{2.28}$$

Condition (2.28) is a constraint equation which has to be satisfied for

any set of parameters α_3, γ_1, γ_2.

Note again that

$$\overline{\Delta X} = \frac{\Delta X}{R} \; ; \qquad \overline{X_o} = \frac{X_o}{R} \; ; \qquad \overline{X_D} = \frac{\overline{X_D}}{R}$$

CHAPTER 3

THE ENERGY APPROACH

3.1 INTERNAL ENERGY OF THE STRUCTURE

The internal energy of the structure is the sum of the work done during the deformation of the membrane by the internal pressure, p, and is obtained from

$$W_p = p\Delta V \tag{3.1.1}$$

where

$$\Delta V = \sum_{i=1}^{3} \Delta V_i \tag{3.1.2}$$

is the total change in volume due to the formation of the inflatable hinges.

Consider a toroidal segment of an undeformed arch membrane of initial central radius R_o as shown in Fig. 12. The initial volume of section ABCD is obtained as

$$V_o = AR_o\,\psi \tag{3.1.3}$$

where A is the cross-section area of the arch segment.

Formation of the inflatable hinge can occur in two ways. The section can bend into an upward direction depicted by Fig. 13. Then for an inextensible membrane

$$(R_o - R)\psi = 2R\alpha$$

or

$$\psi = \frac{2R}{R_o - R}\,\alpha\ . \tag{3.1.4}$$

The change in volume of a toroidal hinge is calculated as

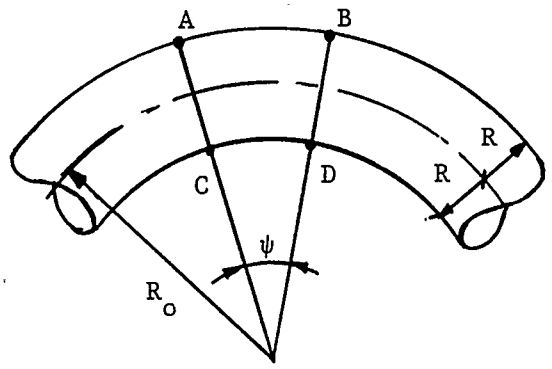

Fig. 12 Arch Segment Before Deformation

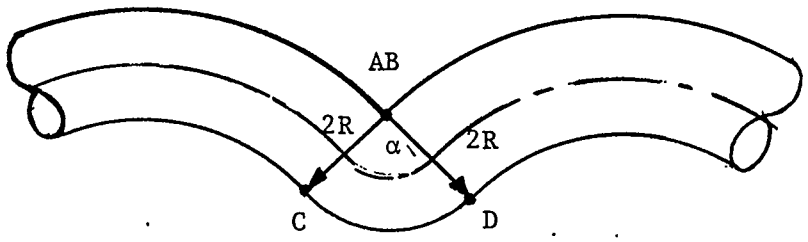

Fig. 13 Segment with Developed Upward Hinge

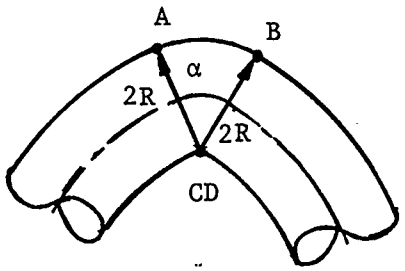

Fig. 14 Segment with Developed Downward Hinge

$$\Delta V_U = V_o - AR\alpha$$

or

$$\Delta V_U = RA \frac{(\overline{R_o}+1)}{(\overline{R_o}-1)} \alpha \ . \qquad (3.1.5)$$

If the section bends in a downward direction, Fig. 14, the ψ angle is given by

$$\psi = \frac{2R}{(R_o+R)} \alpha \ . \qquad (3.1.6)$$

The change in volume is then given by

$$\Delta V_D = RA \frac{(\overline{R_o}-1)}{(\overline{R_o}+1)} \alpha \ . \qquad (3.1.7)$$

It can be seen in Fig. 11 that the hinges described by angles α_1, α_3 are of an upward type whereas the hinge described by α_2 is of a downward type. Making use of equations (3.1.5) and (3.1.7) the total change in volume is obtained as

$$\Delta V = RA \frac{(\overline{R_o}+1)}{(\overline{R_o}-1)} \alpha_1 + RA \frac{(\overline{R_o}-1)}{(\overline{R_o}+1)} \alpha_2 + RA \frac{(\overline{R_o}+1)}{(\overline{R_o}-1)} \alpha_3$$

or, after simplifications,

$$\Delta V = RA \frac{(\overline{R_o}^2-1)}{2\overline{R_o}} (\theta_o-\gamma_1-\gamma_2) \ . \qquad (3.1.8)$$

The internal energy of the structure is then given by

$$W_p = pAR \frac{(\overline{R_o}^2-1)}{2\overline{R_o}} (\theta_o-\gamma_1-\gamma_2) \ . \qquad (3.1.9)$$

3.2 POTENTIAL ENERGY OF THE STRUCTURE

The potential energy of the structure consists of the potential energy of the applied load and the potential energy of the segments of the arch. For reasons of simplicity, the work of the segments of the arch in the gravitational field has not been included in the calculations.

The potential energy of the applied load is given by

$$W_Q = Q\ R\ \overline{DY}\ . \tag{3.2.1}$$

3.3 APPLICATION OF THE LAGRANGE PRINCIPLE

The mathematical formulation of the problem is as follows. Minimize the total potential function

$$V = W_p - W_Q \tag{3.2.2}$$

satisfying the constraint function given by formula (2.28). To solve this problem the method of Lagrange multipliers is used.

Let V^* be a total potential function under the constraint (2.28)

$$V^* = V + \lambda \times \Delta X \tag{3.2.3}$$

where λ is the unknown Lagrange multiplier

For $V^*\ (\alpha_3,\ \gamma_1,\ \gamma_2)$ to be a minimum the following set of equations has to be satisfied

$$\frac{\partial V^*}{\partial \alpha_3} = 0\ ; \qquad \frac{\partial V^*}{\partial \gamma_1} = 0\ ; \qquad \frac{\partial V^*}{\partial \gamma_2} = 0\ .$$

The fourth equation is $\Delta X = 0$. The system equation is then given by

$$\frac{\partial V}{\partial \gamma_1} + \lambda \frac{\partial \Delta X}{\partial \gamma_1} = 0 \qquad (3.2.4)$$

$$\frac{\partial V}{\partial \gamma_2} + \lambda \frac{\partial \Delta X}{\partial \gamma_2} = 0 \qquad (3.2.5)$$

$$\frac{\partial V}{\partial \alpha_3} + \lambda \frac{\partial \Delta X}{\partial \alpha_3} = 0 \qquad (3.2.6)$$

and

$$\overline{\Delta X} = 0 \; . \qquad (3.2.7)$$

Equations (3.2.4 - 7) in a normalised more open form can be written as

$$\frac{1}{2AR} \frac{\partial \Delta V}{\partial \gamma_1} + \overline{Q} \frac{\partial \overline{Y_D}}{\partial \gamma_1} - \frac{\lambda}{2pA} \frac{\partial \overline{X_D}}{\partial \gamma_1} = 0 \qquad (3.2.8)$$

$$\frac{1}{2AR} \frac{\partial \Delta V}{\partial \gamma_2} + \overline{Q} \frac{\partial \overline{Y_D}}{\partial \gamma_2} - \frac{\lambda}{2pA} \frac{\partial \overline{X_D}}{\partial \gamma_1} = 0 \qquad (3.2.9)$$

$$\overline{Q} \frac{\partial \overline{Y_D}}{\partial \alpha_3} - \frac{\lambda}{2pA} \frac{\partial \overline{X_D}}{\partial \alpha_3} = 0 \qquad (3.2.10)$$

and

$$\overline{X_o} - \overline{X_D} = 0 \; . \qquad (3.2.11)$$

Eliminating $\lambda/2pA$ from equations (3.2.8) and (3.2.9) with the help of equation (3.2.10) a new set of three nonlinear equations is obtained

$$\frac{\partial \overline{X_D}}{\partial \alpha_3} \left(\frac{\partial \overline{Y_D}}{\partial \gamma_1} - \frac{\partial \overline{Y_D}}{\partial \gamma_2} \right) - \frac{\partial \overline{Y_D}}{\partial \alpha_3} \left(\frac{\partial \overline{X_D}}{\partial \gamma_1} - \frac{\partial \overline{X_D}}{\partial \gamma_2} \right) = 0 \qquad (3.2.12)$$

$$\frac{1}{RA} \frac{\partial \Delta V}{\partial \gamma_1} \frac{\partial X_D}{\partial \alpha_3} + \overline{Q} \left[\frac{\partial \overline{X_D}}{\partial \alpha_3} \left(\frac{\partial \overline{Y_D}}{\partial \gamma_1} + \frac{\partial \overline{Y_D}}{\partial \gamma_2} \right) - \frac{\partial \overline{Y_D}}{\partial \alpha_3} \left(\frac{\partial \overline{X_D}}{\partial \gamma_1} + \frac{\partial \overline{X_D}}{\partial \gamma_2} \right) \right] = 0 \qquad (3.2.13)$$

$$\overline{X_o} - \overline{X_D} = 0 \qquad (3.2.14)$$

The derivatives summary highlighted in (3.2.12 - 14) is presented below.

$$\frac{\partial \overline{X_D}}{\partial \alpha_3} = 2[\cos\left(\frac{\alpha_1}{2} - \kappa_1\right) - (R_o - 1)\left[\sin\left(\frac{\gamma_1}{2}\right)\sin(\kappa_2) + \sin\left(\frac{\gamma_2}{2}\right)\sin(\kappa_3)\right] + \cos(\alpha_3)] \tag{3.2.15}$$

$$\frac{\partial \overline{Y_D}}{\partial \alpha_3} = 2\left[\sin\left(\frac{\alpha_1}{2} - \kappa_1\right) + (\overline{R_o}+1)\left[\sin\left(\frac{\gamma_1}{2}\right)\cos(\kappa_2) - \sin\left(\frac{\gamma_2}{2}\right)\cos(\kappa_3)\right] - \sin(\alpha_3)\right] \tag{3.2.16}$$

$$\frac{\partial \overline{X_D}}{\partial \gamma_1} - \frac{\partial \overline{X_D}}{\partial \gamma_2} = -(\overline{R_o}-1)\left[\cos\left(\frac{\gamma_1}{2} + \kappa_2\right) + \cos\left(\frac{\gamma_2}{2} + \kappa_3\right)\right] \tag{3.2.17}$$

$$\frac{\partial \overline{Y_D}}{\partial \gamma_1} - \frac{\partial \overline{Y_D}}{\partial \gamma_2} = (\overline{R_o}-1)\left[\sin\left(\frac{\gamma_1}{2} + \kappa_2\right) - \sin\left(\frac{\gamma_2}{2} + \kappa_3\right)\right] \tag{3.2.18}$$

$$\frac{\partial \overline{X_D}}{\partial \gamma_1} + \frac{\partial X_D}{\partial \gamma_2} = (\overline{R_o}-1)\left[\frac{(\overline{R_o}-1)}{\overline{R_o}}\left[\cos\left(\frac{\alpha_1}{2} - \kappa_1\right) + (\overline{R_o}-1)\sin\left(\frac{\gamma_1}{2}\right)\sin(\kappa_2)\right] - \cos\left(\frac{\gamma_1}{2} + \kappa_2\right) + \cos\left(\frac{\gamma_2}{2} + \kappa_3\right)\right] \tag{3.2.19}$$

$$\frac{\partial \overline{Y_D}}{\partial \gamma_1} + \frac{\partial \overline{Y_D}}{\partial \gamma_2} = (\overline{R_o}-1)\left[\frac{(\overline{R_o}-1)}{\overline{R_o}}\left[\sin\left(\frac{\alpha_1}{2} - \kappa_1\right) + (\overline{R_o}-1)\sin\left(\frac{\gamma_1}{2}\right)\cdot\cos(\kappa_2)\right] + \sin\left(\frac{\gamma_1}{2} + \kappa_2\right) + \sin\left(\frac{\gamma_2}{2} + \kappa_3\right)\right] \tag{3.2.20}$$

$$\frac{1}{RA} \times \frac{\partial \Delta V}{\partial \gamma_1} = -\frac{\overline{R_o}^2 - 1}{2\overline{R_o}} \tag{3.2.21}$$

The nonlinear system of equations given by (3.2.12 - 14) can be solved numerically for the prescribed load parameter $\bar{Q}$. This, however, requires advance knowledge of the value of the parameter $\bar{Q}$ with a reasonable set of approximate parameters α_3, γ_1, γ_2. This proved to be an extremely difficult task and, as a result, the numerical routine was unable to converge to the required solution.

3.4 DEFORMATION MODEL OF AN INFLATABLE HINGE

This section of Chapter 3 introduces a new geometrical model describing three dimensional deformations of an inflatable hinge. The previous model, although simple and convenient to use, only corresponds well with the actual deformation pattern for limited values of angle α. To overcome these difficulties a new geometrical model is considered. The constraint that the circular cross-section of the pneumatic hinge before and during the deformation process is unchanged, has been modified. The new model permits the cross-section of the membrane to deform in a prescribed way on condition that the total work done by the pressure moment to collapse the wall of the membrane is minimum.

Consider an inflatable hinge as shown in Fig. 15(a) and 15(b). The area of severe deformation of the membrane is described by angle 2α. It is assumed that outside the angle 2α the cylindrical membrane is undeformed. The arch AB is a segment of a circle of radius R_α. The line of the centroid of the deformed cross-section is described by angle β and radius R_β. It is assumed that the shape of the cross-section of the membrane consists of two elipses, namely, the upper elipse with its short axis equal to b_β, and the lower elipse with its short axis equal to c_β. The long axes are the same and are equal to a_β. It is further

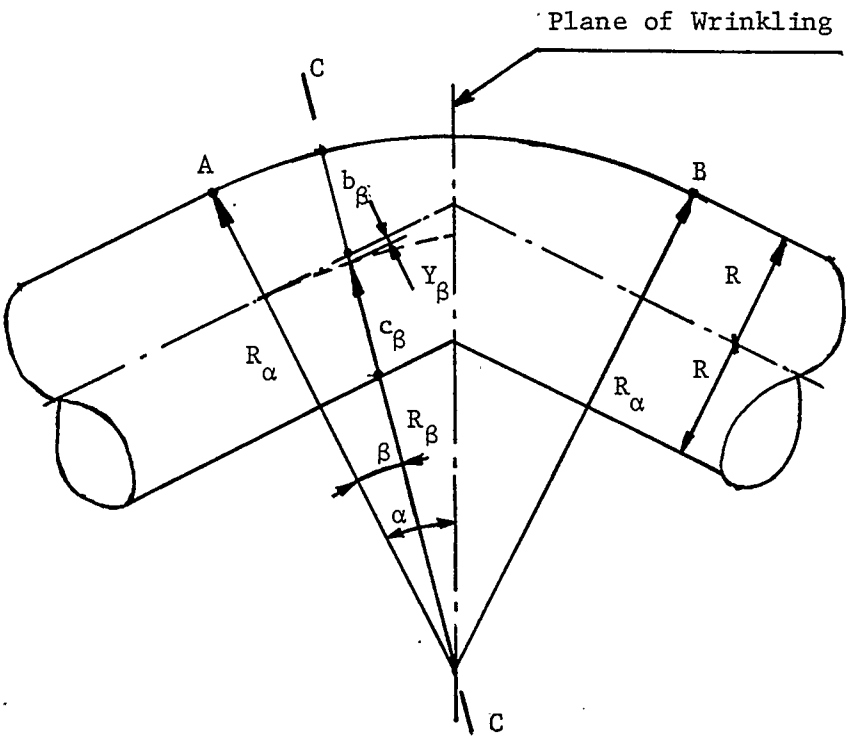

(a)

Section CC

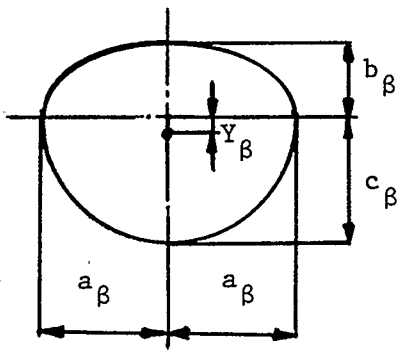

(b)

Fig. 15 Geometry of Inflatable Hinge

assumed that the change of the cross-section from the initial perfect circle at plane A-A to the eliptic one is continuous. In order to satisfy the isometry condition the length of the upper and lower elipse has to be equal to the initial circular length. The circumference of the upper elipse is obtained from an approximate formula [29].

$$L_{1\beta} \cong 2\sqrt{a_\beta^2 + k\, b_\beta^2} \ . \tag{3.4.1}$$

Similarly circumference for the lower elipse is given by

$$L_{2\beta} \cong 2\sqrt{a_\beta^2 + k\, c_\beta^2} \tag{3.4.2}$$

where

$$\kappa = \frac{\pi^2}{4} - 1 \ .$$

The short axis of the elipse in plane B-B is obtained as

$$c_\beta = \frac{R}{\cos\beta} \tag{3.4.3}$$

and

$$b_\beta = R_\alpha \left(1 - \frac{c_\beta}{R}\right) + c_\beta \ . \tag{3.4.4}$$

The centroid of the elipse is obtained as

$$Y_\beta = \frac{4}{3\pi} R_\alpha \left(\frac{c_\beta}{R} - 1\right) \ . \tag{3.4.5}$$

The long axis of the elipse is derived from the isometry condition

$$2\pi R = 2\sqrt{a_\beta^2 + k\, b_\beta^2} + 2\sqrt{a_\beta^2 + k\, c_\beta^2} \tag{3.4.6}$$

and is given by an implicit form of nonlinear equation

$$\sqrt{\left(\frac{a_\beta}{R}\right)^2 + k\left(\frac{b_\beta}{R}\right)^2} + \sqrt{\left(\frac{a_\beta}{R}\right)^2 + k\left(\frac{c_\beta}{R}\right)^2} - \pi = 0 \ . \tag{3.4.7}$$

The radius of the centroid of the elipse in plane C-C is obtained from

$$R_\beta = \frac{R_\alpha - R}{\cos \beta} - Y_\beta \qquad (3.4.8)$$

and is given by

$$R_\beta = \frac{c_\beta}{R} \left[R_\alpha \left(1 - \frac{4R}{3\pi c_\beta} \left(\frac{c_\beta}{R} - 1\right)\right) - R\right] . \qquad (3.4.9)$$

The cross-section area in plane B-B is obtained from

$$A_\beta = \frac{\pi}{2} a_\beta \left(b_\beta + c_\beta\right) \qquad (3.4.10)$$

and after simplification is written as

$$A_\beta = \frac{\pi}{2} a_\beta \left[R_\alpha \left(1 - \frac{c_\beta}{R}\right) + 2c_\beta\right] . \qquad (3.4.11)$$

The volume of the deformed section of the cylindrical membrane described by angle α is given by

$$V_w = \int_o^\alpha A_\beta \, R_\beta \, d\beta . \qquad (3.4.12)$$

Let us introduce a set of non-dimensional parameters

$$\overline{b_\beta} = \frac{b_\beta}{R} ; \quad \overline{c_\beta} = \frac{c_\beta}{R} ; \quad \overline{Y_\beta} = \frac{Y_\beta}{R} ; \quad \overline{a_\beta} = \frac{a_\beta}{R} ; \quad \overline{R_\beta} = \frac{R_\beta}{R} ;$$

$$\overline{A_\beta} = \frac{A_\beta}{\pi R^2} ; \quad \overline{R_\alpha} = \frac{R_\alpha}{R} .$$

Now the geometrical relationships can be written as

$$\overline{c_\beta} = \frac{1}{\cos \beta} \qquad (3.4.13)$$

$$\overline{b_\beta} = \overline{R_\alpha} \left(1 - \overline{c_\beta}\right) + \overline{c_\beta} . \qquad (3.4.14)$$

$\overline{a_\beta}$ is obtained from the numerical solution of an implicit equation given by

$$\sqrt{\overline{a_\beta}^2 + k \, \overline{b_\beta}^2} + \sqrt{\overline{a_\beta}^2 + k \, \overline{c_\beta}^2} - \pi = 0 \qquad (3.4.15)$$

$$\overline{Y_\beta} = \overline{R_\alpha}\ \frac{4}{3\pi}\ (\overline{c_\beta} - 1) \tag{3.4.16}$$

$$\overline{R_\beta} = \overline{c_\beta}\ [\overline{R_\alpha}\ (1 - \frac{4}{3\pi\overline{c_\beta}}\ (\overline{c_\beta} - 1)) - 1] \tag{3.4.17}$$

$$\overline{A_\beta} = \tfrac{1}{2}\ \overline{a_\beta}\ [R_\alpha\ (1 - \overline{c_\beta}) + 2\ \overline{c_\beta}]\ . \tag{3.4.18}$$

The work done by pressure over the change in volume during deformation of the membrane is given by

$$W_p = p(V_o - V_w) \tag{3.4.19}$$

where

$$V_o = \pi R^2 \alpha R_\alpha \tag{3.4.20}$$

is the initial volume of the undeformed membrane.

The work done by the pressure moment over the deformation angle α is given by

$$W_M = \int_o^\alpha M_p\ d\alpha \tag{3.4.21}$$

where

$$M_p = pA_{\beta(\beta=\alpha)} \times [b_{\beta(\beta=\alpha)} + Y_{\beta(\beta=\alpha)}]$$

is the pressure moment calculated in the wrinkling plane and is given by

$$M_p = \frac{p\pi a_\alpha}{2}\ [R_\alpha(1 - \frac{c_\alpha}{R})\ 2c_\alpha][R_\alpha(1 - \frac{c_\alpha}{R})(1 - \frac{4}{3\pi}) + c_\alpha]\ . \tag{3.4.22}$$

Introducing a set of nondimensional parameters

$$\overline{c_\alpha} = \frac{1}{\cos\ \alpha} \tag{3.4.23}$$

$$\overline{b_\beta} = \overline{R_\alpha}\ (1 - \overline{c_\alpha}) + \overline{c_\alpha} \tag{3.4.24}$$

$\overline{a_\alpha}$ is obtained from the solution of

$$\sqrt{\overline{a_\beta}^2 + k\left(\frac{\overline{b_\alpha}}{\cos\alpha}\right)^2} + \sqrt{\overline{a_\alpha}^2 + k\left(\overline{c_\alpha}\cos\alpha\right)^2} - \pi = 0 \qquad (3.4.25)$$

The non-dimensional pressure moment is given by

$$\overline{M_p} = \frac{\overline{a_\alpha}}{2}\left[\overline{R_\alpha}\left(1 - \overline{c_\alpha}\right) + 2\overline{c_\alpha}\right]\left[\overline{R_\alpha}\left(1 - \overline{c_\alpha}\right)\left(1 - \frac{4}{3\pi}\right) + \overline{c_\alpha}\right] \qquad (3.4.26)$$

and

$$\overline{M_p} = \frac{M_p}{p\pi R^3} . \qquad (3.4.27)$$

The variational principle $\delta W = 0$ in which W is the potential energy of the system leads to the following nonlinear algebraic equation

$$\frac{d}{dR_\alpha} W = 0 \qquad (3.4.28)$$

where

$$W = W_p - W_M . \qquad (3.4.29)$$

Equation (3.4.28) written in explicit nondimensional form is given by

$$\bar{W} = \alpha\overline{R_\alpha} - \tfrac{1}{2}\int_o^\alpha \overline{a_\beta}\,\overline{c_\beta}\left[\overline{R_\alpha}\left(1 - \overline{c_\beta}\right) + 2\overline{c_\beta}\right]\left[\overline{R_\alpha}\left(1 - \frac{4}{3\pi\overline{c_\beta}}\left(\overline{c_\beta} - 1\right)\right)\right.$$

$$\left. - 1\right] d\beta - \tfrac{1}{2}\int_o^\alpha \overline{a_\alpha}\left[\overline{R_\alpha}\left(1 - \overline{c_\alpha}\right) + 2\overline{c_\alpha}\right]\left[\overline{R_\alpha}\left(1 - \overline{c_\alpha}\right)\left(1 - \frac{4}{3\pi}\right)\right.$$

$$\left. + \overline{c_\alpha}\right] d\alpha \qquad (3.4.30)$$

where

$$\bar{W} = \frac{W}{p\pi R^3} \quad . \tag{3.4.31}$$

The solution of equation (3.4.30) can be obtained from the direct differentiation of function $\bar{W}$ and by solving the nonlinear algebraic equation, or by numerical minimization of function $\bar{W}$ with respect to parameter $\bar{R}_\alpha$. Because of the very complex trigonometrical relationship describing function $\bar{W}$ the numerical minimization routine is preferable.

The procedure leading to the minimization of equation (3.4.30) with respect to parameter $\bar{R}_\alpha$ as well as the numerical results are presented in Chapter 5.

CHAPTER 4

THE STATIC APPROACH

4.1 GEOMETRY OF THE STRUCTURE

The following analysis, devoted to the theory concerning very large deformations of inflatable arch structures, is based on the geometrical approach described in Chapter 2. This time, however, the geometry of the structure is considered together with the static forces acting on the structure. Consider the half section of the inflatable arch of the central half angle θ_o, arch radius R_o and membrane radius R subjected to the apex load Q/2 as shown in Figure 16. The reference line to which the geometrical parameters as well as the structural forces are reduced is the center line of the arch membrane. Figure 17(a) shows the detailed geometry of the left bottom part of the arch while Figure 17(b) is a "magnification" of the geometry in the neighbourhood of point A.

The horizontal position of point A is given by

$$\overline{X_1} = \overline{a_1'} \cdot \cos(\kappa_1) + \overline{a_2'} \cdot \cos(\kappa_2) - \overline{a_5} \cdot \cos(\kappa_5) \qquad (4.1.1)$$

where

$$\overline{a_1'} = 2 \sin(\frac{\alpha_1}{2}) \qquad (4.1.2)$$

$$\overline{a_2'} = 2\,\overline{R_o} \sin(\frac{\gamma_1}{2}) \qquad (4.1.3)$$

$$\overline{a_5'} = 2 \sin(\frac{\alpha_2}{4}) \qquad (4.1.4)$$

and by

$$\overline{X_2} = \overline{R_o} \sin(\pi - \theta_o) \,. \qquad (4.1.5)$$

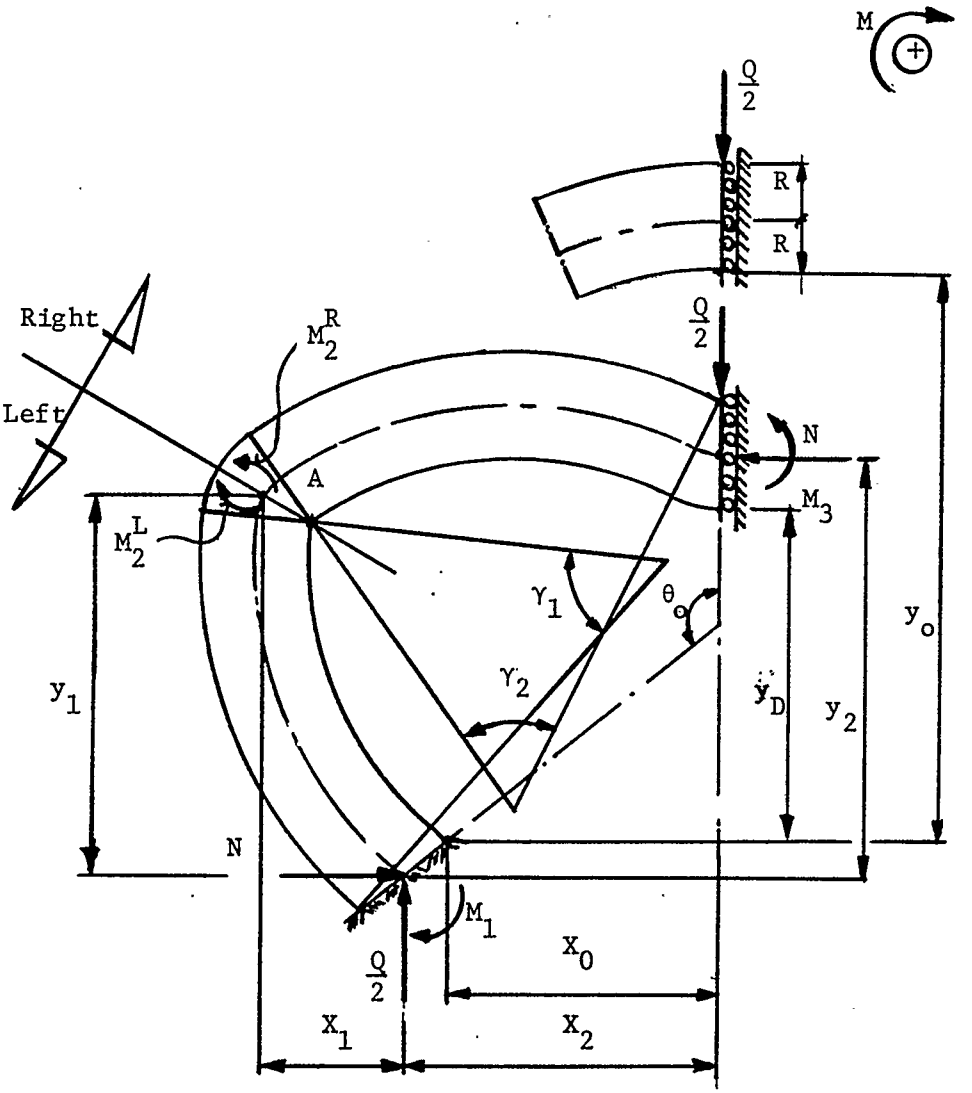

Fig. 16 Static Approach - Geometry of the Arch Structure

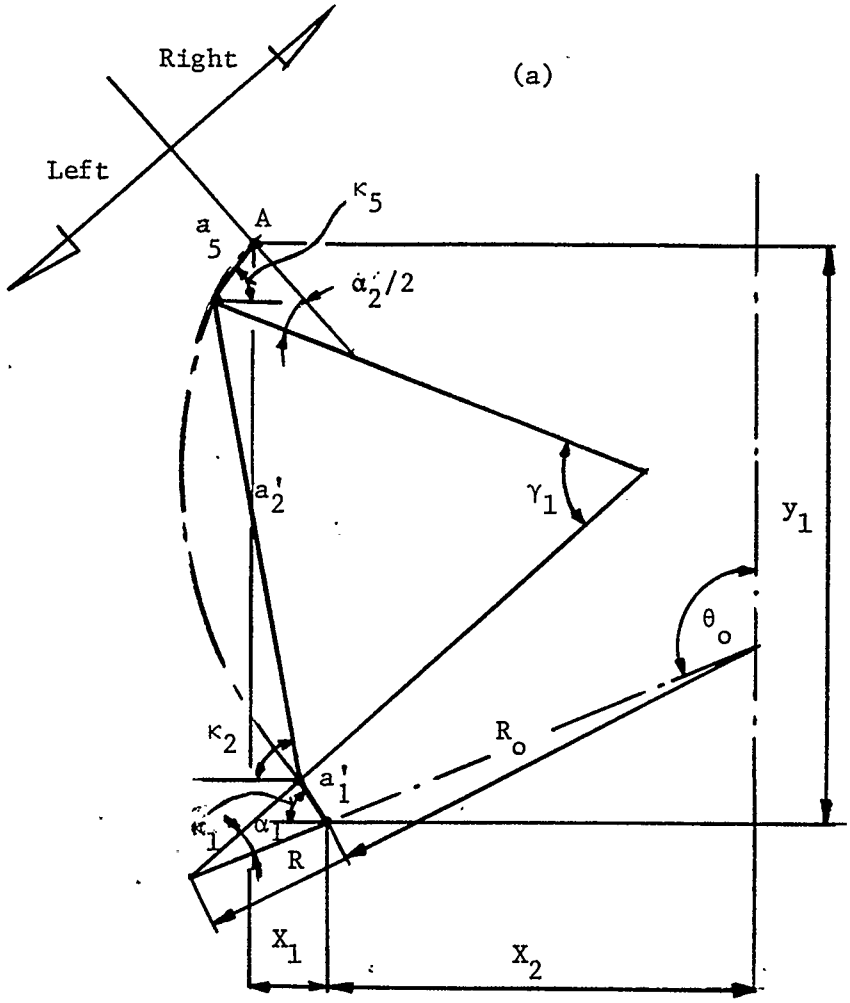

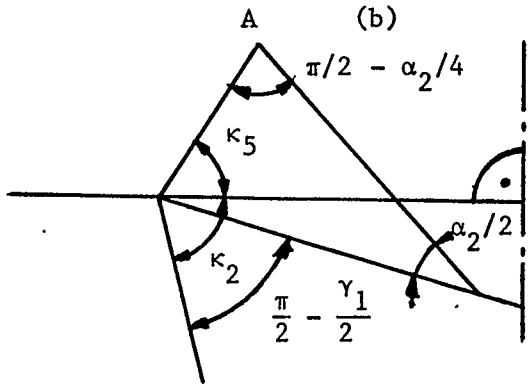

$$\kappa_5 + \kappa_2 = \frac{\pi}{2} - \frac{\gamma_1}{2} + \frac{\pi}{2} - \frac{\alpha_2}{4}$$

$$\kappa_5 = \theta_o + \alpha_1 - \frac{\alpha_2}{4} - \gamma_1$$

Fig. 17 Detailed Angular Relationship of the Deformed Center Line of the Inflatable Arch.

The vertical position of point A is given by

$$\overline{y_1} = \overline{a_1'} \sin(\kappa_1) + \overline{a_2'} \sin(\kappa_2) + \overline{a_5} \sin(\kappa_5) \; . \qquad 4.1.7$$

The vertical position of the point of application of the external load and the static axial force N is given by

$$\overline{y_2} = \overline{Y_D} + 1 + \sin(\theta_o - \tfrac{\pi}{2})$$

where $\overline{Y_D}$ is given by (2.14).

Note that

$$\overline{X_1} = \frac{X_1}{R} \; ; \quad \overline{X_2} = \frac{X_2}{R} \; ; \quad \overline{a_1'} = \frac{a_1'}{R} \; ; \quad \overline{a_2'} = \frac{a_2'}{R} \; ; \quad \overline{a_5} = \frac{a_5}{R} \; ;$$

$$\overline{y_1} = \frac{y_1}{R} \; ; \quad \overline{y_2} = \frac{y_2}{R} \; .$$

4.2 STATIC MODEL OF AN INFLATABLE ARCH STRUCTURE

Consider the model of a deformed arch as shown in Fig. 16. Because of symmetric loading only half of the structure needs to be considered. It is assumed, as before, that the segments described by angles γ_1 and γ_2 are rigid. The length of each toroidal segment changes during the deformation process as the pneumatic hinge development progresses. Each pneumatic hinge carries the horizontal force N over the end-moments M_1, M_2, M_3 and the vertical force equals half of the applied load Q.

The equilibrium condition for the left part of the structure, as indicated in Fig. 16 with respect to point A, can be written as

$$\Sigma M_A^L = 0 \quad : \quad M_2^L - N \cdot y_1 + M_1 - \frac{Q}{2} \cdot X_1 = 0 \qquad (4.2.1)$$

Similarly for the right section of the arch

$$\Sigma M_A^R = 0 \quad : \quad -M_2^R - N \quad (y_2 - y_1) + \frac{Q}{2} (X_1 + X_2) - M_3 = 0 \ . \quad (4.2.2)$$

Equilibrium of the middle hinge requires

$$M_2^L = M_2^R = M_2 \quad (4.2.3)$$

where M_1, M_2, M_3 are reaction moments acting on the hinges.

Using Eq. (4.2.1) and (4.2.2) we can derive the normal force N and load Q as a function of the geometrical parameter and reaction moment

$$N = \frac{1}{y_2} \left(\frac{Q}{2} X_2 + M_1 - M_3\right) \quad (4.2.4)$$

where

$$Q = 2 \left[M_1 \left(1 - \frac{y_1}{y_2}\right) + M_2 + M_3 \frac{y_1}{y_2}\right] / \left(X_1 + X_2 \frac{y_1}{y_2}\right) \ . \quad (4.2.5)$$

4.3 INTERNAL EQUILIBRIUM OF AN INEXTENSIBLE PNEUMATIC HINGE

The pneumatic hinge has not been given a lot of attention in the literature. The collapse model presented here is an idealized pneumatic hinge of perfect toroidal shape and the cross-section is the same as the original structure. If the material of the membrane is inextensional then the tensional force is taken by the most distant fibre of the membrane. The structure is supported only by the internal pressure as the wall of the membrane is unable to support any compressive force. It is assumed that the shear force does not contribute to the cross-sectional stability of the hinge.

The tensional membrane force and the internal pressure acting on the cross-sectional area of the hinge develop a pressure moment, M_P, which, for this model, is constant because of simplified assumptions of an undeformable cross-section. This, however, does not necessarily

mean that the hinge supports the external moment equal in magnitude to the pressure moment M_p.

If the hinge structure is in addition to the bending moment under the action of a resultant axial force N_a, then the reaction moment M_i can be significantly reduced. The explanation of such behaviour is that the pneumatic hinge has to be in equilibrium with the external bending moment M_i and the resultant axial force N_a. This overall equilibrium condition of the hinge can be written as

$$M_P = M_i + N_a R \ . \qquad (4.3.0)$$

If the resultant axial force N_a is increased and $R \cong$ constant then to satisfy equation (4.3.0) the external moment M_i must decrease. Now, let us consider the upper segment of the deformed arch as shown in Fig. 18(a). Pressure force equal to pA where A is the cross-section area of the structure, and the tensional force T, are reduced to the restoring pressure moment M_p. The resultant moment with respect to point A_i from the horizontal force N and the external bending moment M_i cannot be greater than the pressure moment M_p. Considering the equilibrium of the pneumatic hinge with respect to point A_3 we can write

$$M_P - N\,R - M_3 = 0 \ , \qquad (4.3.1)$$

and similarly with respect to point A_2

$$M_P - N \sin \phi_3 \, R - \frac{Q}{2} \cos \phi_2 \, R - M_2 = 0 \ , \qquad (4.3.2)$$

finally with respect to point A_1, see Fig. 18(b)

$$-M_P - N \sin \phi_1 \, R + \frac{Q}{2} \cos \phi_1 \, R + M_1 = 0 \ . \qquad (4.3.3)$$

From the above set of equilibrium equations the reaction moments M_1, M_2, M_3 can be derived as functions of known value of the pressure moment M_p

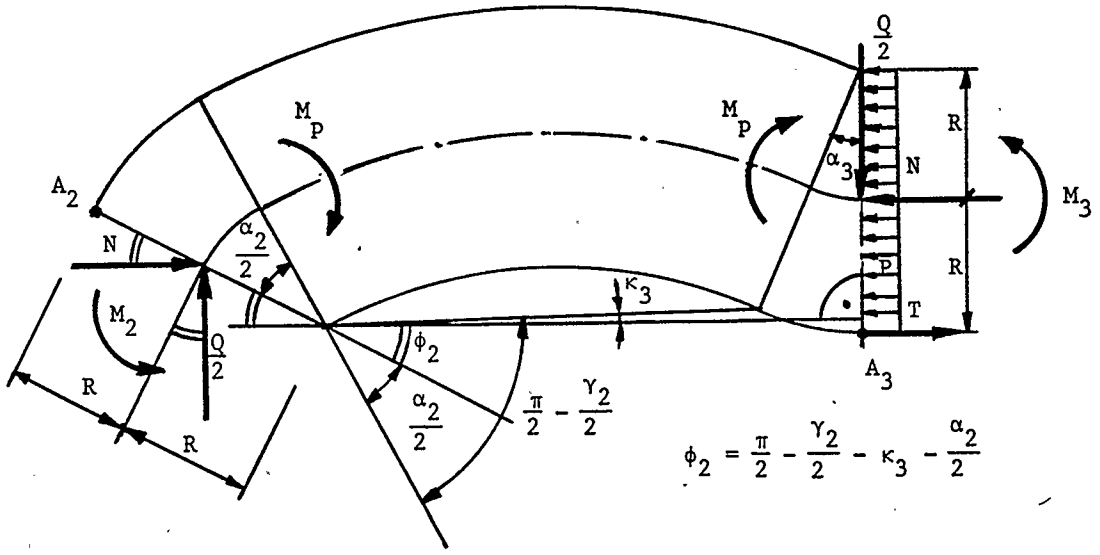

(a) Force Diagram for Upper Segment of the Arch Structure

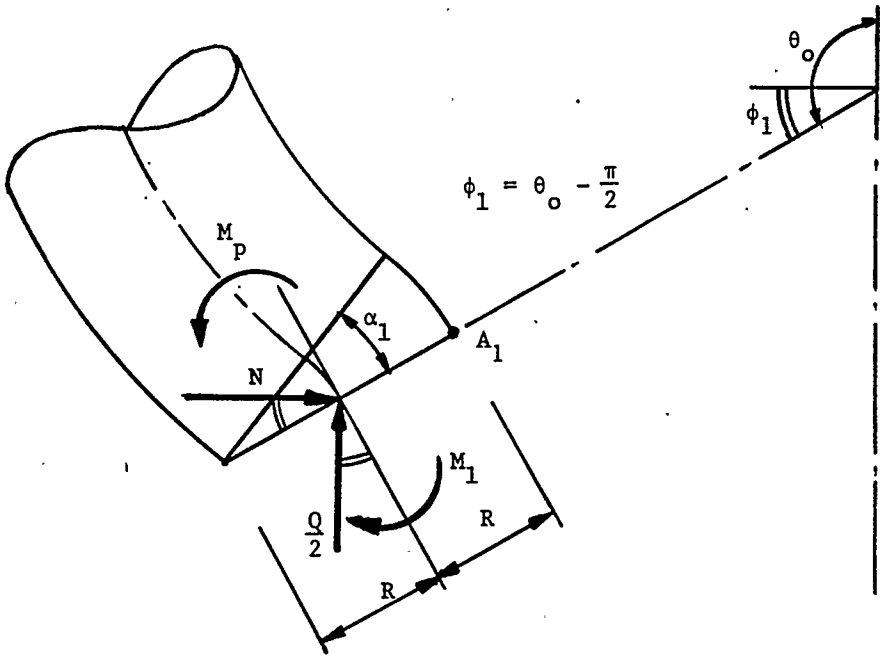

(b) Force Diagram for Lower Segment of the Arch Structure

Fig. 18 Force Diagrams for Different Segments of the Inflatable Arch Structure

and the unknown horizontal force N and load Q. These three equations complete the set of five linear equations describing the state of the static equilibrium of the arch structure as well as the local equilibrium of the hinge structures. The complete set of equilibrium equations can be written as

$$M_1 = M_P + N\,R \sin \phi_1 - \frac{Q}{2} R \cos \phi_1 \tag{4.3.4}$$

$$M_2 = M_P - N \cdot R \sin \phi_2 - \frac{Q}{2} R \cos \phi_2 \tag{4.3.5}$$

$$M_3 = M_P - N \cdot R \tag{4.3.6}$$

$$N = \frac{1}{y_2} \left(\frac{Q}{2} X_2 + M_1 - M_3\right) \tag{4.3.7}$$

and

$$Q = 2 \left[M_1 \left(1 - \frac{y_1}{y_2}\right) + M_2 + M_3 \frac{y_1}{y_2}\right] \left(X_1 + X_2 \frac{y_1}{y_2}\right) . \tag{4.3.8}$$

The method of solution of the above equations is as follows. Using the direct substitution approach, the system of the first four equations is solved in the form

$$M_1 = M_P + \frac{Q}{2} R\, f \tag{4.3.9}$$

$$M_2 = M_P - \frac{Q}{2} R \left[g \sin \phi_2 + \cos \phi_2\right) \tag{4.3.10}$$

$$M_3 = M_P - \frac{Q}{2} R\, g \tag{4.3.11}$$

$$N = \frac{Q}{2} g \tag{4.3.12}$$

where

$$f = \frac{X_2 \sin \phi_1 - (y_2 - R) \cos \phi_1}{y_2 - R(1 + \sin \phi_1)} \tag{4.3.13}$$

$$g = \frac{X_2 + R \cdot f}{y_2 - R} . \tag{4.3.14}$$

It is convenient to express all parameters in nondimensional form.

Let

$$\overline{X_1} = \frac{X_1}{R} \; ; \quad \overline{y_1} = \frac{y_1}{R}; \quad \overline{X_2} = \frac{X_2}{R} \; ; \quad \overline{y_2} = \frac{y_2}{R}$$

$$\bar{Q} = \frac{Q}{2pA} \; ; \quad \overline{M_1} = \frac{M_1}{pAR} \; ; \quad \overline{M_2} = \frac{M_2}{pAR} \; ; \quad \overline{M_3} = \frac{M_3}{pAR} \; ; \quad \overline{M_P} = \frac{M_P}{pAR} \; .$$

Then Eqs. (4.3.9) through (4.3.14) are written as

$$\overline{M_1} = \overline{M_P} + \bar{Q}\,\bar{f} \tag{4.3.15}$$

$$\overline{M_2} = \overline{M_P} - \bar{Q}\,(\bar{g}\,\sin\phi_2 + \cos\phi_2) \tag{4.3.16}$$

$$\overline{M_3} = \overline{M_P} - \bar{Q}\,\bar{g} \tag{4.3.17}$$

$$\bar{N} = \bar{Q}\,\bar{g} \tag{4.3.18}$$

$$\bar{Q} = \frac{\overline{M_1}\,(1 - \dfrac{\overline{y_1}}{\overline{y_2}}) + \overline{M_2} + \overline{M_3}\,\dfrac{\overline{y_1}}{\overline{y_2}}}{\overline{X_1} + \overline{X_2}\,\dfrac{\overline{y_1}}{\overline{y_2}}} \tag{4.3.19}$$

$$\bar{f} = \frac{\overline{X_2}\,\sin\phi_1 - (\overline{y_2} - 1)\,\cos\phi_1}{\overline{y_2} - 1 - \sin\phi_1} \tag{4.3.20}$$

$$\bar{g} = \frac{\overline{X_2} + \bar{f}}{\overline{y_2} - 1} \; . \tag{4.3.21}$$

After substitution of (4.3.15 - 18) into (4.19) and after simplifications the load $\bar{Q}$ in terms of geometrical parameters only is given by

$$\bar{Q} = \frac{2\,\overline{M_P}}{\overline{X_1} + (\overline{X_2} + \bar{f} + \bar{g})\,\dfrac{\overline{y_1}}{\overline{y_2}} - \bar{f} + \bar{g}\,\sin\phi_2 + \cos\phi_2} \,. \qquad (4.3.22)$$

4.4 EXTENSIBILITY OF THE HINGE MEMBRANE

In this chapter the influence of the elasticity of the material of the membrane on the pressure moment and the transition from the state of first wrinkling to the state of fully developed pressure moment is analysed. This is quite interesting nonlinear behaviour and is similar to the plastic deformation of a beam under the action of a bending moment. Consider the cross-section of the cylindrical membrane in the state of first wrinkling as shown in Fig. 19. As the external moment increases the spread of wrinkling described by angle ϕ grows to the point where the whole cross-section has wrinkled. As the spread of wrinkling continues, the top tensioned part of the membrane becomes smaller causing the rapid buildup of tensional stress. This field of high local stress stretches the membrane in the area OD, (see Fig. 19), and is depicted by angle α_E. The equilibrium of the axial forces of the membrane in plane DE is given by

$$p\,\pi R^2 - 2\int_0^{\phi} \sigma(\beta)\,t\,R\,d\beta = 0 \qquad (4.4.1)$$

where the distribution of the stress can be obtained from

$$\sigma(\beta) = \frac{z}{\rho}\,E\,, \qquad (4.4.2)$$

and

$$z = R\,(\cos\beta - \cos\phi) \qquad (4.4.3)$$

is the distance from point 0 to the coming fiber.

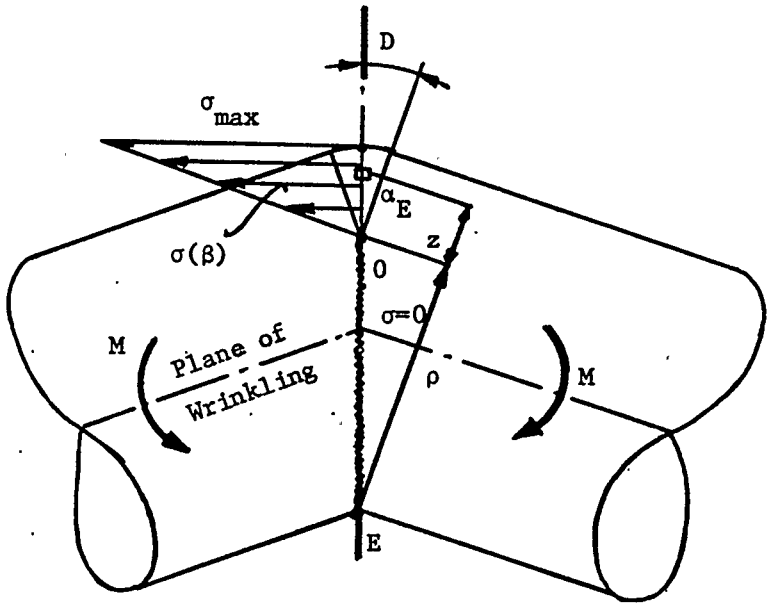

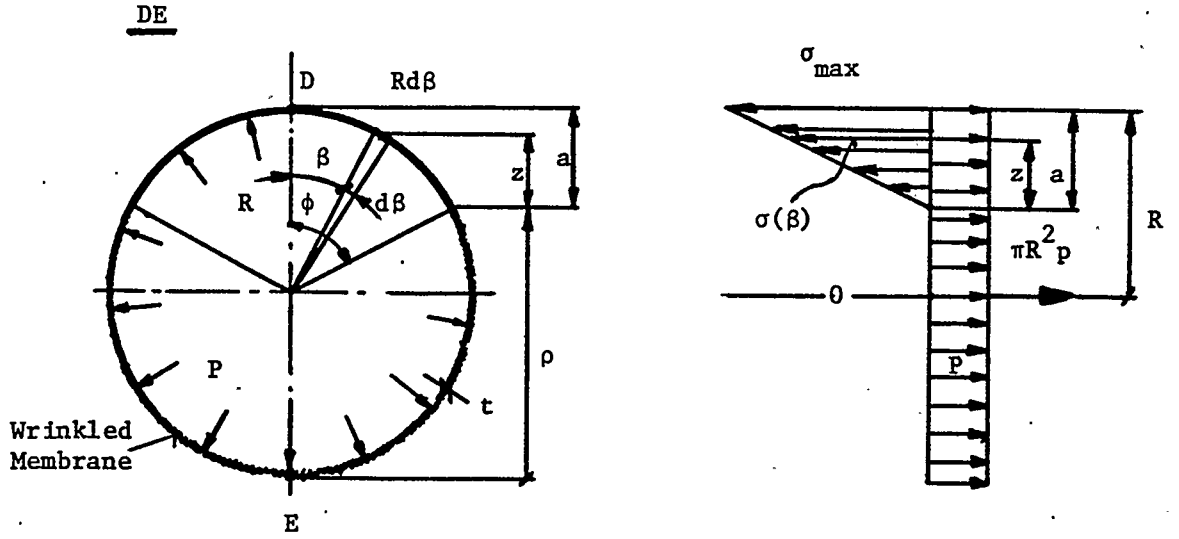

Fig. 19 The Force Diagram and Cross-Sectional Geometry of Cylindrical Membrane

$$\rho = R\ (1 + \cos\ \phi) \qquad (4.4.4)$$

is the radius of the curvature of the stretched segment of the membrane.

Introducing Eq. (4.4.2 - 4) into (4.4.1) and integrating, the following equation of equilibrium will be obtained

$$p\pi R - \frac{Et}{1 + \cos\ \phi}\ 2\ (\sin\ \phi - \phi\ \cos\ \phi)\ . \qquad (4.4.5)$$

The maximum tensional stress developed in the most external fibre of the hinge membrane is given by

$$\sigma_{max} = \frac{a}{\rho}E \qquad (4.4.6)$$

where

$$a = R\ (1 - \cos\ \phi) \qquad (4.4.7)$$

is the height of the stretched segment of the membrane as shown on Fig. 19.

Substituting a and ρ in Eq. (4.4.6) by Eq. (4.4.7) and (4.4.4) respectively to get

$$\frac{E}{1 + \cos\ \phi} = \frac{\sigma_{max}}{1 - \cos\ \phi}\ . \qquad (4.4.8)$$

introducing Eq. (4.4.8) into Eq. (4.4.5) and simplifiying it, a relationship of the maximum tensile stress versus the spread of wrinkling is established and is given by

$$\sigma_{max(\phi)} = \frac{p\pi R}{2t}\ \frac{1 - \cos\ \phi}{\sin\ \phi - \phi\ \cos\ \phi}\ . \qquad (4.4.9)$$

The "post-initial wrinkling" moment the pneumatic hinge can support is calculated from

$$M = 2 \int_o^{\phi} \sigma_{(\beta)}\ (R - a + z)\ t\ Rd\beta \qquad (4.4.10)$$

Performing integration one will obtain

$$M = \frac{Et}{1 + \cos\ \phi}\ R^2\ (\phi - \sin\ \phi\ \cos\ \phi)\ . \qquad (4.4.11)$$

Making use of Eq. (4.4.5) the pressure moment is obtained as

$$M(\phi) = \frac{\pi p R^3}{2} \quad \frac{\phi - \sin\phi \cos\phi}{\sin\phi - \phi\cos\phi} \,. \tag{4.4.12}$$

The angle of elastic deformation α_E can be obtained from the relationship

$$\alpha_E = \frac{\Delta L}{a} = \frac{\sigma_{max}}{aE} \cdot \ell \tag{4.4.13}$$

where ℓ is the mean length of the elongated area of the apex part of the hinge membrane.

Introducing Eq. (4.47) and Eq. (4.4.9) into (4.4.13) yields

$$\alpha_E(\phi) = \frac{\pi p \ell}{2Et} \quad \frac{1}{\sin\phi - \phi\cos\phi} \,. \tag{4.4.14}$$

The analysis presented in this chapter does not pretend to be exact. Such analysis is beyond the scope of the thesis. This, however, does not diminish the usefulness of the derivations presented here. They provide sufficient theoretical base to investigate the phenomena of transition from the first wrinkling to the totally wrinkled section of the membrane just before formation of the pneumatic hinge. This "transition effect" is most profound at the initial stages of deformation of the arch structure when the hinge angles are small.

The graphical representation of Eqs. (4.4.9) (4.4.12) and (4.4.14) in non-dimensional form is shown on Fig. 20. Fig. 21 shows the relationship between the pressure moment $\bar{M}$ and the hinge angle $\bar{\alpha}_E$. If one compares the behaviour of the pressure moment of the pneumatic hinge to the bending moment of a solid beam (Fig. 22), the similarities are quite evident. Point b) in Fig. 22 corresponds to the point of first wrinkling moment in Fig. 21. Both curves are linear before that point and non-linear asymptotically approaching the limit bending moment after

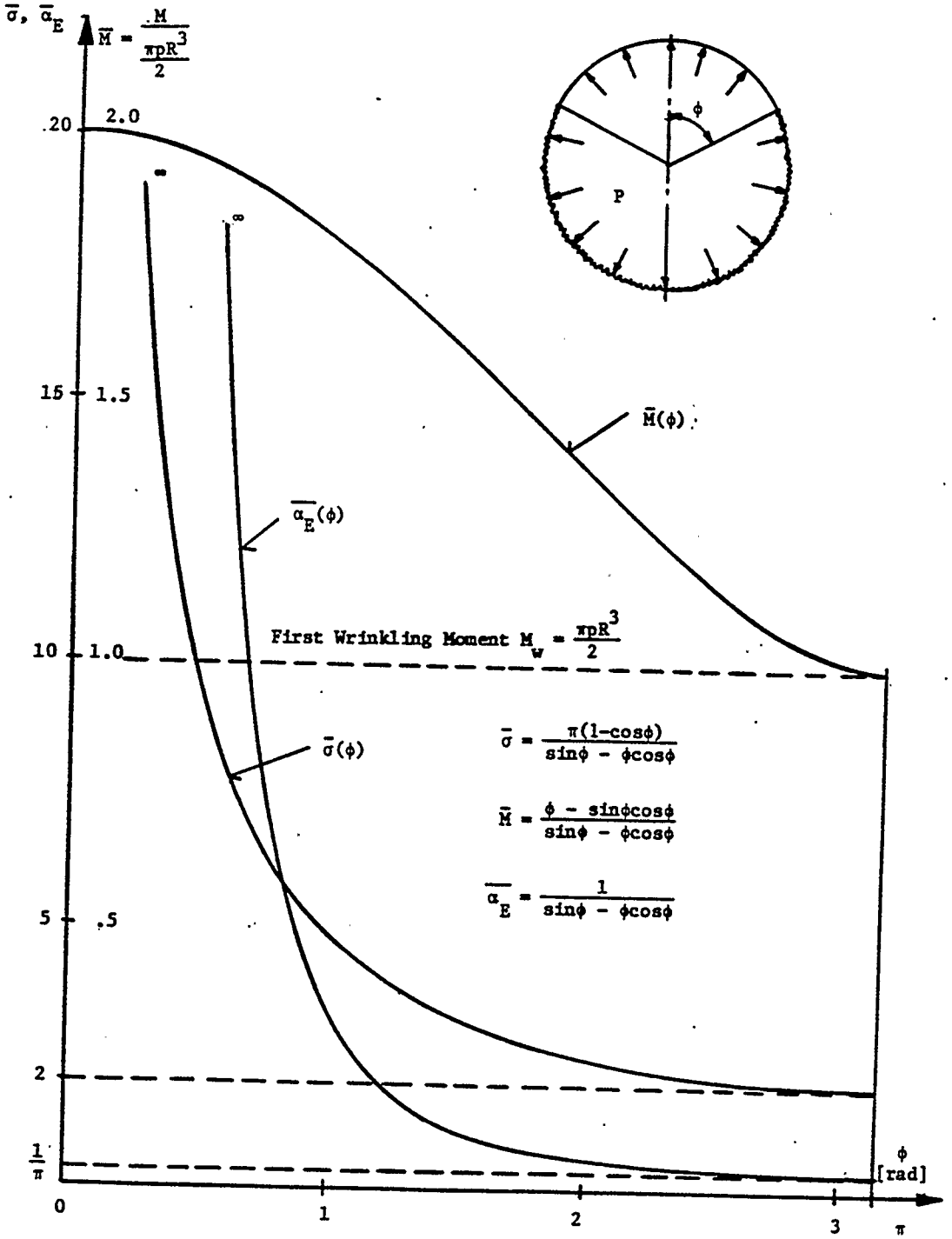

Fig. 20 Post Wrinkling Relations for Cylindrical Membrane

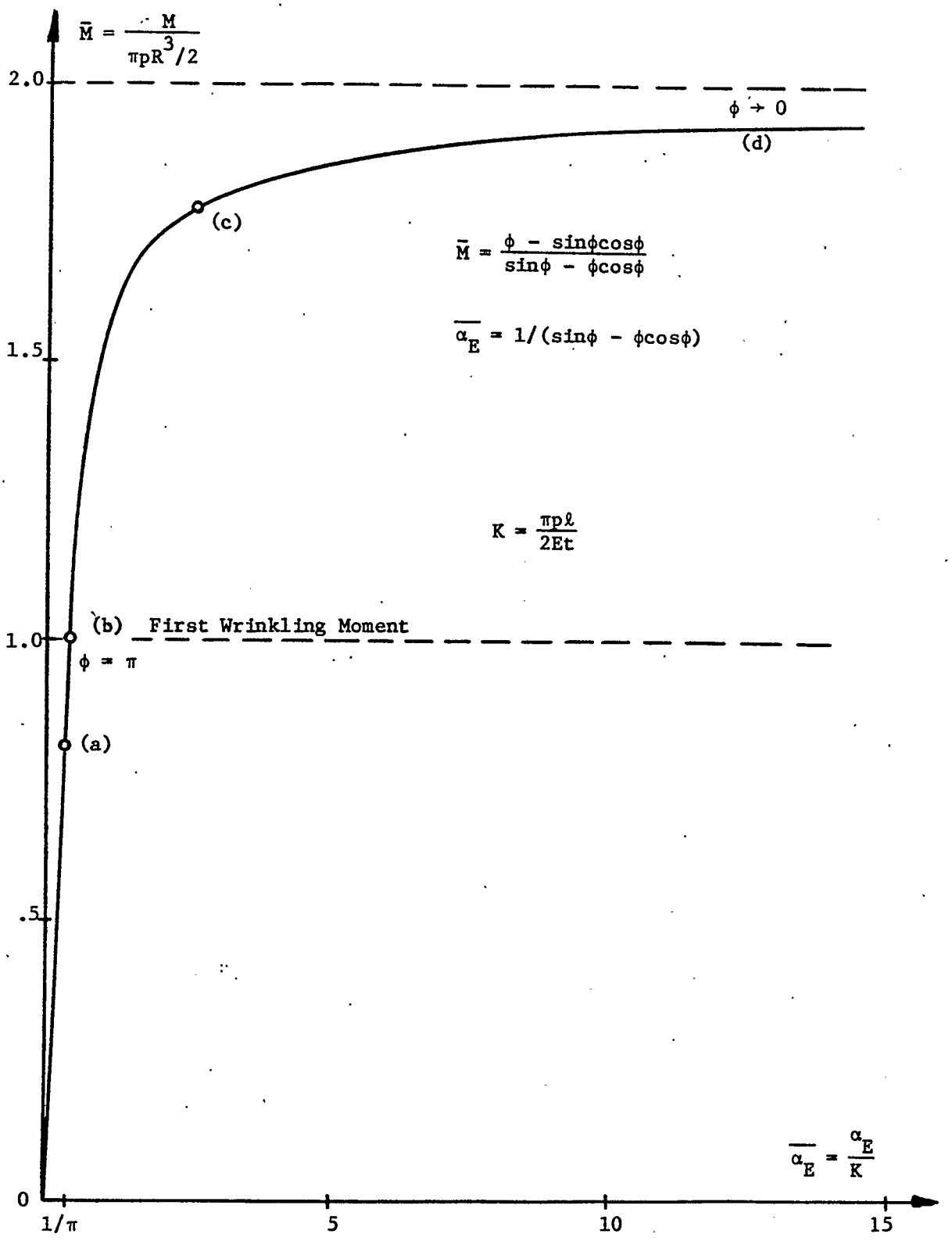

Fig. 21 Moment-Hinge Angle Relation for the Inflatable Cylindrical Membrane

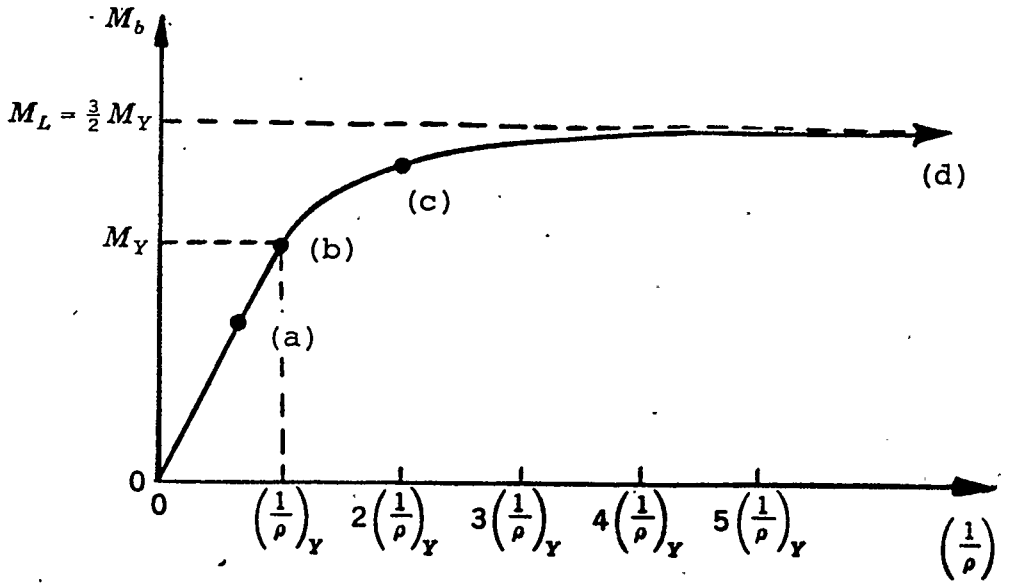

Fig. 22 Moment-Curvature Relation for the Rectangular Beam [26]

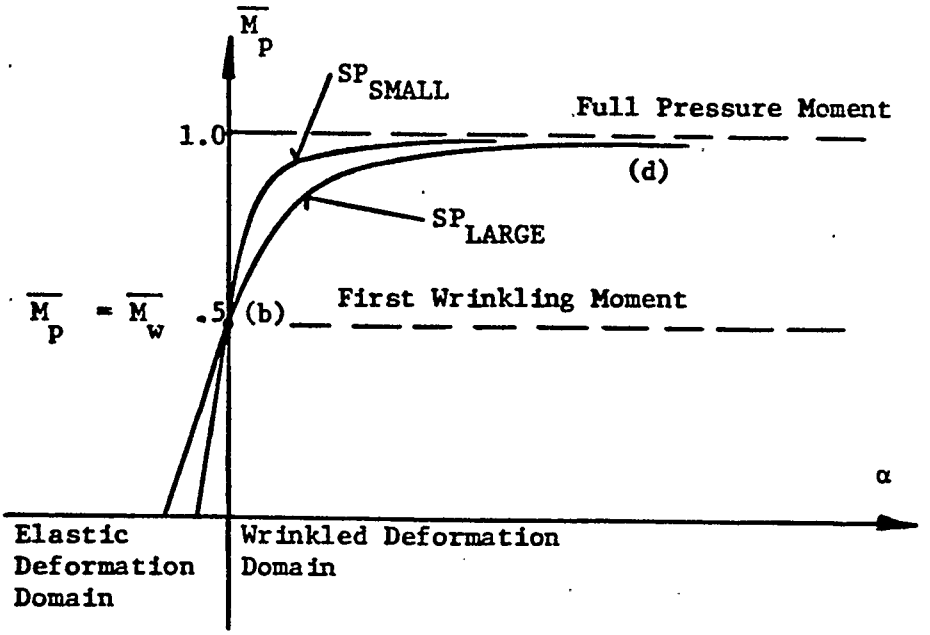

Fig. 23 Moment-Hinge Angle Relation for Pneumatic Cylindrical Membrane

it. The limit moment is twice the first wrinkling moment for the pneumatic structure where the yielding moment is one and half times that of the solid beam.

The application of extensibility of the membrane can be confined only to the localized area of the pneumatic hinge without sacrificing the accuracy of the theoretical model. This can be done either by the exact calculation of the relationship of the pressure moment vs the hinge angle or by a semi-empirical function which may include some coefficients difficult, if not impossible, to obtain theoretically. In this thesis such a function has been used. The argument for this approach is that both the real structure and the experimental one have some geometrical, material, or other imperfections which are difficult to account for. Therefore, a function which will preserve the general relationship depicted in Fig. 21 yet be flexible enough to accommodate, by means of a coefficient, the influence of the different stiffnesses of a membrane, can be a useful analytical tool.

Consider a function describing a pressure moment as a function of the hinge angle and a flexibility coefficient of the membrane given by

$$\overline{M_{Pi}} = \tfrac{1}{2}\left(1 + \frac{\alpha_i}{SP + \alpha_i}\right) \qquad i = 1, 2, 3 \qquad (4.4.15)$$

where

$\overline{M_{Pi}}$ is the non-dimensional pressure moment at "i" hinge

α_i is the "i" hinge angle

SP is the flexibility coefficient of the arch membrane.

Analysing Eq. (4.4.15) we see that for the given coefficient SP, as α_i approaches zero, the pressure moment $\overline{M_{Pi}}$ converges to $\frac{1}{2}$ and

vice-versa, as α_i increases to ∞, moment $\overline{M_{Pi}}$ converges to 2. The coefficient SP controls the growth rate of the pressure moment. For the very stiff or almost inextensible membrane SP $\to$ 0 and the pressure moment $\overline{M_{Pi}}$ reaches its maximum theoretical value for the very small value of hinge angle α_i. This is schematically depicted in Fig. 23.

Replace constant pressure moment $\overline{M_P}$ in Eq. (4.3.15) to (4.3.18) by function (4.4.15) to get

$$\overline{M_1} = \tfrac{1}{2}\left(1 + \frac{\alpha_1}{SP + \alpha_1}\right) + \bar{Q} \cdot \bar{f} \qquad (4.4.16)$$

$$\overline{M_2} = \tfrac{1}{2}\left(1 + \frac{\alpha_2}{SP + \alpha_2}\right) - \bar{Q}\left(\bar{g} \sin \phi_2 + \cos \phi_2\right) \qquad (4.4.17)$$

$$\overline{M_3} = \tfrac{1}{2}\left(1 + \frac{\alpha_3}{SP + \alpha_3}\right) - \bar{Q} \cdot \bar{g} \,. \qquad (4.4.18)$$

Then the load function $\bar{Q}$ in terms of new pressure moments is obtained as

$$\bar{Q} = \frac{\overline{M_{P1}} + \overline{M_{P2}} + \left(\overline{M_{P3}} - \overline{M_{P1}}\right) \cdot \dfrac{\overline{y_1}}{\overline{y_2}}}{\overline{X_1} + \left(\overline{X_2} + \bar{f} + \bar{g}\right) \dfrac{\overline{y_1}}{\overline{y_2}} - \bar{f} + \bar{g} \sin \phi_2 + \cos \phi_2} \,. \qquad (4.4.19)$$

The load function $\bar{Q}$ given by (4.4.19) is a function of the three parameters α_3, γ_1, γ_2. Assuming α_3 as the given parameter for which the value of the load $\bar{Q}$ is to be found eliminates one parameter. The second parameter can be calculated from the constraint function given by Eq. (2.28). This brings $\bar{Q}$ to be a function of one parameter (either γ_1 or γ_2). The last step is to minimize $\bar{Q}$ with respect to the remaining parameter. The minimization routine is described in the following chapter.

CHAPTER 5

NUMERICAL PROCEDURE

5.1 OPTIMIZATION ROUTINE

The optimization routine is based on the elimination scheme, which is a highly efficient computational procedure for all functions which have only one minimum within the search interval.

Suppose we place two search points at the end of the interval, located a very small distance from each other, as shown in Fig. 24, where

XL = left end of the search interval

XR = right end of the search interval

XL1 = left-hand interior search point

XR1 = right-hand interior search point

EPS = distance between XL1 and XR1 .

The function Q is evaluated at XL1 and XR1. Let us call these values QL1 and QR1 respectively. If QL1 turns out to be greater than QR1 then a new search interval is generated at the left end equal to XL1 and at the right end equal to XR, with a new set of interior search points located at the interval center.

On the other hand, suppose QL1 turns out to be smaller than QR1. This indicates that the new search interval should lie between point XL and XR1 with new interior search points again located in the center of the interval. The procedure is continued until the search interval becomes smaller than 3 EPS. Each time the comparison between QL1 and QR1 is made, that portion of the search interval which contains the larger value of Q is eliminated. If both interior values of

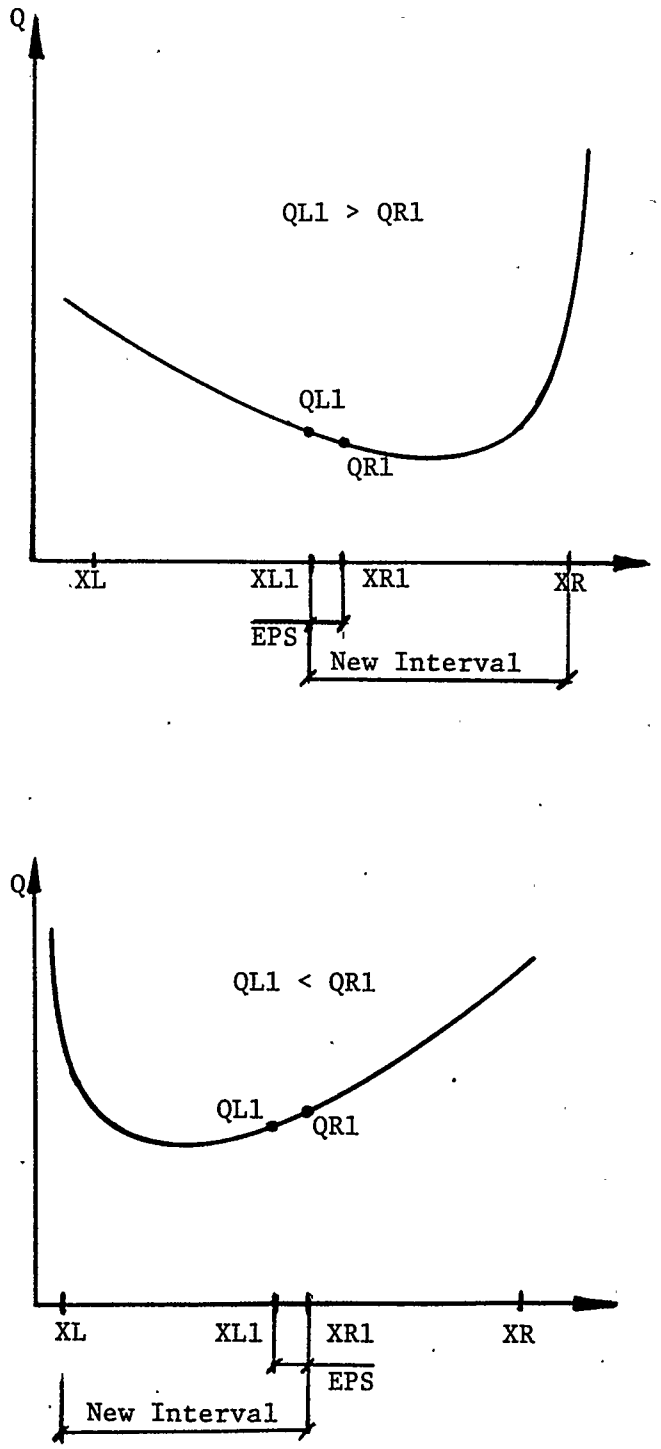

Fig. 24 - Placement of Search Intervals Over Argument Axes of Minimized Function Q

Q should happen to be identical, the search procedure stops, and the minimum is assumed to occur at the center of the two search points.

Once the search has ended, either because the search interval has become sufficiently small or because the two interior points yield identical values of Q, the approximate value of Q_{min} is calculated as

$$Q_{min} = \tfrac{1}{2} (QL1 + QR1) \qquad (5.1)$$

which occurs at approximately

$$X_{min} = \tfrac{1}{2} (XL1 + XR1) \; . \qquad (5.2)$$

5.2 OTHER NUMERICAL ROUTINES

If Q is a function of two variables represented by other equations, then before function Q is evaluated the equation has to be solved. In the case of load function Q this additional equation is a condition set on the horizontal movement of load Q given by (2.28). Equation (2.28) is a nonlinear trigonometrical equation with one variable which can be solved by many iterative techniques. The one used in this thesis is taken from the Harwell Subroutine Library. The subroutine NS01A uses the ideas of Newton-Raphson and Steepest Descent, coupled with Broyden's method for improving Jacobian matrices (see A.E.R.E. Report M.J.D. Powell "A Fortran Subroutine for Solving Systems of Nonlinear Algebraic Equations").

The numerical integration has been performed with the help of Simpson's Composite Algorithm [27].

5.3 NUMERICAL RESULTS

Numerical calculations were performed on Sun Microsystem 3/50

using single precision digits. The numerical solutions of equations containing trigonometrical functions are well known to the researchers for their convergence difficulties [24]. This was also the case in the present work. As mentioned in Chapter 3.3 the solution of the three nonlinear equations describing the equilibrium position of applied load derived from the Energy Approach has not been found. The most probable cause of the lack of convergence is the highly complex trigonometrical formulation of each function. The equations contain multivalued functions and consequently have a number of solutions, all of which satisfy the governing equations. The routine is trapped in the local minimum and does not converge to the required solution. To avoid these difficulties and improve the convergence of the solution, the static formulation of the problem was considered. This time, to find the minimum of the load function, direct differentiation of the minimized function had been avoided. Instead, a numerical algorithm has been used. This has proved to be a very powerful method of obtaining the numerical solution to the minimization problem of complex trigonometric functions.

The first application of the minimization routine was related to the pneumatic hinge model development. The numerical results are listed in Table 1-2. As can be seen, the obtained solution is not free from some convergence difficulties. One may expect the value of parameters M_p, A, B to lie on a smooth curve and to be independent of the number of integration intervals m when the deformation angle ALFA is gradually increased. Nevertheless the results are very interesting. They show that the hinge radius R_α changes significantly from the very high value at $\alpha \to 0$ rad to the lowest one comparable to the diameter of

Table 1 Computer Printout for Pneumatic Hinge Structure, m = 10

PNEUMATIC HINGE -SHAPE OPTIMIZATION
PROGRAM phm.f

NUMERICAL RESULTS

ALFA	PAR Ra	PAR Mp	PAR A	PAR B	PAR C
0.30303e-01	0.16986e+03	0.96790e+00	0.10535e+01	0.92244e+00	0.10005e+01
0.60606e-01	0.16758e+03	0.82483e+00	0.11802e+01	0.69360e+00	0.10018e+01
0.90909e-01	0.10999e+03	0.71300e+00	0.12388e+01	0.54805e+00	0.10041e+01
0.12121e+00	0.27497e+02	0.90377e+00	0.11206e+01	0.80415e+00	0.10074e+01
0.15152e+00	0.27492e+02	0.82930e+00	0.11749e+01	0.69298e+00	0.10116e+01
0.18182e+00	0.24056e+02	0.77191e+00	0.12067e+01	0.61358e+00	0.10168e+01
0.21212e+00	0.18044e+02	0.77181e+00	0.12051e+01	0.60923e+00	0.10229e+01
0.24242e+00	0.13534e+02	0.78582e+00	0.11955e+01	0.62247e+00	0.10301e+01
0.27273e+00	0.10454e+02	0.80128e+00	0.11845e+01	0.63717e+00	0.10384e+01
0.30303e+00	0.84743e+01	0.81050e+00	0.11764e+01	0.64319e+00	0.10477e+01
0.33333e+00	0.74157e+01	0.80305e+00	0.11776e+01	0.62629e+00	0.10582e+01
0.36364e+00	0.63779e+01	0.80690e+00	0.11718e+01	0.62373e+00	0.10700e+01
0.39394e+00	0.55398e+01	0.81294e+00	0.11642e+01	0.62342e+00	0.10829e+01
0.42424e+00	0.49105e+01	0.81687e+00	0.11572e+01	0.61961e+00	0.10973e+01
0.45455e+00	0.44653e+01	0.81587e+00	0.11524e+01	0.60837e+00	0.11130e+01
0.48485e+00	0.41869e+01	0.80594e+00	0.11513e+01	0.58485e+00	0.11303e+01
0.51515e+00	0.20107e+01	0.97100e+00	0.99512e+00	0.84927e+00	0.11491e+01
0.54545e+00	0.19925e+01	0.96674e+00	0.99082e+00	0.83153e+00	0.11697e+01
0.57576e+00	0.19901e+01	0.96172e+00	0.98844e+00	0.80970e+00	0.11922e+01
0.60606e+00	0.19876e+01	0.95547e+00	0.98493e+00	0.78599e+00	0.12167e+01

Table 2 Computer Printout for Pneumatic Hinge Structure, m = 20

PNEUMATIC HINGE -SHAPE OPTIMIZATION
PROGRAM phm.f

NUMERICAL RESULTS

ALFA	PAR Ra	PAR Mp	PAR A	PAR B	PAR C
0.30303e-01	0.15894e+03	0.97033e+00	0.10503e+01	0.92746e+00	0.10005e+01
0.60606e-01	0.15009e+03	0.84849e+00	0.11653e+01	0.72577e+00	0.10018e+01
0.90909e-01	0.10321e+03	0.73637e+00	0.12297e+01	0.57620e+00	0.10041e+01
0.12121e+00	0.25800e+02	0.91265e+00	0.11148e+01	0.81669e+00	0.10074e+01
0.15152e+00	0.25798e+02	0.84556e+00	0.11683e+01	0.71261e+00	0.10116e+01
0.18182e+00	0.24190e+02	0.77341e+00	0.12127e+01	0.61135e+00	0.10168e+01
0.21212e+00	0.18149e+02	0.77442e+00	0.12131e+01	0.60681e+00	0.10229e+01
0.24242e+00	0.14056e+02	0.77965e+00	0.12113e+01	0.60673e+00	0.10301e+01
0.27273e+00	0.10705e+02	0.80161e+00	0.12001e+01	0.62754e+00	0.10384e+01
0.30303e+00	0.94930e+01	0.78326e+00	0.12122e+01	0.59455e+00	0.10477e+01
0.33333e+00	0.83072e+01	0.77546e+00	0.12183e+01	0.57436e+00	0.10582e+01
0.36364e+00	0.41526e+01	0.92485e+00	0.11079e+01	0.77943e+00	0.10700e+01
0.39394e+00	0.31132e+01	0.95543e+00	0.10721e+01	0.82471e+00	0.10829e+01
0.42424e+00	0.31112e+01	0.94756e+00	0.10852e+01	0.79464e+00	0.10973e+01
0.45455e+00	0.29512e+01	0.94837e+00	0.10882e+01	0.77949e+00	0.11130e+01
0.48485e+00	0.29493e+01	0.94045e+00	0.11026e+01	0.74607e+00	0.11303e+01
0.51515e+00	0.29013e+01	0.93540e+00	0.11141e+01	0.71645e+00	0.11491e+01
0.54545e+00	0.28993e+01	0.92616e+00	0.11311e+01	0.67761e+00	0.11697e+01
0.57576e+00	0.28521e+01	0.92102e+00	0.11443e+01	0.64401e+00	0.11922e+01
0.60606e+00	0.28280e+01	0.91315e+00	0.11611e+01	0.60389e+00	0.12167e+01

the membrane when angle α is large. The numerical model also predicts that the pressure moment M_p is initially equal to twice the first wrinkling moment slowly decreases because of the change of cross-sectional geometry and reaches its lowest value $M_p \cong .77$ at angle $\alpha \cong .20$ (Table 2). After that, the pressure moment gradually increases to up to $\alpha \cong .39$, where it begins to decrease again. The behaviour of the cross-section of the membrane at the wrinkling plane is shown by parameters A, B, C. As can be seen, when the hinge angle ALFA is small, the cross-section of the membrane approaches a circle. As the deformations of the hinge structure continue to develop, the theoretical model predicts that the upper, tensioned surface of the membrane described by parameter B will flatten opposite to the lower wrinkled surface of the membrane depicted by parameter C which will become more oval. The width of the theoretical hinge structure described by parameter A also undergoes nonlinear transformations. Initially equal to the diameter of the membrane, it becomes larger as the hinge angle continues to increase and approaches a maximum value at the point when the pressure moment is at its minimum. After that point the width of the hinge slightly decreases up to $\alpha \cong .39$ where it increases again.

The second application of the minimization routine was devoted to the theoretical model of the double surface inflatable arch structure. From a numerical solution of the equations derived in the previous sections, analytical predictions for the large deflection and stability behaviour of these inflatables were obtained which are shown in Fig. N1 and Fig. N2 and given numerically for an abitrary parameter SP = .05 in Table 3.

Figure N1 presents the analytical results in non-dimensional

Table 3 Computer Printout for Arch Structure

SYMMETRICALLY LOADED ARCH
PROGRAM lam.f

INITIAL GEOMETRY

R= 6.500000 TE0= 1.818000 PARAMETER SP= 5.00000e-02

NUMERICAL RESULTS

ALFA 3	ALFA 2	ALFA 1	GAMA 1	GAMA 2	DELTA Y	LOAD Q
0.00000e+00	0.00000e+00	0.00000e+00	0.90900e+00	0.90900e+00	-0.47684e-06	0.19148e+00
0.20000e-01	0.41219e-01	0.21668e-02	0.92852e+00	0.87043e+00	0.15916e+00	0.24948e+00
0.40000e-01	0.82651e-01	0.44477e-02	0.90723e+00	0.87257e+00	0.32216e+00	0.27044e+00
0.60000e-01	0.12430e+00	0.68441e-02	0.88593e+00	0.87461e+00	0.48892e+00	0.27937e+00
0.80000e-01	0.16561e+00	0.90602e-02	0.86819e+00	0.87326e+00	0.65711e+00	0.28280e+00
0.10000e+00	0.20686e+00	0.11244e-01	0.85044e+00	0.87194e+00	0.82778e+00	0.28325e+00
0.12000e+00	0.24805e+00	0.13396e-01	0.83270e+00	0.87065e+00	0.10009e+01	0.28190e+00
0.14000e+00	0.28918e+00	0.15517e-01	0.81496e+00	0.86938e+00	0.11763e+01	0.27939e+00
0.16000e+00	0.33026e+00	0.17607e-01	0.79721e+00	0.86813e+00	0.13539e+01	0.27607e+00
0.18000e+00	0.37128e+00	0.19665e-01	0.77947e+00	0.86692e+00	0.15337e+01	0.27218e+00
0.20000e+00	0.41224e+00	0.21692e-01	0.76172e+00	0.86573e+00	0.17156e+01	0.26785e+00
0.22000e+00	0.45465e+00	0.24501e-01	0.74043e+00	0.86742e+00	0.19056e+01	0.26318e+00
0.24000e+00	0.49563e+00	0.26540e-01	0.72269e+00	0.86622e+00	0.20919e+01	0.25820e+00
0.26000e+00	0.53836e+00	0.29518e-01	0.70139e+00	0.86776e+00	0.22872e+01	0.25297e+00
0.28000e+00	0.58133e+00	0.32625e-01	0.68010e+00	0.86920e+00	0.24853e+01	0.24748e+00
0.30000e+00	0.62668e+00	0.37012e-01	0.65526e+00	0.87308e+00	0.26942e+01	0.24175e+00
0.32000e+00	0.67263e+00	0.41723e-01	0.63042e+00	0.87668e+00	0.29067e+01	0.23575e+00
0.34000e+00	0.72173e+00	0.48133e-01	0.60203e+00	0.88237e+00	0.31318e+01	0.22945e+00
0.36000e+00	0.77191e+00	0.55117e-01	0.57364e+00	0.88757e+00	0.33611e+01	0.22282e+00
0.38000e+00	0.82929e+00	0.65972e-01	0.53815e+00	0.89654e+00	0.36151e+01	0.21578e+00
0.40000e+00	0.89234e+00	0.79882e-01	0.49911e+00	0.90643e+00	0.38858e+01	0.20823e+00
0.42000e+00	0.96617e+00	0.99585e-01	0.45298e+00	0.91844e+00	0.41858e+01	0.20000e+00
0.44000e+00	0.10673e+01	0.13395e+00	0.38910e+00	0.93559e+00	0.45542e+01	0.19075e+00
0.46000e+00	0.13086e+01	0.24376e+00	0.24714e+00	0.96597e+00	0.52174e+01	0.17936e+00

form. It shows the load deflection behaviour of a toroidal inflatable arch structure subjected to the uniform line load Q with zero load eccentricity and with the initial central half-angle $\theta_o = 1.818$ and the structure radius $\overline{R}_o = 6.5$. The analytical results are plotted for the different values of the membrane flexiblity parameter SP. As can be seen, the load deflection relationship is highly nonlinear, typical of the snap-through systems with the 'limit load' point. The reader should note that the load deflection curves do not show the linear part of the deflections corresponding to the state of the membrane before wrinkling. The zero displacement corresponds therefore to the load causing the first wrinkling of the membrane leading later on to the formation of pneumatic hinges. The theoretical model predicts that the load carrying capability extends beyond the first wrinkling load and that the stiffness of the hinge membrane significantly influences the value of the ultimate or critical load of the structure as well as the stability behaviour. As the flexibility of the membrane increases the value of the critical load decreases. Also the stability behaviour undergoes some changes. With the flexible membrane the region of stable behaviour is larger than when the membrane is stiffer and corresponds to the moderate slope of the load deflection curve. This suggests that if the hinge membrane is stiff the arch structure experiences a much higher degree of instability than if the hinge membrane is flexible. This phenomenon can easily be observed when Fig. N1 and Fig. N2 are compared. The solid line on both figures corresponds to the perfectly stiff or inextensible hinge membrane. For such structures the value of the critical load is the highest of all the membranes and the structure is unstable over the entire region of vertical deformation. However, if a

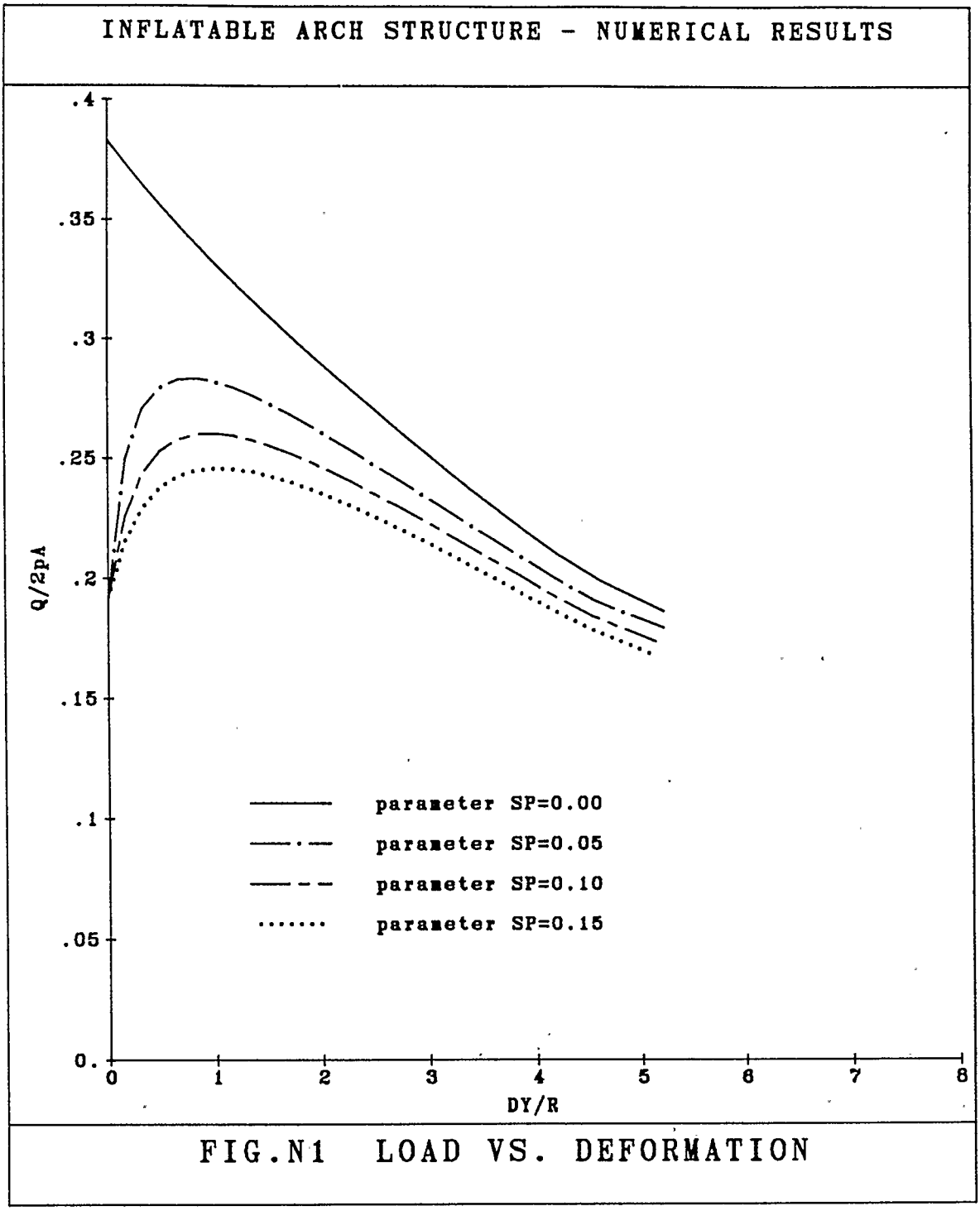

FIG.N1 LOAD VS. DEFORMATION

Relationship for large values of parameter SP and central half angle θ_o = 1.818 rad.

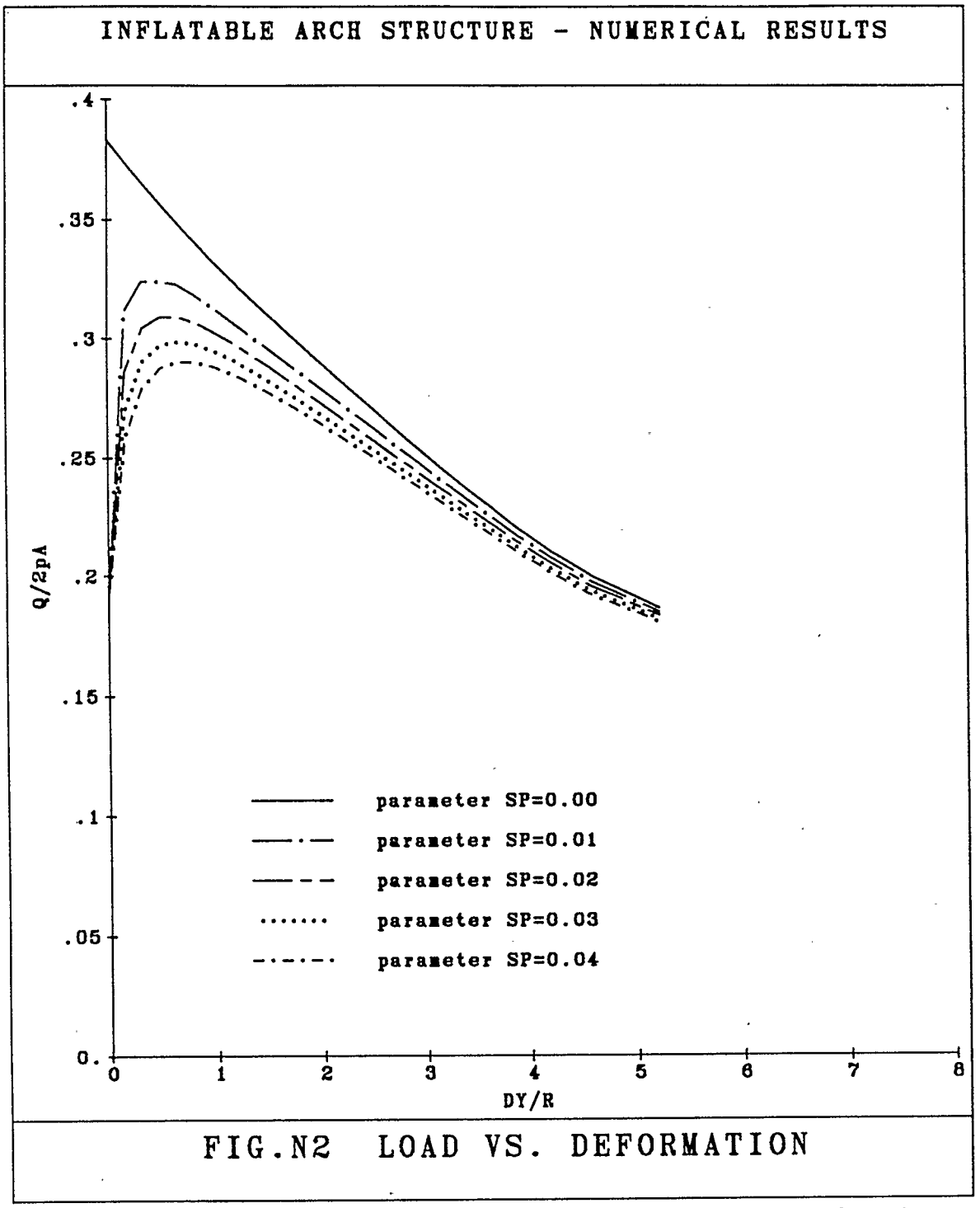

FIG.N2 LOAD VS. DEFORMATION

Relationship for small values of parameter SP and central half angle θ_o = 1.818 rad.

small extensibility of the membrane is admitted, the value of the critical load drops rapidly by some 12% for the flexibility parameter SP = .01. Further increase of the flexibility parameter by .01 does not correspond to the same ratio of decrease of the value of critical load which means that this relationship is nonlinear. Theoretical analysis indicates that the arch structure is vertically stable over the vertical displacement range up to the "ultimate load" point on the load deflection curve. After that the structure is vertically unstable. Furthermore, if the flexibility of the hinge membrane is low even a very small change in the membrane stiffness may significantly reduce the critical load as well as the load carrying capacity of the structure. This nonlinear effect slowly diminishes as the vertical displacement ΔY continues to increase.

CHAPTER 6

TESTS ON A SMALL SCALE MODEL

6.1 MODEL DESCRIPTION

In designing the apparatus and deciding on the appropriate procedures, the assumptions and conditions used in the analytical work had to be considered. The theoretical model used is an inflatable toroidal membrane of circular cross-section with the ends fixed in the support. Thus, the model had to be either a circular hose or, for all practical purposes, made of a couple of circular hoses. The membrane at the support has to be permanently attached to it which can easily be built into the model by raising the inside part of the support above the floor which was represented by a sheet of stiff foam. Finally, the membrane was assumed to be inextensible except in the localized area of high tension where the pneumatic hinges are developed. The membrane was also assumed to be weightless, an assumption which had some consequences, particularly at low inflation pressures. This point will be discussed when comparing the experimental results with the analytical predictions.

From experience in previous experiments on the ponding instability of cylindrical and spherical inflatable structures [16,24], it was decided that it would be easier to keep the line load constant for a particular experiment and to decrease the pressure thereby establishing the critical internal pressure.

The model used was assembled from toroidal segments establishing a formation of four cylindrical shells, Fig. 25. Each shell was made of 18 subsegments to conform to a circular shape

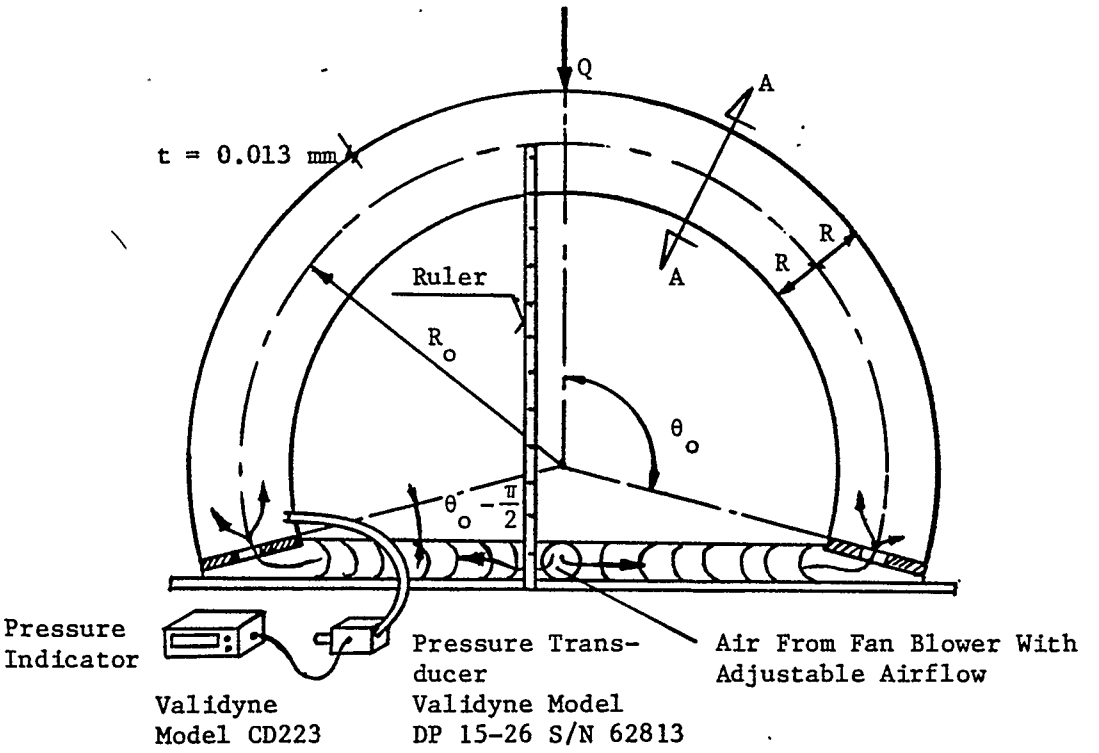

A-A

Dimensions in [mm]

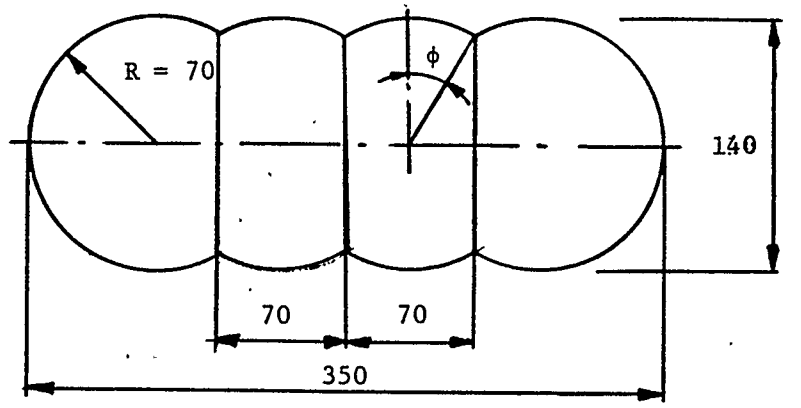

The cross section area is given by:

$$A = [\pi + 3\ (2\phi + \sin\phi\cos\phi)]\ R^2$$

Fig. 25 Experimental Model Setup and Geometry

as close as possible. The membrane material was .5 mil microwave plastic film, of which the modulus of elasticity obtained from a tension test was found to be E = .429 GPa. Segments were connected by hot-ironing them together with the help of a set of contoured forms. Although extreme care was taken during the assembly process to join all the pieces precisely the final membrane structure was not free from assembly-imposed wrinkling. This was the main reason for using a semi-empirical function to describe the transition effect instead of the relationship shown in Fig. 21.

After final assembly the arch structure was inflated and the geometry was measured. The central radius was R_o = .495 m, the membrane radius R = .07 m and the central half angle θ_o = 1.818 rad. Support for the membrane was achieved by clamping a certain portion of the circumference around shaped to the cross-section of the membrane boards of rigid foam which had been fixed to the floor at an angle $\theta_o - \pi/2$. The structure was inflated by a fan blower with adjustable air flow providing appropriate inflation pressure through a .114 m (4.5 in) diameter expandable hose, connected to the base structure. The air entered the inflatable membrane arch on each side of the structure through .049 m diameter air inlet holes.

The pressure was monitored by means of a Validyne pressure transducer, Model No. DP 15-26, with a pressure range from 0.-3.25 kPa. The transducer was connected to a Validyne Model CD233 pressure readout box, displaying the pressure to within an accuracy of 1.10^{-4} kPa. While monitoring the pressure, it was connected to a transducer flexible tube running from the inlet placed on the base level of the structure as shown in Fig. 25.

The line load was made out of plastic hose .23 m long and filled with sand. Vertical displacement was measured using a standard metric ruler with an accuracy of 1 mm.

6.2 TESTING PROCEDURE

The main objective of the test was to establish the load-deflection relationship and to compare it to the theoretical prediction. Another objective was to test if the structure was pressure sensitive by repeating the experiment for different values of line load Q. It was also interesting to check how the application of the line load influenced the shape of load deflection curve and to observe the hysteresis effect during pressure reversal.

The structure was initially inflated by means of the caged-fan blowers to a pressure well above the first wrinkling pressure. The line load was placed on the top surface in line with the apex of the structure. All experiments consisted of slowly decreasing the pressure and recording the displacement of the bottom surface of the structure just below the line load. At the same time the internal pressure was recorded and the overall displacement mechanism, as well as the severe deformations of the membrane at the point of application of the load, was observed. The pressure was decreased until the structure touched the floor, then the pressure was increased and the experiment started in reverse order.

Next the load was glued by means of self-adhesive tape to the bottom surface in line with the apex of the structure. This was done to prevent severe membrane deformations due to sinking of the load in the inflatable hinge. The experiment was repeated again with smaller values of the load.

6.3 EXPERIMENTAL RESULTS

The data obtained from the tests on the small-scale model described above are presented in non-dimensional form in Figures T1-T4. The points on Fig. T1 and Fig. T2 are obtained for the line load $Q = 2.87$ N while the points on Fig. T3 and Fig. T4 are obtained for $Q = 2.286$ N and $Q = 1.256$ N respectively. As can be seen, the load deflection behaviour is highly nonlinear. There is significant "hysteresis effect" corresponding to reversing the direction of the vertical displacement of the load. This behaviour can be explained if we look more closely into the overall deformation mechanism of the inflatable arch structure. As mentioned in Chapter 2, when the pressure drops below the first wrinkling pressure, the arch structure breaks into circular segments described by angles γ_1, γ_2 connected by inflatable hinges described by angles α_1, α_2, α_3. Formation of each inflatable hinge requires, firstly, severely wrinkling the membrane and, next, pushing it inside the inflatable hinge. This happens in the plane of wrinkling of the inflatable hinge. This behaviour corresponds to a resistance force in the direction opposite to the direction of the deformation of the hinge and can be considered as a frictional force. This force, when the load is going down, is supportive thus increasing the load-carrying capacity of the arch structure and when the load is going up, it does just the opposite, leading to the "hysteresis effect" on the load-deflection plot.

The post first wrinkling load-deflection behaviour of the inflatable arch structure shows the typical characteristic of snap-through instability with the "limit point", i.e. the highest point on the load deflection curve. There are three distinct regions of

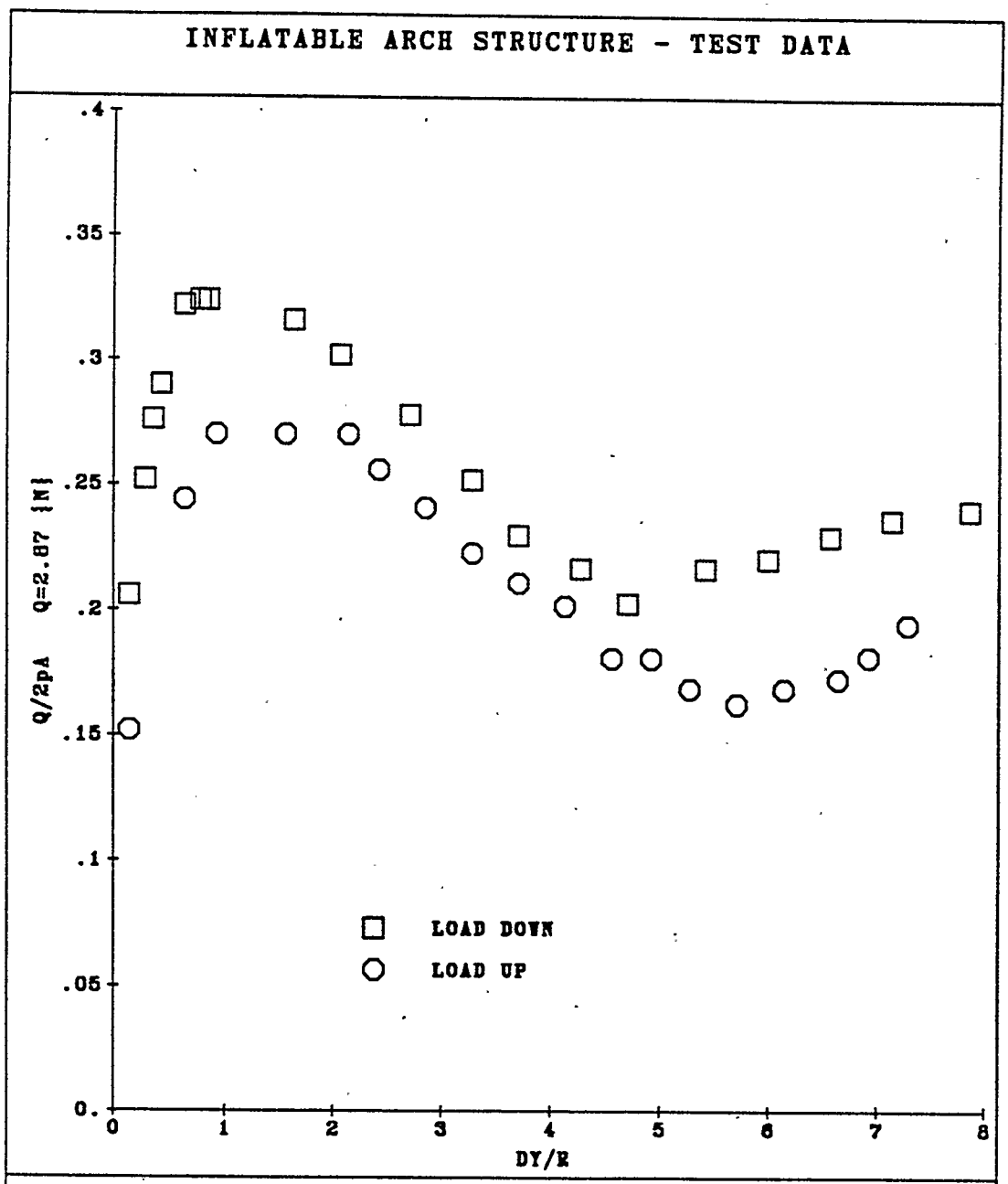

FIG.T1 LOAD VS. DEFORMATION

First trial, apex load Q = 2.87 N
Central half angle θ_o = 1.818 rad

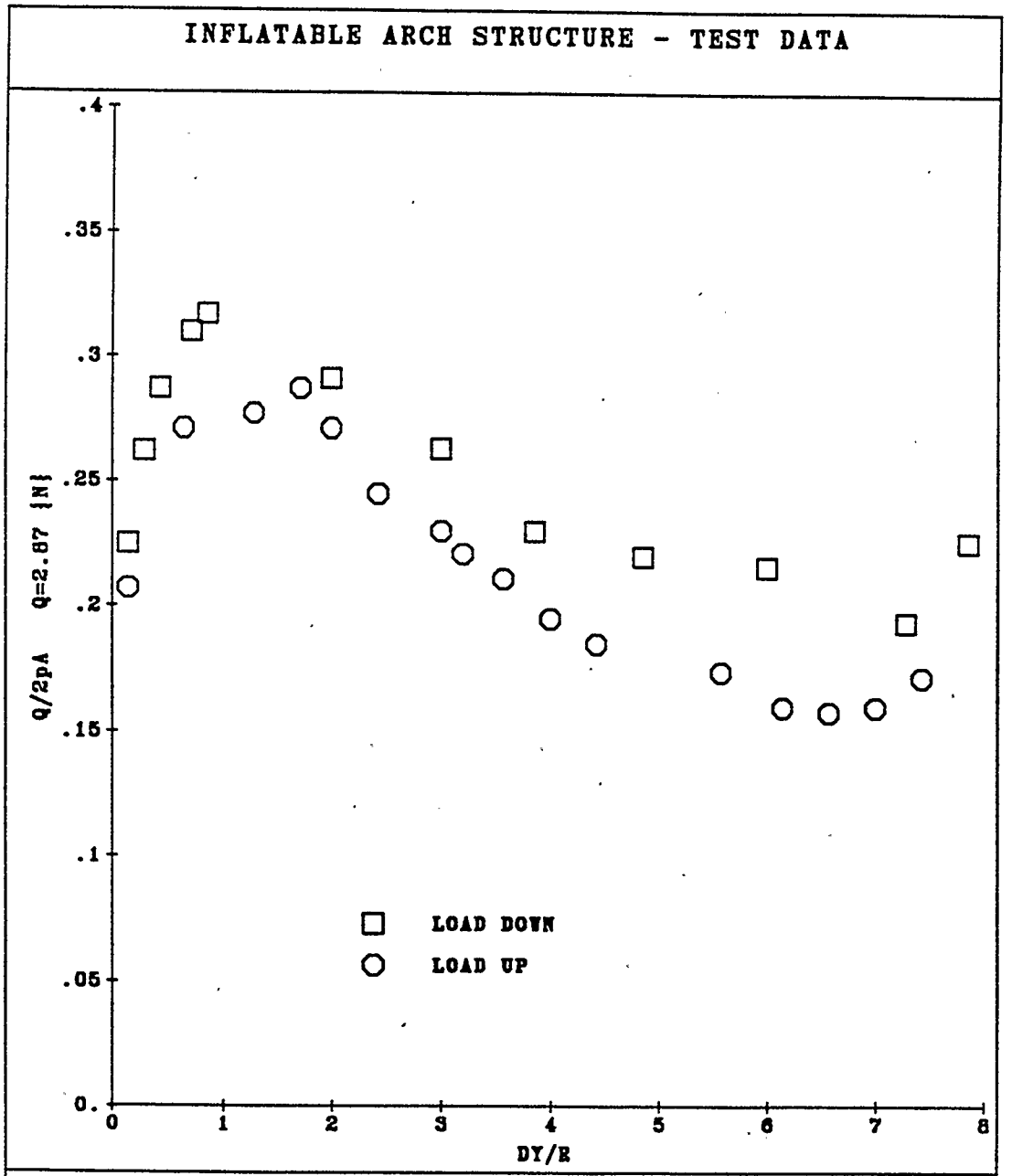

FIG.T2 LOAD VS. DEFORMATION

Second trial, apex load Q = 2.87 N
Central half angle θ_o = 1.818 rad

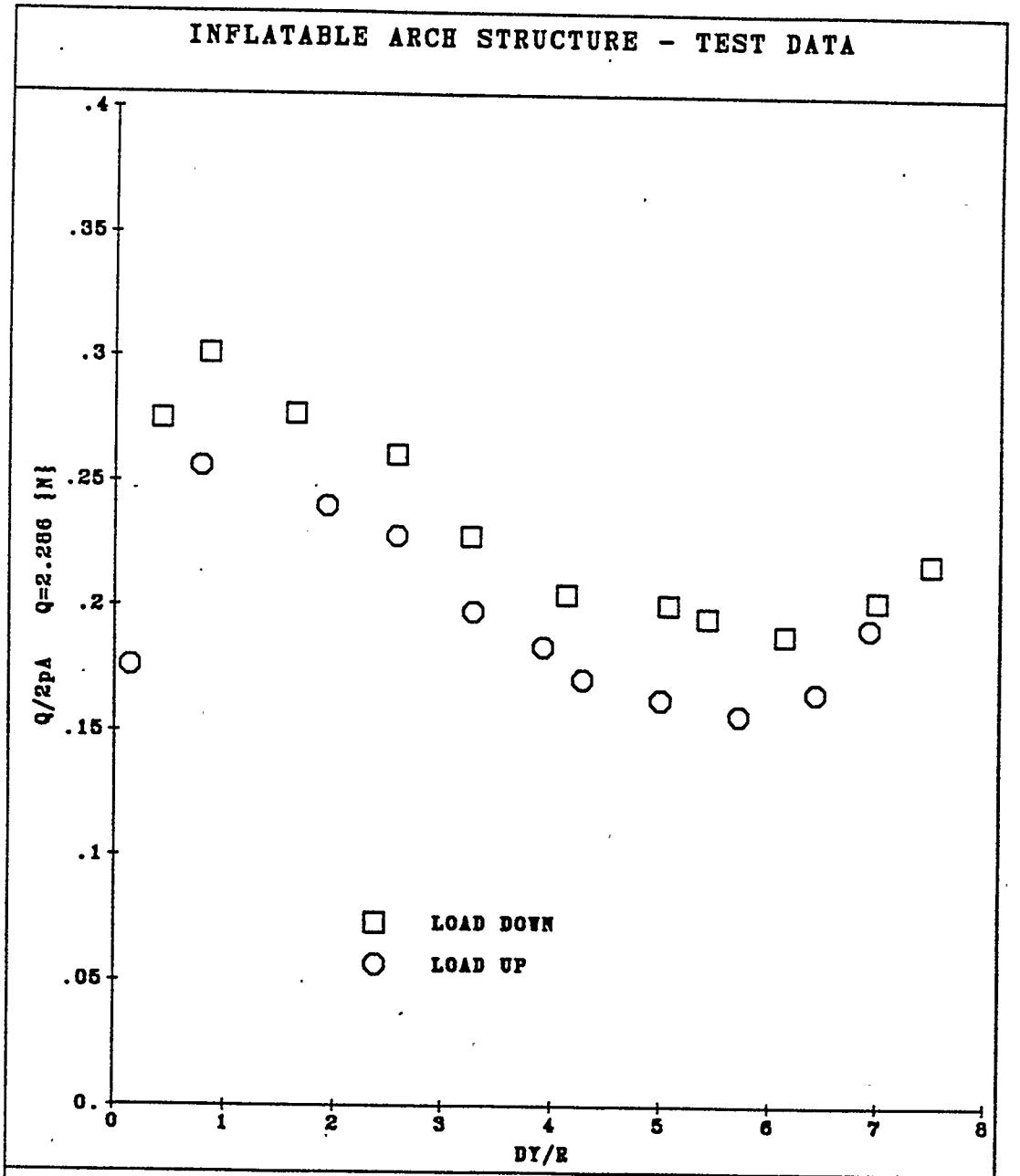

FIG.T3 LOAD VS. DEFORMATION

Third trial, apex load Q = 2.286 N
Central half angle θ_o = 1.818 rad

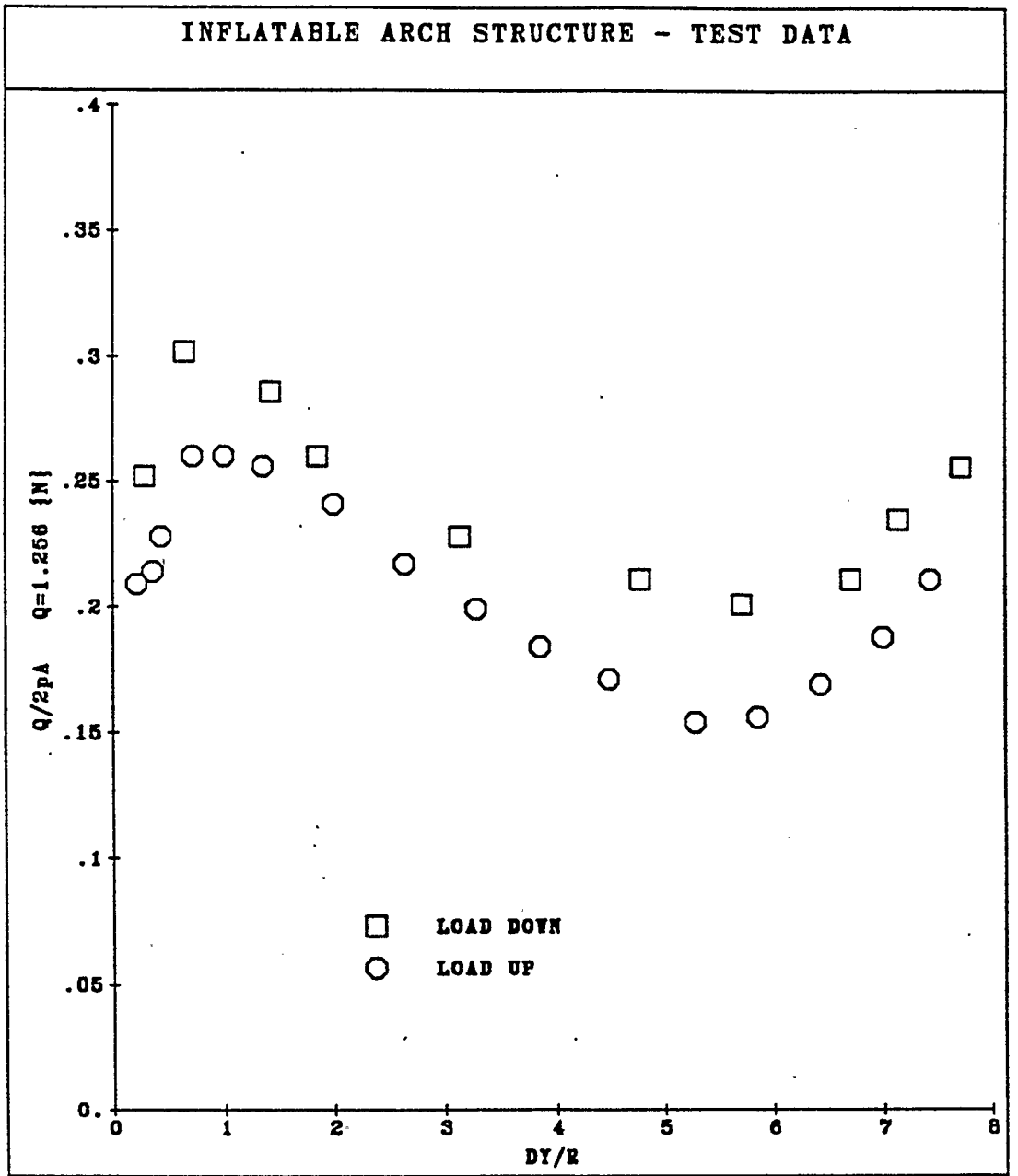

FIG.T4 LOAD VS. DEFORMATION

Fourth trial, apex load Q = 1.256 N
Central half angle θ_o = 1.818 rad

stability closely related to the state of deformation of the inflatable hinges. The first one can be attributed to the "transition effect" experienced by the pneumatic hinge made of extensible membrane. In this region the structure is stable. The load-carrying capacity grows rapidly followed by the small vertical displacement of the structure up to the "ultimate load" or "critical load" which is about 50% higher than the first wrinkling load. Second, the unstable region of the load-deflection curve is when the pneumatic hinges are developed and this corresponds to the vertical displacements in the range of DY = 1÷5.5. Finally, the structure becomes stable again as the pneumatic hinges (mostly hinges described by angle α_2, α_3) become severely squashed and wrinkled thus contributing to the overall change of the geometry of the structure. At this point, another type of instability of the arch membrane was observed. The pneumatic hinge depicted by the angle α_2 not only deformed angularly but also moved circumferentially in a downward direction to the new stable position which can be seen by comparing Plate 3 with Plate 4. In Plate 4 the right vertical segment of the structure is relatively shorter than the same segment shown in Plate 3. This behaviour of the inflatable hinge has not been included in the theoretical analysis.

Comparing the value of the non-dimensional critical load for the arch structure with different values of the applied control load Q, Fig. 1 and Fig. 4, it can be seen that the structure is, to a certain degree, inflation pressure dependent. The difference in the "ultimate load" value is about 7%. This, however, can be attributed to the "softening effect" of the structural wrinkles of the arch membrane.

Another factor to be considered is the weight of the membrane.

Fig. 26 "Overlapping Effect" of Hinge Membrane

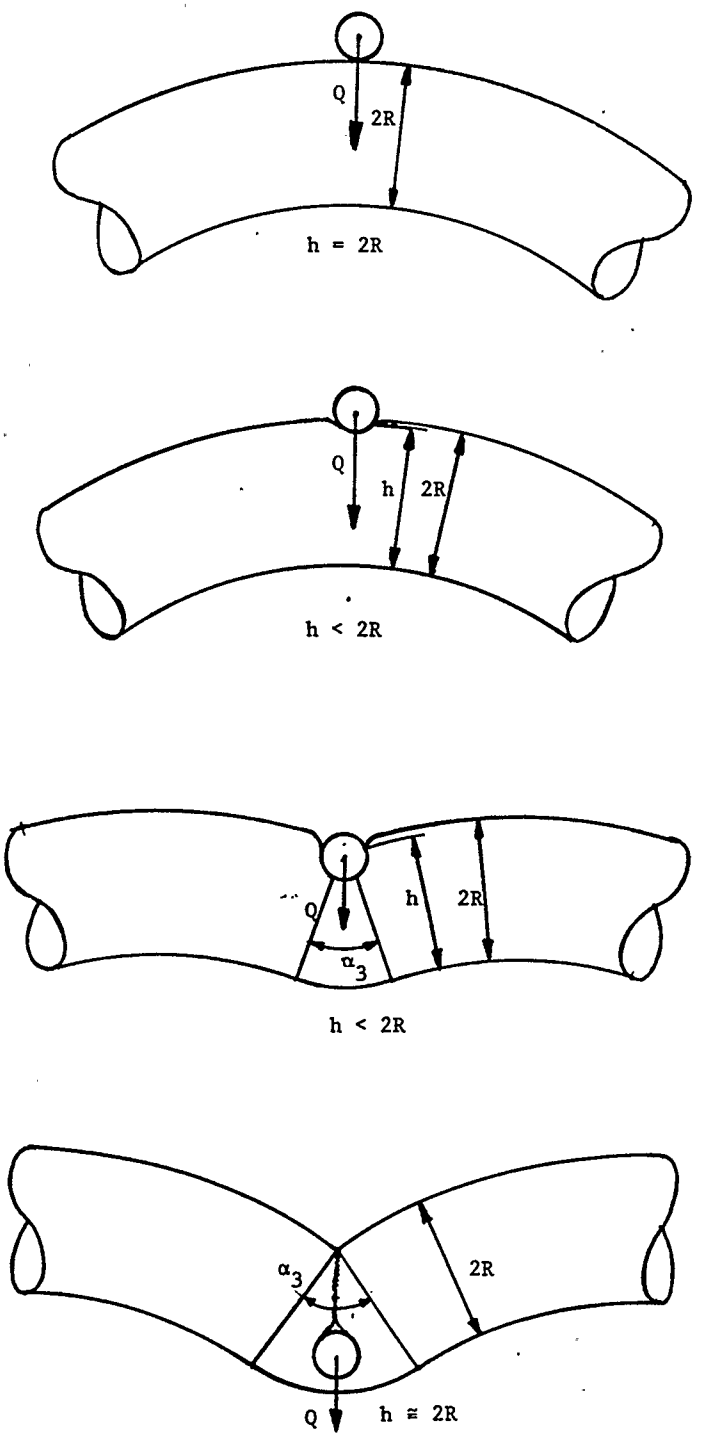

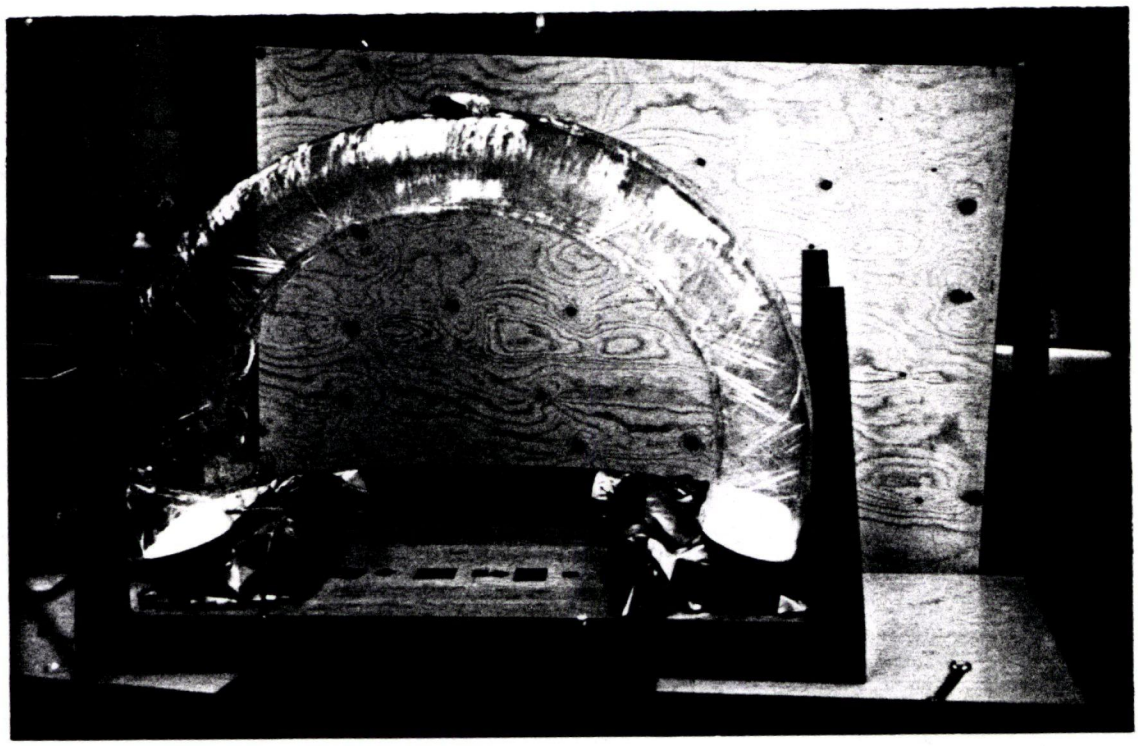

PLATE 1: Experimental Set-up - Membrane Fully Inflated.

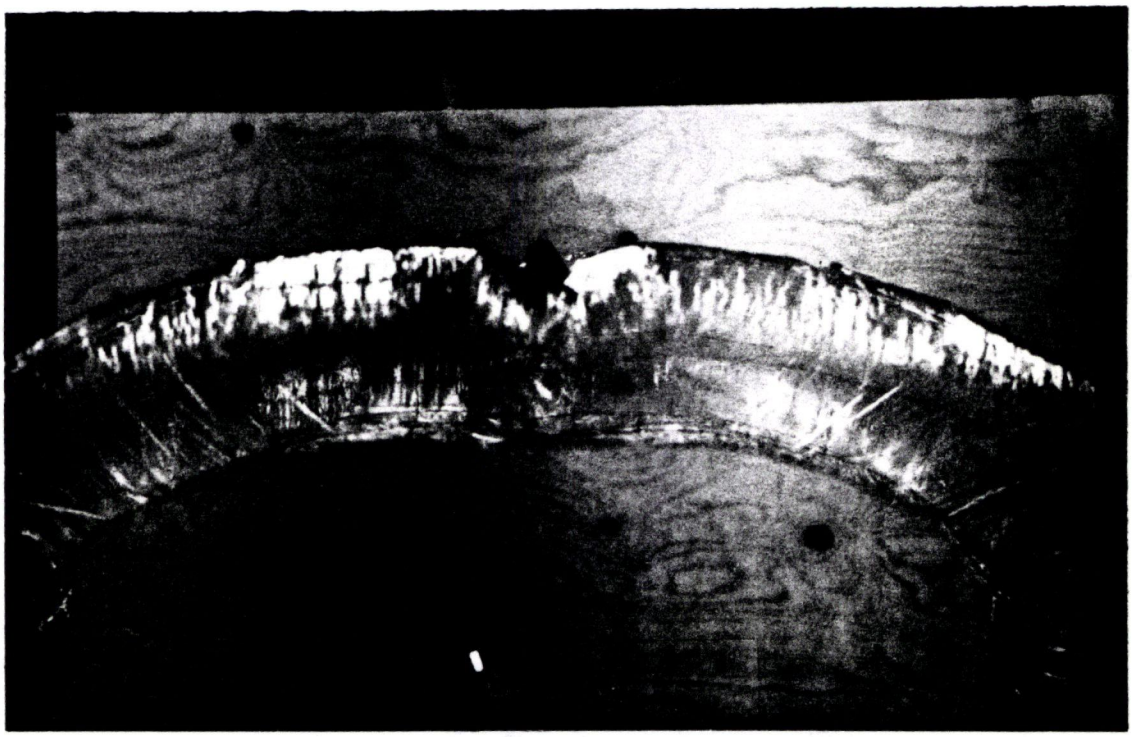

PLATE 2: "Overlapping Effect" - Localized Deformations of Upper Surface of the Arch Structure.

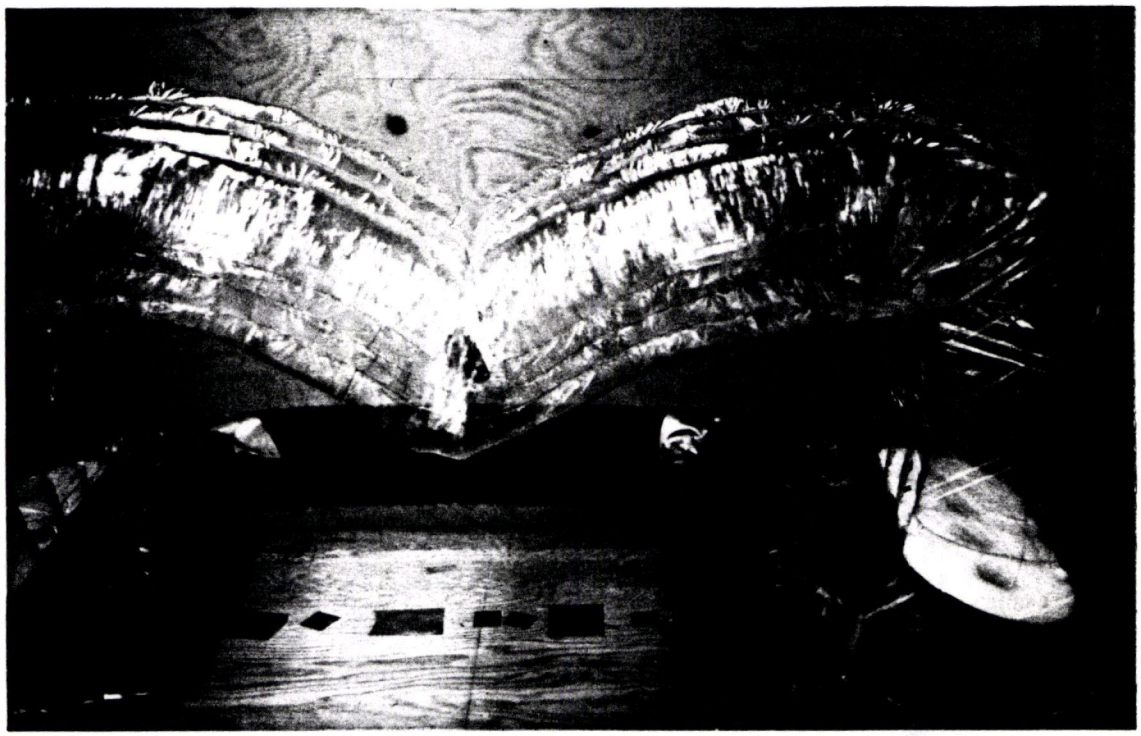

PLATE 3: "Overlapping Effect" - Applied Load Submerged in the Pneumatic Hinge, $\overline{\Delta Y} \cong 3.5$.

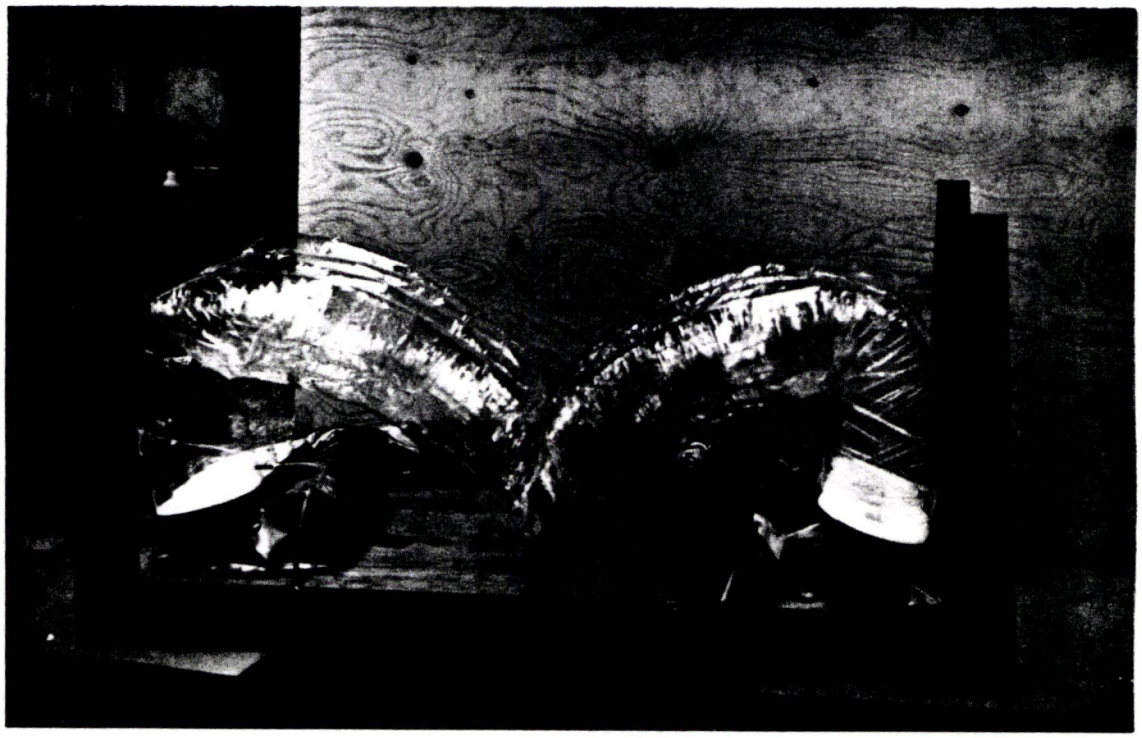

PLATE 4: Inflatable Arch Structure - Very Large Vertical Deflection $\overline{\Delta Y} \cong 7.5$.

For small values of the load the influence becomes more pronounced when the experimental non-dimensional load $\bar{Q}$ is calculated. The inflation pressure required to support the uniformly distributed weight of the membrane and the load Q is higher than the pressure needed to support the load Q only. Since the pressure parameter is in a denominator the net effect on the experimental load displacement curve is such that the experimentally calculated value of the parameter $\bar{Q}$ is lower than the one calculated theoretically.

Peculiar behaviour of the membrane was noted when the load Q was applied to the top surface of the structure. When the inflation pressure was decreased the tension of the top surface of the membrane rapidly disappeared due to the action of the apex bending moment. This caused the load Q to descend into the membrane even before the first wrinkling moment occured. When the pressure continued to drop, the pneumatic hinge at the apex of the arch developed and the load Q slid with the rest of the wrinkled membrane inside the hinge where it was totally enclosed by the membrane. This initial displacement of the load decreased the apex cross-section of the membrane, thus the value of the pressure moment decreased. The net effect in the load-displacement curve is that the membrane appears to be made of more flexible material. This phenomenum is evident until the load is totally submerged in the membrane. It has been found from experiment that the critical load is smaller by about 10% than that when the load is applied to the bottom surface of the arch structure. One may expect a much higher percentage of "ultimate load" drop but, because of the "overlapping effect" of the membrane wall, the working cross-section of the membrane is only slightly smaller than the initial cross-section of the inflatable hinge.

This is schematically depicted in Fig. 26 and can be seen in Plates 1-4. It can be deduced that, as the body of the load Q becomes more "flexible", the "overlapping effect" will be stronger, thus improving the load-carrying capacity of the structure. This localized unstable behaviour of a double-surface inflatable structure under bending and axial force subjected to a point load needs further theoretical as well as experimental work.

CHAPTER 7

DISCUSSION OF RESULTS

7.1 PNEUMATIC HINGE MODEL

The analytical predictions of the geometry of the inflatable hinge are compared to the geometry of the test model presented in [25] and are shown in Fig. 27a-d and Fig. 28. The experimental model was constructed using thin polyethylene membrane and was covered by a rectangular grid of lines, so as to be able to photograph the deformed configuration of the model as well as to observe and measure the shape and extent of the wrinkled region. In Fig. 27 the radius shown by the solid line was drawn to scale obtained from the theoretical analysis (see Table 2), where the dashed line describes the experimental radius drawn so as to conform closely to the shape of the experimental model. As can be seen in Fig. 27a, b, for the small and moderate values of angle α_i the theoretical predictions regarding the non-dimensional radius parameter $\bar{R}_{\alpha i}$ are too high. Since the theoretical and experimental values of the deformation angle α are the same, the theoretical value of parameter $\bar{b}$ describing the flatness of the tensioned section of the hinge in a wrinkling plane is smaller than the one obtained from the experiment. Therefore, the analytically calculated cross-section area, as well as the pressure moment, have lower values than found in the real pneumatic hinge. When the deformation angle becomes larger the divergence between the theoretical and the experimental predictions quickly disappears, see Fig. 27c, d. Here the analytically predicted shape agrees very well with the experimental one. The disagreement between the theoretical and experimental results for the small values of

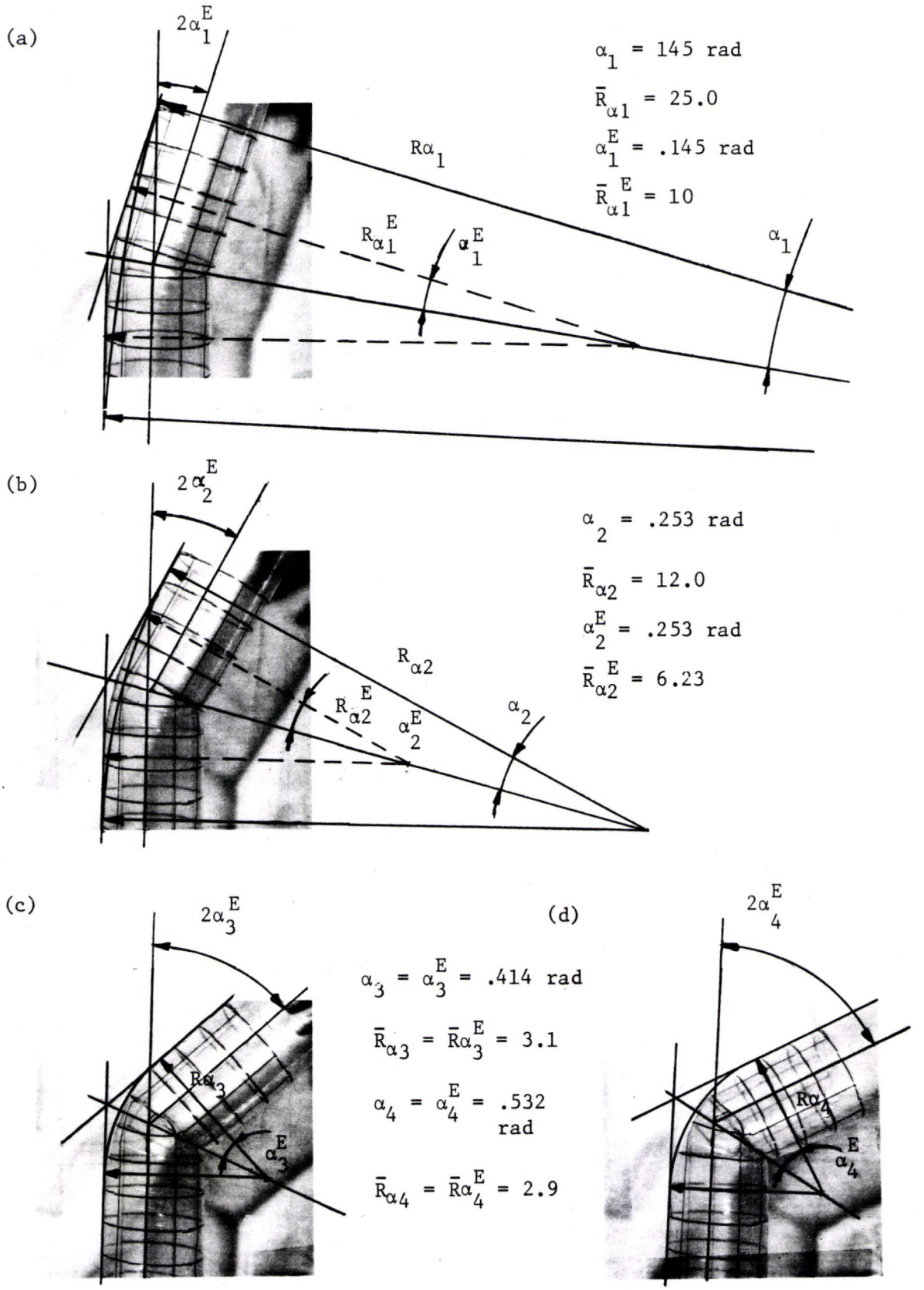

Fig. 27 Inflatable Hinge-Geometry Comparison [25] ⟵ Theoretical Radius
⟵----- Experimental Radius, E - experimental

the hinge deformation angle α may be attributed to either too simple parametric description of the geometry of the theoretical model or, more likely, to the numerical convergence difficulties due to residual errors of calculated integrals coupled with the "flat shape" of the total potential function $\bar{W}$ in the vicinity of the minimum of the function. Nevertheless, the geometrical parametric model presented here explains two important relationships: (1) how the pressure moment of an initially cylindrical membrane changes with respect to the angular deformations of the structure and (2) how the cross-sectional deformations of the membrane influence the pressure moment in the wrinkling plane. On the basis of the theoretical and experimental results it is shown that the cylindrical membrane, when subjected to large angular deformations, undergoes substantial cross-sectional deformations but without a significant decrease in the value of the pressure moment. The calculated nondimensional pressure moment minimum value of .77 at an angle $\alpha \cong .2$ (Table 2) seems to be too low and most likely is in the neighborhood of .96. This, however, has yet to be proven by an improved numerical procedure. When the angular deformations are large, i.e. $\alpha >$ .40, the pressure moment is about 5% to 10% below its initial value, $\overline{M_p}$ = 1.0 (Fig. 28). Therefore, a very simple toroidal model of a pneumatic hinge with a constant pressure moment $\overline{M_p} = 1.0$ is quite a good first approximation of the real structure especially when considered in the static approach. The energy approach, based on the total change in volume of the pneumatic hinge, may not be as well suited. A simplified assumption that the change in volume of the pneumatic hinge is a linear function of the deformation angle α may not be justified. At this stage, however, it is difficult to discuss this problem since even the

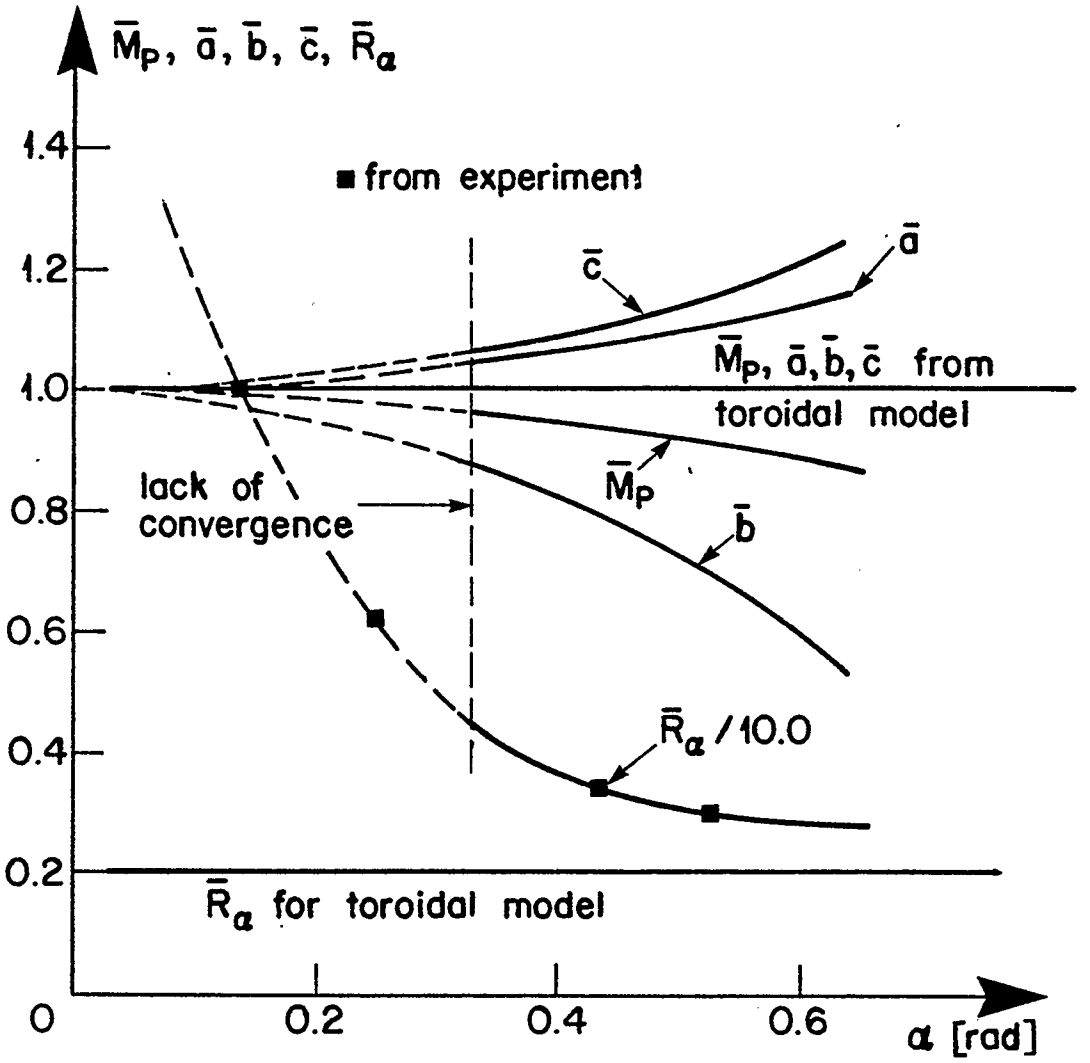

Fig. 28 - Inflatable Hinge - Theoretical Relationships for Different Geometrical Parameters.

solution with a simplified assumption has not been obtained.

7.2 PNEUMATIC ARCH STRUCTURE

The theoretical predictions of load displacement behaviour are compared to the experimental data throughout in Figs. NT1 - NT4. As can be seen, there is a good correlation of results over the vertical non-dimensional displacement interval .0 to 5.2. Particularly, excellent agreement can be observed in the interval 1.5 to 5.2 if the hysteresis effect is taken into account. In this area, for the first set of experimental data initially described by Fig. T1, the flexibility parameter SP can be estimated to be in the range of .02. Following the theoretical load displacement curve of $SP_1 \cong .02$ in the interval .0 to 1.5, we observe that the experimental load deflection curve has shifted in the direction of the increased vertical deformation parameter DY. This behaviour can be attributed mainly to the way the line load Q was applied to the arch structure. Since all the experimental data presented here has been obtained for the load Q applied to the top surface of the arch structure, the "sinking" of the load inside the pneumatic hinge is the main contributor. During this process the applied load Q descends into the hinge body causing a small depression due to local tensional forces, thus locally decreasing the cross-section area of the hinge. This, in effect, decreases the pressure moment M_p, lowers the slope and shifts the load displacement curve to the right, Fig. NT1. Such behaviour stops completely when the applied load is totally overlapped by the hinge membrane, which happens at the vertical displacement $DY \cong 2.0$. This pattern can be seen in all the NT1-4 figures but to a smaller degree in Fig. NT3-4. Evaluating the

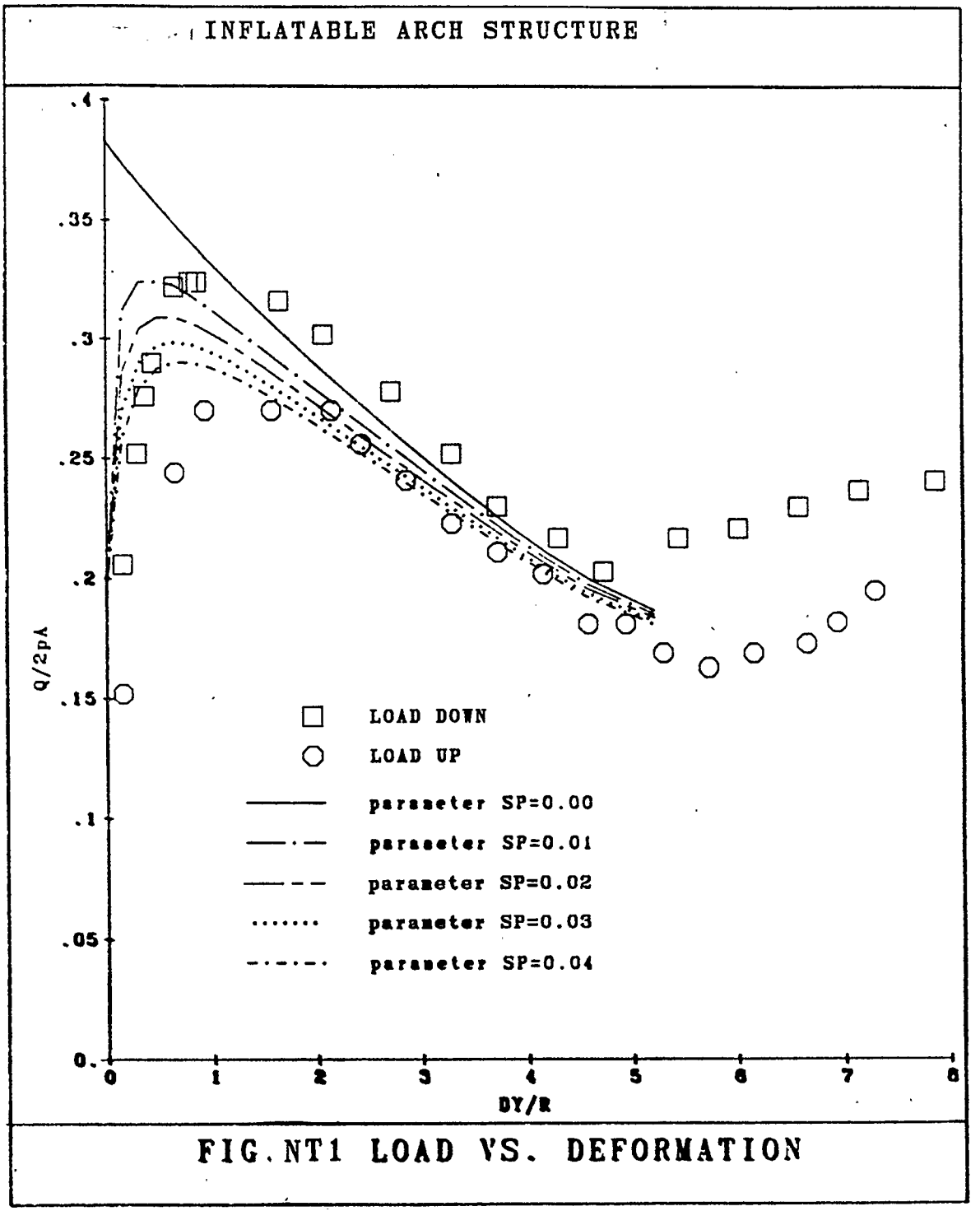

FIG.NT1 LOAD VS. DEFORMATION

Comparison of first set of experimental data to the theoretical predictions, θ_o = 1.818 rad.

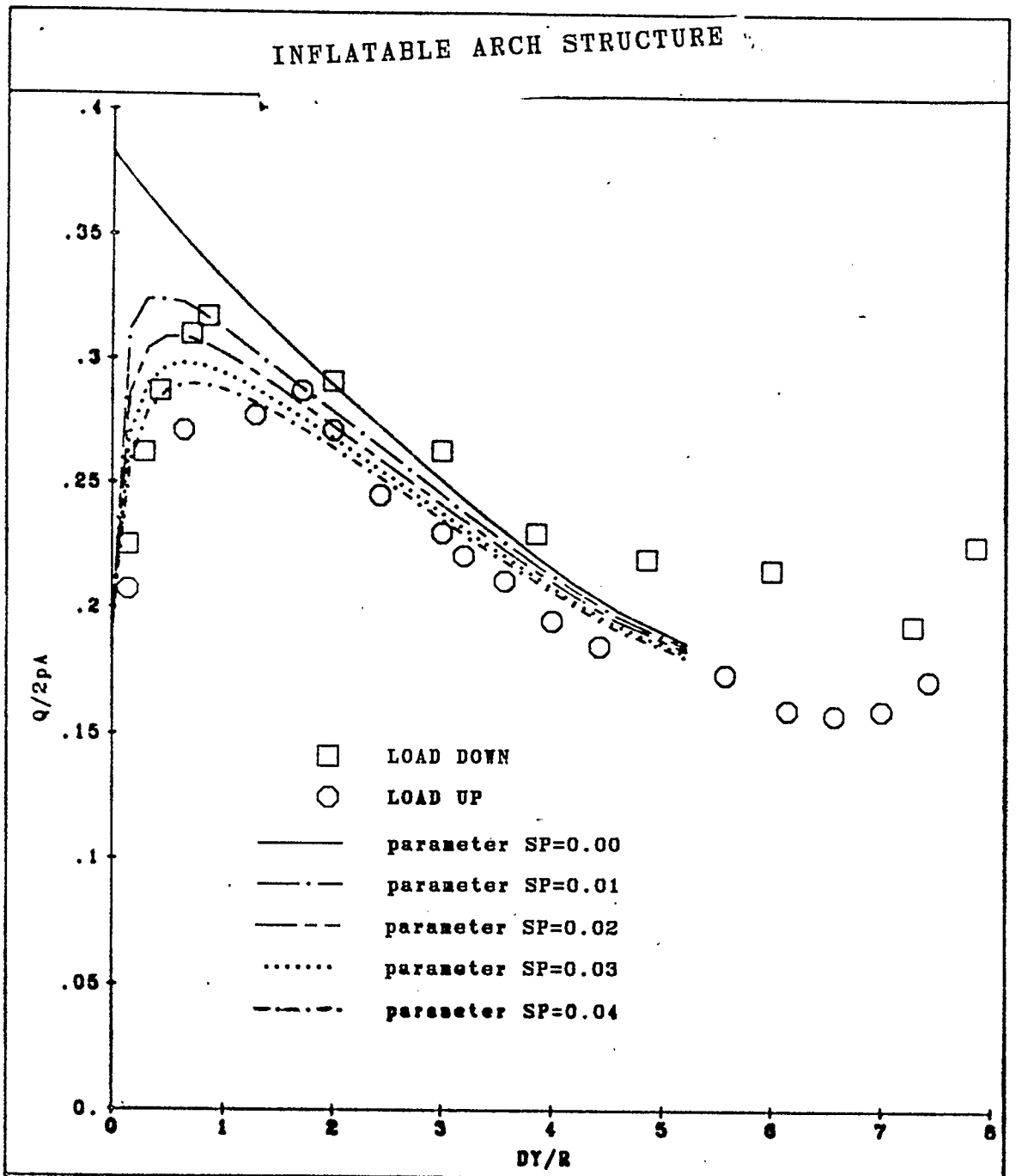

FIG:NT2 LOAD VS. DEFORMATION

Comparison of second set of experimental data to the theoretical predictions, θ_o = 1.818 rad.

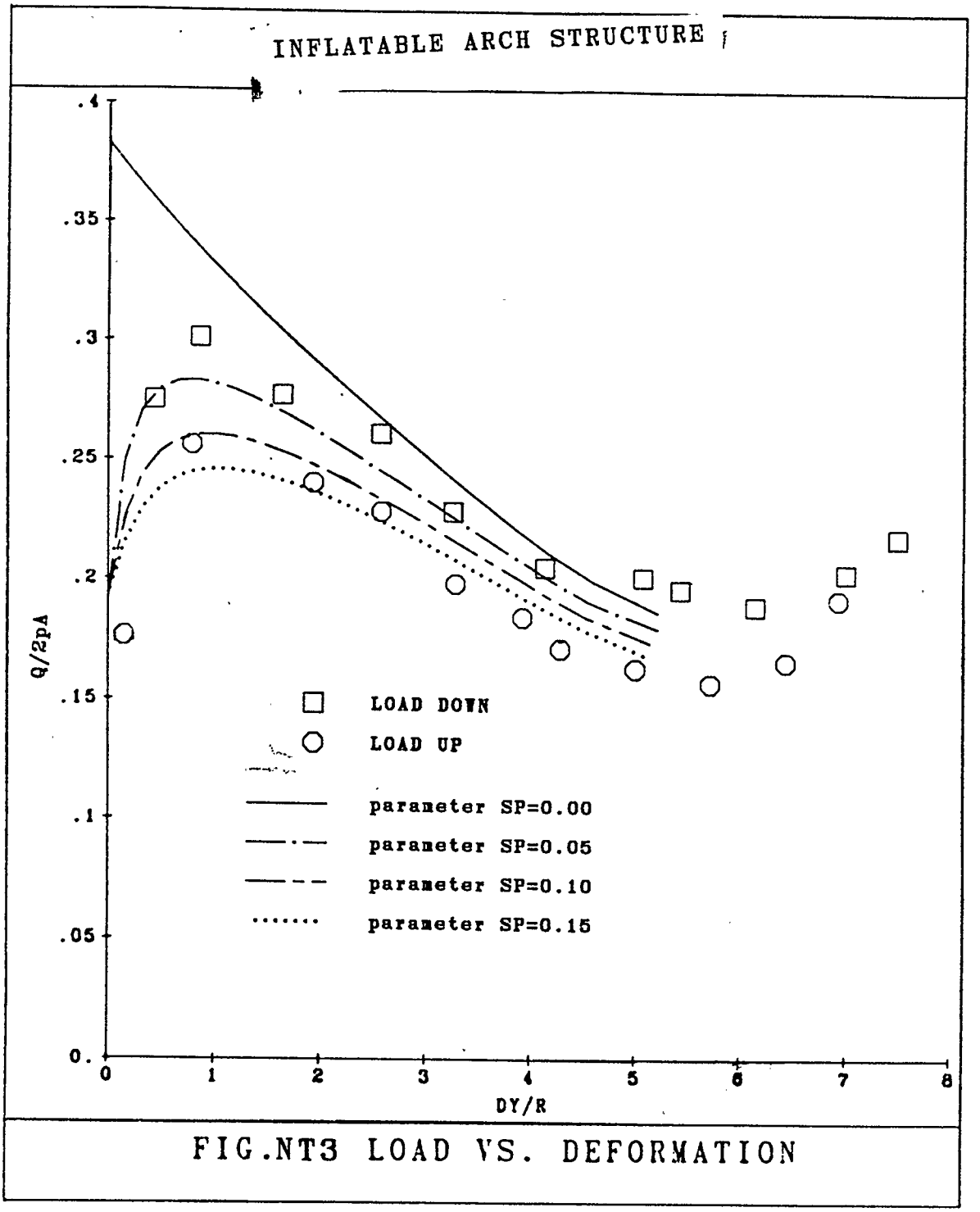

FIG.NT3 LOAD VS. DEFORMATION

Comparison of third set of experimental data to the theoretical predictions, θ_o = 1.818 rad.

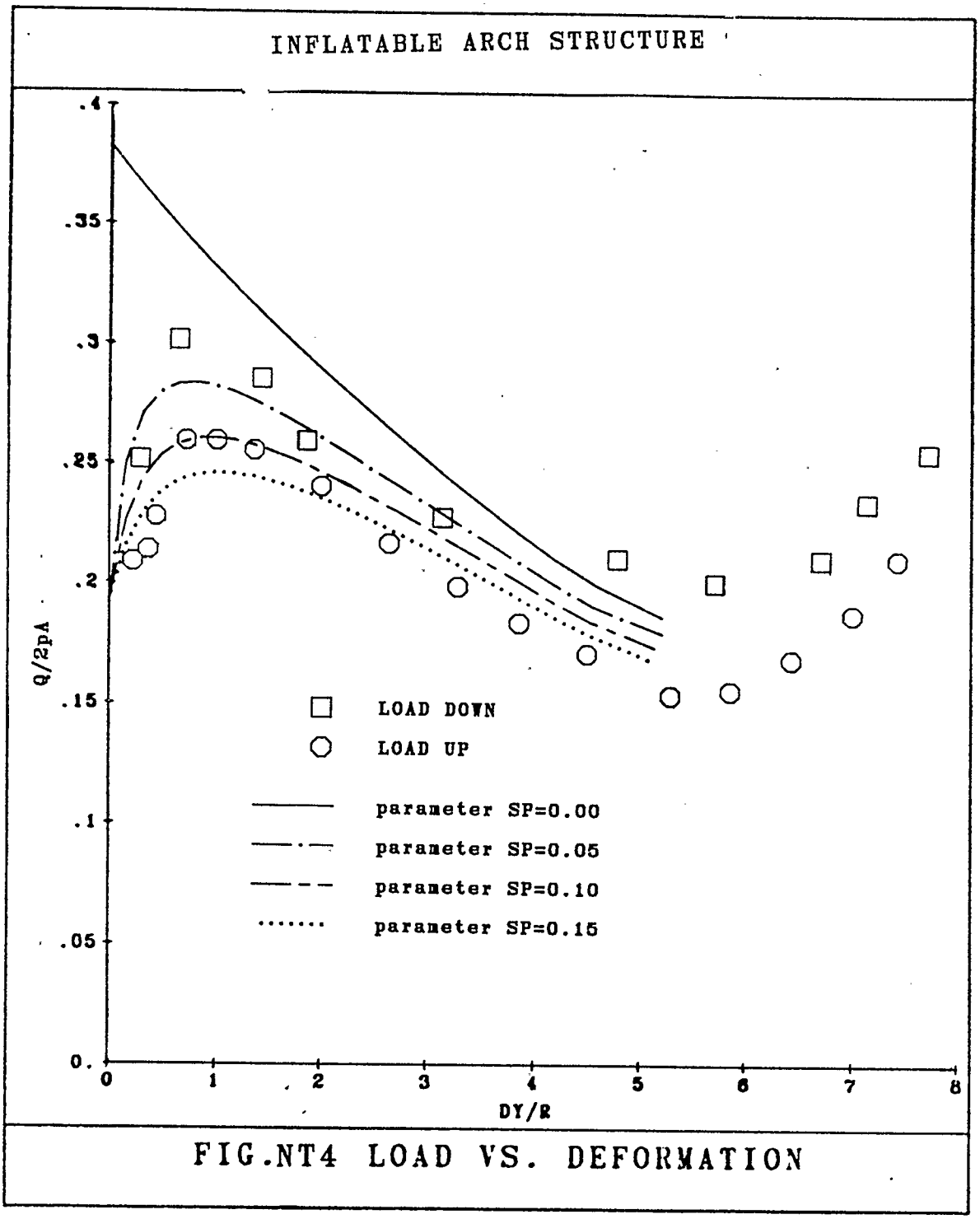

FIG.NT4 LOAD VS. DEFORMATION

Comparison of fourth set of experimental data to the theoretical predictions, θ_o = 1.818 rad.

flexibility parameter SP for different values of the applied load Q, one can arrive at $SP_2 \cong .03$ from Fig. NT2, $SP_3 \cong .06$ from Fig. NT3 and $SP_4 = .08$ from Fig. NT4. This inconsistency of the flexibility parameter in the experimental model can be explained by manufacturing imposed wrinkling as discussed in Chapter 6.

The overall performance of the theoretical model of the inflatable arch structure was very good, especially since the influence of the complex side-effect during the derivation process was not taken into consideration. Thus the way is paved to more exact theoretical analysis.

CHAPTER 8

CONCLUSIONS

The analysis of the large deflection and stability behaviour of a toroidal inflatable arch structure subjected to symmetric uniform line loads has been presented. The formulation is based on the static equilibrium and the geometric relations incorporating the extensibility of the membrane in the localized area of the pneumatic hinge. The results of the analysis are presented in non-dimensional graphical form showing the load deflection curves. The initial geometry is defined by the central half angle θ_o and the ratio of radius R_o versus the membrane radius R. The analysis clearly indicates vertical instability at certain load levels and shows that the failure load is very much influenced by the membrane extensional stiffness in the area of the stress concentration of the pneumatic hinge. The analysis predicts that the load carrying capability extends beyond the first wrinkling load and that the deformation mechanism of the inflatable arch structure is similar to the collapse mechanism of a rigid-plastic frame with developed plastic hinges. The static axial forces have to be considered together with the static bending moments as they significantly influence the overall load carrying capacity of the structure. The experiments show that the shear forces can be neglected, except in the localized areas, where the application of the concentrated load collapses the membrane and changes locally the cross-sectional geometry.

The analysis of the large deformation of the pneumatic hinge model subjected to external bending was also presented. The formulation is based on the minimization of the total potential energy function and

the geometric relations. The formulation admits cross-sectional deflections of the membrane but assumes that the effect of extensibility of the membrane on the overall large deformation relationship to be negligible. The governing equations, although relatively simple in appearance, contain functions which are multi-valued, leading to convergence difficulties.

The results of the analysis presented in non-dimensional form show parameters describing the geometry of the structure in the wrinkling plane and the pressure moment developed by the pneumatic hinge with respect to the hinge angle α.

The analysis indicates that the pressure moment does not change significantly over the investigated angular deformation interval and that the simple toroidal model of deformation of the cylindrical membrane [25] can be successfully applied in the theoretical investigations of cylindrical or double surface toroidal membranes.

The experimental data obtained from tests on a small scale toroidal inflatable arch structure are also presented and compared with the analytical predictions. Good agreement between numerical and experimental results confirm the validity of the theory and assumptions used in its derivations.

RECOMMENDATIONS

The analysis of the large deformation behaviour of an inflatable arch structure can be broadened in several areas. The dead weight of the membrane can be taken into account, thus improving the

theoretical results for a small value of the applied line-load. The theoretical work can also be undertaken to investigate the localized deformation of the apex of the external surface of the arch structure due to the application of the concentrated line-load. The future research could include the side effects of the two other phenomena not apparent at the initial stages of earlier theory development. These are:

- additional work required to wrinkle arch membrane during the development of the pneumatic hinge. It is present because the hinge membrane is not perfectly flexible and is responsible for hysteresis effect on the load deflection curve.
- initial imperfections of the surface of the arch membrane. This factor is most difficult to be established as it is random in nature, from the analytical formulation of the problem results, that the non-dimensional load is independent of the internal membrane pressure. The effect of these imperfections show up as we found from the experiments that the load carrying capability of the arch structure is pressure dependent. For larger internal pressure the arch structure develops higher nondimensional critical load.

Finally, the convergence difficulties encountered in the present work can be reduced by an improved numerical procedure and higher precision of numerical calculations (double precision).

REFERENCES

1. Bulson, P.S., "The Behaviour of Some Experimental Inflated Structures", IASS Ist International Conference on Pneumatic Structures, Stuttgart, May 1967, pp. 68-77.
2. Bird, W.W., "The Development of Pneumatic Structures, Past, Present and Future", IASS. 1st Int. Coloquium on Pneumatic Structures, Stuttgart, May (1967).
3. Geiger, D.H., "U.S. Pavillion at Expo 70 Features Air Supported Gable Roof", Civil Engineering, ASCE, March (1970), pp. 48-50.
4. Glockner, P.G. and Malcolm, D.J., "The Use of Inflatables in Agriculture and Exploration Industry" Proc. CIB and IASS, International Symposium on Air Supported Structures, Venice, Italy, June 1977, pp. 337 - 407.
5. Kinnius, R.A., "The Modern Concept of Air-Supported Structures", CIB/IASS Int. Symposium on Air-Supported Structures, Venice, June (1977), pp. 43-49.
6. Malcolm, D.J. and Glockner, P.G., "Collapse by Ponding of Air-Suppported Spherical Caps", Department of Mechanical Engineering, Report No. 174, The University of Calgary, September (1980).
7. Malcolm, D.J. and Glockner, P.G., "Collapse by Ponding of Air-Supported Membranes", Proc. ASCE, 104, No. ST9, Proc. Paper 14002, September 1978, pp. 1525 - 1532.
8. Malcolm, D.J. and Glockner, P.G., "Ponding Stability of an Air-Supported Spherical Membrane", Proc. Seventh Can. Congress Appl. Mech., CANCAM '79, Sherbrook, P.Q., May 27-June 1, 1979, 1, pp. 135-136.

9. Malcolm, D.J., "Ponding Instability of Air-Supported Cylinders - Some Experimental Results", Department of Mechanical Engineering, Report No. 137, The University of Calgary, December (1978).

10. Oden, J.T., and Kubitza, W.K., "Numerical Analysis of Nonlinear Pneumatic Structures", IASS 1st International Colloquium on Pneumatic Structures, Stuttgart, May 1967, pp. 87-107.

11. Ahmadi, G. and Glockner, P.G., "Collapse by Ponding of Pneumatic Elastic Spherical Caps Under Distributed Loads", Can. J. Civ. Eng., 10, (1983), pp. 740-747.

12. Lukasiewicz, S. and Glockner, P.G., "Ponding Instability of Cylindrical Air-Supported Membranes Under Nonsymmetrical Loadings", J. Struct. Mech., 10(4), (1982-1983), pp. 419-499.

13. Winship, C. and Powell-Jones, O.C., "Investigation of a Cylindrical Inflated Beam-Column Structure", Department of Aeronautical Engineering, Report No. 301, University of Bristol, June 1983.

14. Szyszkowski, W. and Glockner, P.G., "Finite Deformation and Stability Behaviour of Spherical Inflatables Under Axisymmetric Concentrated Loads", Department of Mechanical Engineering, Report No. 253, The University of Calgary, April 1983.

15. Szyszkowski, W. and Glockner, P.G., "Finite Deformation and Stability Behaviour of Spherical Inflatables Subjected to Axi-Symmetric Hydrostatic Loading", Department of Mechanical Engineering, Report No. 254, The University of Calgary, April 1983.

16. Szyszkowski, W. and Glockner, P.G., "Finite Deformation and Stability Behaviour of Spherical Inflatables Under Axisymemtric Concentrated and Hydrostatic Loading", Department of Mechanical Engineering, Report No. 255, The University of Calgary, April 1983.

17. Szyszkowski, W., Lukasiewicz, S. and Glockner, P.G., "Lateral Stability of Symmetrically Loaded Cylindrical Inflatables", Proc. IASS Congress on Spatial Roof Structures, Dortmund, Sept. 1984, 1, pp. 1.3.051-1.3.082.

18. Szyszkowski, W. and Glockner, P.G., "Finite Deformation and Stability Behaviour of Cylindrical Membranes Subjected to Symmetric Line Loads", Report No. 291, Dept. of Mech. Engg., The University of Calgary, April 1984.

19. Herzog, T., "PNEUMATIC STRUCTURES A Handbook for the Architect and Engineer", Crosby Lockwood Staples, London, (1977).

20. Dent, R.N., "Principles of PNEUMATIC ARCHITECTURE", London, (1972).

21. Frei, O., "Tensile Structures, Volume One, Pneumatic Structures", The M.I.T. Press, Massachusetts Institute of Technology, Cambridge, Massachusetts, and London, England (1969).

22. Frei, O., "Tensile Structures, Volume Two, Cable Structures", The M.I.T. Press, Massachusetts Institute of Technology, Cambridge, Massachusetts, and London, England (1969).

23. "Wandelbare Pneus-Convertible Pneus", Institute for Lightweight Structures (1L12), University of Stuttgart, Germany, (1975).

24. Lukasiewicz, S., Balas, L. and Glockner, P.G., "Stability and Large Deformation Behavior of Nonsymmetrically Loaded Cylindrical Membranes", Journal of Struct. Mech., 14(2), June (1986), pp. 229-254.

25. Lukasiewicz, S. and Glockner, P.G., "Stability of Lofty Air-Supported Cylindrical Membranes", J. Struct. Mech., 12(4), 1984, pp. 543-555.

26. Crandall, S.M., Dahl, N.C. and Lardner, T.J., "An Introduction to the Mechanics of Solids", McGraw-Hill Book Company, USA, (1972).

27. Burden, R.L., Faires, J.D. and Reynolds, A.C., "Numerical Analysis", Prindle, Weber and Schmidt, Boston, Massachusetts, (1981).

28. Gottfried, B.S., "Programming with Fortran IV", Quantum Publishers Inc., New York, (1972).

29. Krolikowski, J. and Steckiewicz, C., "MATEMATYKA wzory, definicje, tablice", Wydawnictwa Komunikacji Lacznosci, Warszawa, (1972).

APPENDIX A

DERIVATION OF GEOMETRICAL PARAMETERS FOR THE PNEUMATIC ARCH STRUCTURE

Derivations of Rotation Angles κ_i of Stiff Segments of the Arch

Angle κ_1 is obtained from the relationship (see Fig. A1)

$$\alpha_1 + \theta_o - \frac{\pi}{2} + \frac{\pi}{2} - \frac{\alpha_1}{2} + \kappa_1 = \pi$$

$$\kappa_1 = \pi - \theta_o - \frac{\alpha_1}{2} . \qquad (A.1)$$

Angle κ_2 is obtained from the relationship (see Fig. A2)

$$\alpha_1 + \theta_o - \frac{\pi}{2} + \frac{\pi}{2} - \frac{\gamma_1}{2} + \kappa_2 = \pi$$

$$\kappa_2 = \pi - \theta_o - \alpha_1 + \frac{\gamma_1}{2} . \qquad (A.2)$$

Angle κ_3 is obtained from the relationship (see Fig. A3)

$$\kappa_3 = \frac{\pi}{2} - \frac{\gamma_2}{2} - \alpha_2 + \frac{\pi}{2} - \frac{\gamma_1}{2} - \kappa_2$$

$$\kappa_3 = \pi - \alpha_2 - \frac{\gamma_1}{2} - \frac{\gamma_2}{2} - \pi + \theta_o + \alpha_1 - \frac{\gamma_1}{2}$$

$$\kappa_3 = \theta_o + \alpha_1 - \alpha_2 - \gamma_1 - \frac{\gamma_2}{2} . \qquad (A.3)$$

Angle κ_3 can also be obtained from the relationship (see Fig. A5)

$$\pi = \kappa_3 + \frac{\pi}{2} + \alpha_3 + \frac{\pi}{2} - \frac{\gamma_2}{2}$$

$$\kappa_3 = \frac{\gamma_2}{2} - \alpha_3 . \qquad (A.4)$$

Angle κ_4 is obtained from the relationship (see Fig. A4)

$$\kappa_4 = \frac{\pi}{2} - \frac{\alpha_3}{2} - \frac{\pi}{2} + \alpha_3$$

$$\kappa_4 = \frac{\alpha_3}{2} . \qquad (A.5)$$

The continuity condition of the inside surface of the arch structure is given by

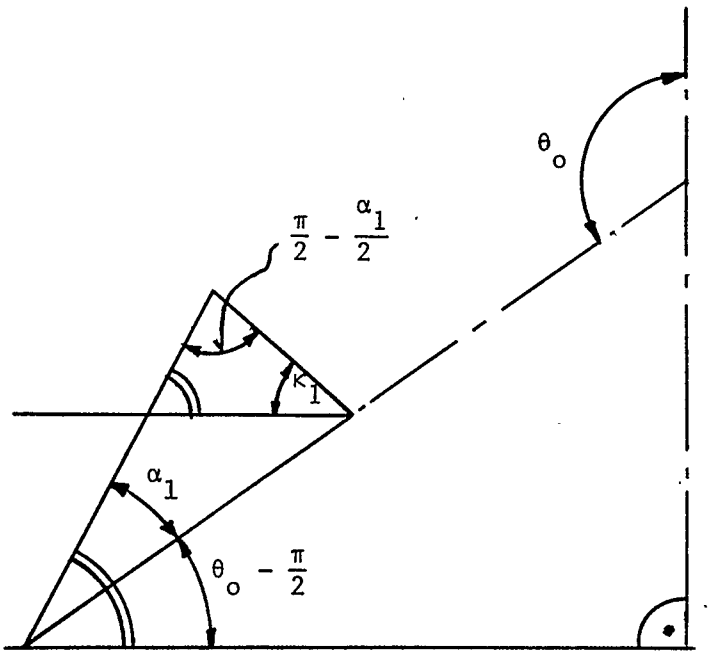

Fig. A1 Geometry for κ_1 Derivation

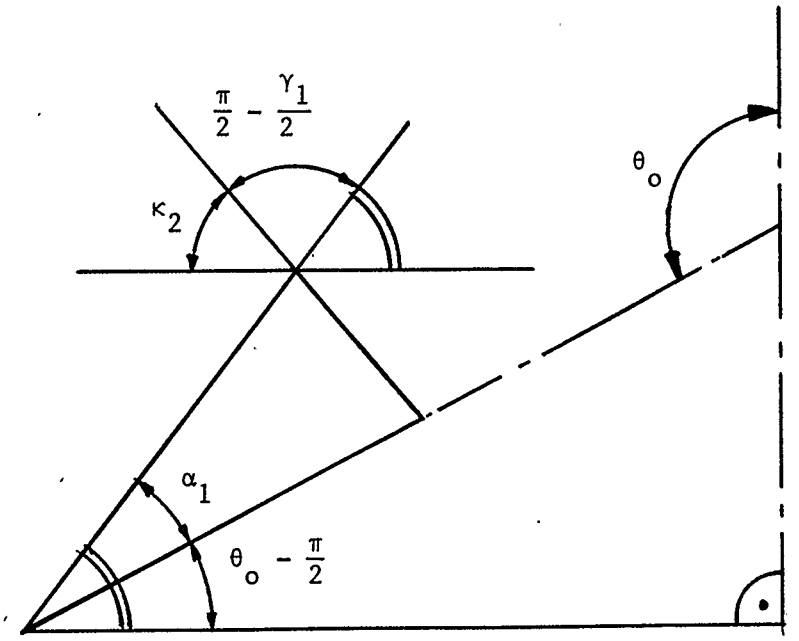

Fig. A2 Geometry for κ_2 Derivation

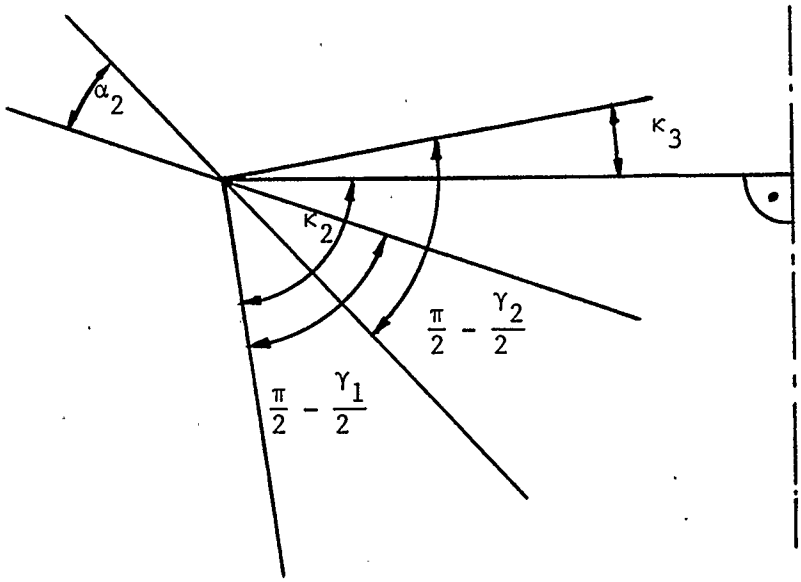

Fig. A3 Geometry for κ_3 Derivation

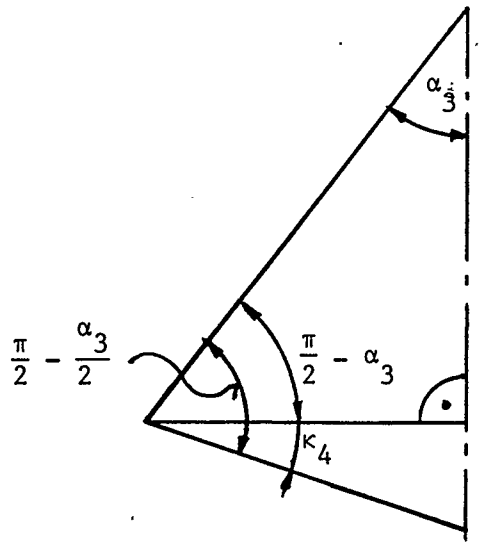

Fig. 4 Geometry for κ_4 Derivation

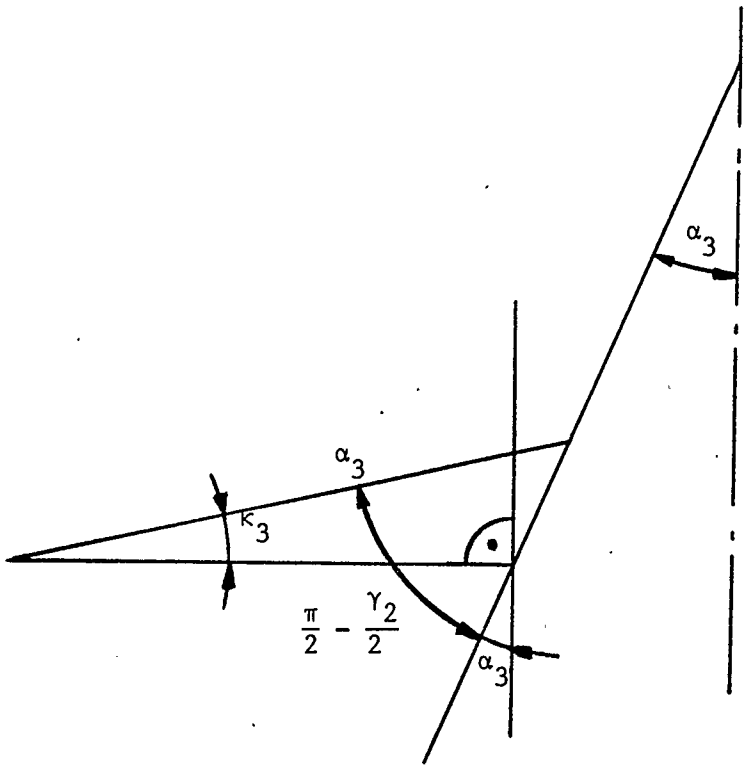

Fig. A5 Geometry for κ_3 Derivation

$$\theta_o (R_o-R) = 2R\alpha_1 + (R_o-R)\gamma_1 + \frac{2R}{R_o+R} \alpha_2 (R_o-R) + (R_o-R)\gamma_2$$

$$+ 2R\alpha_3$$

and after simplifications

$$\theta_o = \frac{2}{\overline{R_o}-1} \alpha_1 + \frac{2}{\overline{R_o}+1} \alpha_2 + \frac{2}{\overline{R_o}-1} \alpha_3 + \gamma_1 + \gamma_2 \quad . \qquad (A.6)$$

Using Eq. (A.3) and Eq. (A.4) to get

$$\theta_o + \alpha_1 - \alpha_2 - \gamma_1 - \frac{\gamma_2}{2} = \frac{\gamma_2}{2} - \alpha_3$$

$$\theta_o + \alpha_1 - \alpha_2 + \alpha_3 = \gamma_1 + \gamma_2 \; . \qquad (A.7)$$

Using Eq. (A.7) and Eq. (A.6) to get

$$\theta_o - \frac{2}{\overline{R_o}-1} \alpha_1 - \frac{2}{\overline{R_o}+1} \alpha_2 - \frac{2}{\overline{R_o}-1} \alpha_3 = \theta_o + \alpha_1 - \alpha_2 + \alpha_3$$

after simplifications one will obtain

$$\alpha_1 = \frac{(\overline{R_o}-1)^2}{(\overline{R_o}+1)^2} \alpha_2 - \alpha_3 \; . \qquad (A.8)$$

Using Eq. (A.7) and Eq. (A.8) to get

$$\theta_o + \frac{(\overline{R_o}-1)^2}{(\overline{R_o}+1)^2} \alpha_2 - \alpha_3 - \alpha_2 + \alpha_3 = \gamma_1 + \gamma_2$$

after simplifications

$$\alpha_2 = \frac{(\overline{R_o}+1)^2}{4\overline{R_o}} (\theta_o - \gamma_1 - \gamma_2) \; . \qquad (A.9)$$

Introducing Eq. (A.9) into Eq. (A.8) to get

$$\alpha_1 = \frac{(\overline{R_o}-1)^2}{(\overline{R_o}+1)^2} \frac{(\overline{R_o}+1)^2}{4\overline{R_o}} (\theta_o - \gamma_1 - \gamma_2) - \alpha_3$$

$$\alpha_1 = \frac{(\overline{R_o}-1)^2}{4\overline{R_o}} (\theta_o - \gamma_1 - \gamma_2) - \alpha_3 \ . \qquad (A.10)$$

Having derived α_1 and α_2 as a function of γ_1, γ_2, α_3 let us introduce them into Eqs. (A.1) and Eq. (A.2). Introducing Eq. (A.10) into Eq. (A.1) to get

$$\kappa_1 = \pi - \theta_o - \frac{(\overline{R_o}-1)^2}{8\overline{R_o}} (\theta_o - \gamma_1 - \gamma_2) + \frac{\alpha_3}{2}$$

or

$$\kappa_1 = \pi - [1 + \frac{(\overline{R_o}-1)^2}{8\overline{R_o}}] \theta_o + \frac{\alpha_3}{2} + \frac{(\overline{R_o}-1)^2}{8\overline{R_o}} (\gamma_1+\gamma_2) \ . \qquad (A.11)$$

Similarly introducing Eq. (A.10) into Eq. (A.2) to get

$$\kappa_2 = \pi - \theta_o - \frac{(\overline{R_o}-1)^2}{4\overline{R_o}} (\theta_o-\gamma_1-\gamma_2) + \alpha_3 + \frac{\gamma_1}{2}$$

or

$$\kappa_2 = \pi - [1 + \frac{(\overline{R_o}-1)^2}{4\overline{R_o}}] \theta_o + \alpha_3 + [\tfrac{1}{2} + \frac{(\overline{R_o}-1)^2}{4\overline{R_o}}] \gamma_1$$

$$+ \frac{(\overline{R_o}-1)^2}{4\overline{R_o}} \gamma_2 . \qquad (A.12)$$

Angles κ_3 and κ_4 are given by Eq. (A.4) and Eq. (A.5) respectively.

APPENDIX B

COMPUTER PROGRAMS

- MINIMIZATION OF LOAD FUNCTION Q FOR STATIC APPROACH
- MINIMIZATION OF TOTAL POTENTIAL W FOR HINGE SHAPE OPTIMIZATION

```
 1  *
 2  *      PROGRAM SYMMETRICALLY LOADED ARCH
 3  *      AIR-SUPPORTRED STRUCTURE
 4  *      STATIC APPROACH
 5  *      PROGRAM lam.f
 6  *
 7  *      THIS PROGRAM MINIMIZE LOAD FUNCTION Q
 8  *      WITH CONSTRAINT DELTAX=0
 9  *
10  *       VARIABLE TYPES
11  *
12         REAL mp
13         COMMON /PARS/r,rn,pi,t0/PARXY/x0,y0,x2,y20
14         COMMON /PARC/c1,c2/ANGL/al3,sam1/PARF/fi1,sp
15         COMMON /PARAL/al1,al2/NSO1B/LP,LPD,IERR
16         COMMON /PARM/mp
17         CHARACTER *18 NAME
18  *
19  *      OUTPUT HEADING
20  *      INPUT DATA
21  *
22         WRITE(6,*)'FILE NAME'
23         READ(5,10)NAME
24         WRITE(6,*)'INPUT SHAPE PARAMETER  SP'
25         READ(5,*)sp
26    10   FORMAT(A18)
27         OPEN (UNIT=12,FILE= NAME)
28         WRITE(12,*)'SYMMETRICALLY LOADED ARCH'
29         WRITE(12,*)'PROGRAM lam.f'
30  *
31         pi=4.*ATAN(1.)
32         r=6.5
33         t0=1.818
34         rp=r+1.
35         rn=r-1.
36  *
37         x0=rn*sin(pi-t0)
38         y0=rn*(1.+cos(pi-t0))
39         x2=r*sin(pi-t0)
40         y20=sin(t0-pi/2.)
41         fi1=t0-pi/2.
42  *
43         c1=rn*rn/(4.*r)
44         c2=rp*rp/(4.*r)
```

```
*
*     OUTPUT INITIAL GEOMETRY
*
      WRITE(12,*)
      WRITE(12,*)'INITIAL GEOMETRY'
      WRITE(12,*)
      WRITE(12,*)'R=',r,'TE0=',t0,'PARAMETER SP=',sp
      WRITE(12,*)
      WRITE(12,*)'NUMERICAL RESULTS'
      WRITE(12,*)
      WRITE(12,15)
15    FORMAT(3x,' ALFA 3',6x,' ALFA 2',6x,' ALFA 1',6x,' GAMA 1',6x,
     &       ' GAMA 2',6x,'DELTA Y',6x,'DELTA X',6x,'LOAD Q',6x,
     &       'MOMENT MP')
      WRITE(12,*)
*
*     SET INITIAL APROXIMATION
*
      eps=.001
      DO 18 i1=1,35
      s11=0.
      s1r=t0
      al3=float(i1-1)*.02
      CALL OPTI(s11,s1r,eps,s1m,s2m,am,dy,dx,error)
*
*     OUTPUT CURRENT DATA
*
      if(error.EQ.1.) GO TO 25
      if(IERR.GT.0) GO TO 26
      WRITE(12,20)al3,al2,al1,s1m,s2m,dy,dx,am,mp
20    FORMAT(E12.5,(8(1x,E12.5)))
      GO TO 18
 25   WRITE(12,*)'ERROR FROM OPTI,I>1000'
      GO TO 18
 26   WRITE(12,*)'ERROR FROM NSO1A,IERR=',IERR
*
18    CONTINUE
*
*     END MAIN PROGRAM
*
      STOP
      END
*****************************************************************
```

```
      SUBROUTINE OPTI(s11,s1r,eps,s1m,s2m,am,dy,dx,error)
      COMMON /PARS/r,rn,pi,t0/PARXY/x0,y0,x2,y20
      COMMON /ANGL/al3,sam1/PARAL/al1,al2/XDYD/xd,yd
      COMMON /NS01B/LP,LPD,IERR
      REAL x(1),F(1),A(1,1),W(7)
*
      N=1
      ACC=.000001
      MAXFUN=10000
      IPRINT=MAXFUN
      STEP=.01
      STPMAX=.5
      LP=0
      LPD=0
      i=1
*     CALCULATE INTERIOR POINT FOR GAMA1 LEFT
100   s11=s11+(s1r-s11-eps)/2.
*     SOLVE CONSTRAINT EQUATION FOR GAMA2 LEFT
      x(1)=t0-s11
      sam1=s11
      CALL NS01A (N,x,F,A,STEP,STPMAX,ACC,MAXFUN,IPRINT,W)
      s21=x(1)
      CALL LOADQ(s21,q)
      q1=q
*     CALCULATE INTERIOR POINT FOR GAMA1 RIGHT
      s1r1=s11+eps
*     SOLVE CONSTRAINT EQUATION FOR GAMA2 RIGHT
      x(1)=t0-s1r1
      sam1=s1r1
      CALL NS01A (N,x,F,A,STEP,STPMAX,ACC,MAXFUN,IPRINT,W)
      s2r1=x(1)
      CALL LOADQ(s2r1,q)
      qr1=q
*     DETERMINE POSITION OF THE MINIMUM
      IF(q11-qr1)2,5,3
2     s1r=s1r1
      GO TO 4
3     s11=s11
*     TEST FOR END OF SEARCH
4     IF(i.GT.1000) GO TO 6
      i=i+1
      IF(s1r-s11.GT.3.*eps) GO TO 100
5     s1m=(s11+s1r1)/2.
```

```
*     SOLVE CONSTRAINT EQUATION FOR GAMA2 MINIMUM
      x(1)=(g2l1+g2r1)/2.
      gam1=g1m
      CALL NS01A (N,x,F,A,STEP,STPMAX,ACC,MAXFUN,IPRINT,W)
      g2m=x(1)
      CALL LOADQ(g2m,q)
      qm=q
      dx=x0-xd
      dy=y0-yd
      GO TO 7
*
6     error=1.
7     RETURN
      END
*************************************************************
*
      SUBROUTINE GEOM(x)
      REAL k1,k2,k3,k4,x(1)
      COMMON /PARC/c1,c2/PARS/r,rn,pi,t0
      COMMON /PARAL/al1,al2/PARA/a1,a2,a3,a4
      COMMON /PARK/k1,k2,k3,k4/ANGL/al3,gam1
*
      al1=c1*(t0-gam1-x(1))-al3
      al2=c2*(t0-gam1-x(1))
*
      k1=pi-(1.+c1/2.)*t0+al3/2.+c1*(gam1+x(1))/2.
      k2=pi-(1.+c1)*t0+al3+(.5+c1)*gam1+c1*x(1)
      k3=x(1)/2.-al3
      k4=al3/2.
*
      a1=4.*sin(al1/2.)
      a2=2.*rn*sin(gam1/2.)
      a3=2.*rn*sin(x(1)/2.)
      a4=4.*sin(k4)
*
      RETURN
      END
*************************************************************
```

```
      SUBROUTINE LOADQ(sam2,a)
      REAL k1,k2,k3,k4,k5
      REAL m1,m2,m3,mp
      COMMON /PARS/r,rn,pi,t0/PARF/fi1,sp
      COMMON /PARA/a1,a2,a3,a4/ANGL/al3,sam1
      COMMON /PARK/k1,k2,k3,k4/PARAL/al1,al2
      COMMON /PARXY/x0,y0,x2,y20/XDYD/xd,yd
      COMMON /PARM/mp
*
      k5=t0+al1-al2/4.-sam1
      a5=2.*sin(al2/4.)
      ap1=a1/2.
      ap2=2.*r*sin(sam1/2.)
*
      xd=a3*cos(k3)+a4*cos(k4)-a1*cos(k1)-a2*cos(k2)
      yd=a1*sin(k1)+a2*sin(k2)+a3*sin(k3)-a4*sin(k4)
*
      x1=ap1*cos(k1)+ap2*cos(k2)-a5*cos(k5)
      y1=ap1*sin(k1)+ap2*sin(k2)+a5*sin(k5)
      y2=yd+1.+y20
*
      fi2=pi/2.+al3-al2/2.-sam2
      f=(x2*sin(fi1)-(y2-1.)*cos(fi1))/(y2-1.-sin(fi1))
      s=(x2+f)/(y2-1.)
*
      m1=.5*(1.+al1/(sp+al1))
      m2=.5*(1.+al2/(sp+al2))
      m3=.5*(1.+al3/(sp+al3))
      mp=m1+m2+(m3-m1)*y1/y2
*
      a=mp/(x1+(x2+f+s)*y1/y2-f+s*sin(fi2)+cos(fi2))
*
      RETURN
      END
*****************************************************************
      SUBROUTINE CALFUN(N,x,F)
      REAL x(1),F(1)
      REAL k1,k2,k3,k4
      INTEGER N
      COMMON /PARA/a1,a2,a3,a4/PARXY/x0,y0,x2,y20
      COMMON /PARK/k1,k2,k3,k4
*
      CALL GEOM(x)

*
      F(1)=(x0-(a3*cos(k3)+a4*cos(k4)-a1*cos(k1)-a2*cos(k2)))
*
      RETURN
      END
*****************************************************************
```

```
      *       THIS PROGRAM MINIMIZE TOTAL POTENTIAL
      *       FUNCTION W FOR PNEUMATIC HINGE MODEL
      *       PROGRAM phm.f
      *
              REAL mp
              COMMON/PAR/pi,p1,p2,p3,ax
              COMMON/PBC/b,c
              COMMON/NS01B/LP,LPD,IERR
              REAL x(1),F(1),A(1,1),W(7)
              CHARACTER *18 NAME
      *
              N=1
              ACC=.000001
              MAXFUN=10000
              IPRINT=MAXFUN
              STEP=.01
              STPMAX=.5
              LP=0
              LPD=0
              pi=4.*atan(1.)
              p1=pi*pi/4.
              p2=p1-1.
              p3=4./(3.*pi)
              ax=1.2
      *
              WRITE(6,*)'FILE NAME'
              READ(5,10)NAME
      10      FORMAT(A18)
              OPEN(UNIT=12,FILE=NAME)
              WRITE(12,*)'PNEUMATIC HINGE -SHAPE OPTIMIZATION'
              WRITE(12,*)'PROGRAM phm.f'
              WRITE(12,*)
              WRITE(12,*)'NUMERICAL RESULTS'
              WRITE(12,*)
              WRITE(12,15)
      15      FORMAT(3x,' ALFA  ',6x,' PAR Ra',6x,' PAR Mp',6x,
             &          ' PAR  A',6x,' PAR  B',6x,' PAR  C')
              rm=1500.
              do 18 j=1,20
              al=float(j)/33.
              m=10*j
              r1=.0
              rr=rm
              eps=1.E-3
      *
      *       START OF MINIMIZATION ROUTINE
      *       CALCULATE INTERIOR POINTS
      *
```

```
      1        rl1=rl+.5*(rr-rl-eps)
               rr1=rl1+eps
      *        CALCULATE VALUE OF FUNCTION W
               CALL FUNW(al,rl1,m,fw)
               wl1=fw
               CALL FUNW(al,rr1,m,fw)
               wr1=fw
               if(wl1-wr1)2,5,3
      2        rr=rr1
               GO TO 4
      3        rl=rl1
      4        if(i.ge.1000) GOTO 6
               i=i+1
               if(rr-rl.gt.3.*eps) GOTO 1
      5        rm=.5*(rl1+rr1)
      *        END OF MINIMIZATION ROUTINE
               c=1./cos(al)
               c1=1.-c
               b=rm*c1+c
               x(1)=ax
               CALL NS01A(N,x,F,A,STEP,STPMAX,ACC,MAXFUN,IPRINT,W)
               ax=x(1)
               mp=.5*ax*(b+c)*(rm*c1*(1.-p3)+c)
               WRITE(12,30)al,rm,mp,ax,b,c
      30       FORMAT(E12.5,(5(1x,E12.5)))
               GOTO 18
      6        WRITE(12,*)'ERROR RETURN, N>1000'
      18       CONTINUE
               STOP
               END
      ********************************************
               SUBROUTINE FUNW(al,ra,m,fw)
               a0=.0
               CALL INTEG1(a0,al,ra,m,xi)
               wv=xi
               CALL INTEG2(a0,al,ra,m,xi)
               wm=xi
               fw=al*ra-wv-wm
               RETURN
               END
      ********************************************
               SUBROUTINE FUN1(xa,r,fx)
               COMMON/PAR/pi,p1,p2,p3,ax
               COMMON/PBC/b,c
               COMMON/NS01B/LP,LPD,IERR
               REAL x(1),F(1),A(1,1),W(7)
               N=1
               ACC=.000001
               MAXFUN=10000
               IPRINT=MAXFUN
```

```
      STEP=.01
      STPMAX=.5
      LP=0
      LPD=0
      c=1./cos(xa)
      c1=1.-c
      b=r*c1+c
      x(1)=ax
      CALL NS01A(N,x,F,A,STEP,STPMAX,ACC,MAXFUN,IPRINT,W)
      ax=x(1)
      fx=.5*c*ax*(b+c)*(r*(1.+p3*c1/c)-1.)
      RETURN
      END
**********************************************
      SUBROUTINE FUN2(xa,r,fx)
      COMMON/PAR/pi,p1,p2,p3,ax
      COMMON/PBC/b,c
      COMMON/NS01B/LP,LPD,IERR
      REAL x(1),F(1),A(1,1),W(7)
      N=1
      ACC=.000001
      MAXFUN=10000
      IPRINT=MAXFUN
      STEP=.01
      STPMAX=.5
      LP=0
      LPD=0
      c=1./cos(xa)
      c1=1.-c
      b=r*c1+c
      x(1)=ax
      CALL NS01A(N,x,F,A,STEP,STPMAX,ACC,MAXFUN,IPRINT,W)
      ax=x(1)
      fx=.5*ax*(b+c)*(r*c1*(1.-p3)+c)
      RETURN
      END
**********************************************
*     NUMERICAL INTEGRATION BY
*     SIMPSON'S COMPOSITE ALGORITHM
*
      SUBROUTINE INTEG1(a,b,r,m,xi)
      h=(b-a)/float(2*m)
      CALL FUN1(a,r,fx)
      fa=fx
      CALL FUN1(b,r,fx)
      fb=fx
      x10=fa+fb
      x11=.0
      x12=.0
```

```
148           do 5 i=1,(2*m-1)
149           x=a+float(i)*h
150           k=i/2
151           if(i.eq.2*k) GOTO 10
152           CALL FUN1(x,r,fx)
153           x11=x11+fx
154           GOTO 5
155   10      CALL FUN1(x,r,fx)
156           x12=x12+fx
157   5       CONTINUE
158           xi=h*(x10+2.*x12+4.*x11)/3.
159           RETURN
160           END
161   ***********************************************
162   *       NUMERICAL INTEGRATION BY
163   *       SIMPSON'S COMPOSITE ALGORITHM
164   *
165           SUBROUTINE INTEG2(a,b,r,m,xi)
166           h=(b-a)/float(2*m)
167           CALL FUN2(a,r,fx)
168           fa=fx
169           CALL FUN2(b,r,fx)
170           fb=fx
171           x10=fa+fb
172           x11=.0
173           x12=.0
174           do 5 i=1,(2*m-1)
175           x=a+float(i)*h
176           k=i/2
177           if(i.eq.2*k) GOTO 10
178           CALL FUN2(x,r,fx)
179           x11=x11+fx
180           GOTO 5
181   10      CALL FUN2(x,r,fx)
182           x12=x12+fx
183   5       CONTINUE
184           xi=h*(x10+2.*x12+4.*x11)/3.
185           RETURN
186           END
187   ***********************************************
188           SUBROUTINE CALFUN(N,x,F)
189           REAL x(1),F(1)
190           COMMON/PAR/pi,p1,p2,p3,ax
191           COMMON/PBC/b,c
192           F(1)=sqrt(x(1)**2.+p2*b*b)+sqrt(x(1)**2.+p2*c*c)-pi
193           RETURN
194           END
195   ***********************************************
```